TOHOKU UNIVERSITY

Graduate School of Engineering

Engineering Dynamic DNA Structures Driven by Physico-Chemical Interactions

(物理化学的相互作用により駆動される動的DNA構造のエンジニアリング)

A dissertation submitted for the degree of Doctor of Philosophy (Engineering)

Department of Bioengineering and Robotics

by

Keitel Abraham CERVANTES SALGUERO

May 18, 2017

Contents

1

Introduction

Contents

1.1 Outline

This thesis is a contribution to molecular engineering, a sub-field of nanotechnology. In this field, molecules are designed, synthesized and used as building materials for fabricating high-order structures. Initial efforts have focused on, under thermodynamic equilibrium, creating static structures. Later, with the growing but still incomplete mastering of static structures, dynamic structures were developed and used as components for functional devices in applications including health, energy, and computation, to name a few. Giving its potential, ongoing research in molecular engineering seeks to establish new routes to provide dynamics to, otherwise, static structures. For this purpose, there are diverse approaches such as synthesizing inorganic molecules; approach that recently has been awarded with the 2016 Nobel prize in chemistry [1]. Using biomolecules for creating dynamic structures is another interesting approach. In the same way as life is powered by biomolecules, nanotechnology is founded on harnessing the properties of biomolecules by careful molecular design. In this context, DNA has been widely used for nanotechnology because information (molecular programs for self-assembly, computation and so on) can be written directly in its structure. Programming molecular interactions with DNA is an insight, five times recognized by the renowned Feynman prize [2]. The aim of this thesis is to show novel methods for making dynamic structures made of DNA molecules. To elaborate more

on the thesis aim, the contents of this chapter Introduction and the thesis are orderly presented as follows.

In chapter one, the background to this thesis is divided into two parts. In the first part, as general background, I describe the DNA molecule and its properties. Structural properties, as well as physical, chemical, and electrical properties of DNA are reviewed. Then, I explain the DNA base-pairing rule, which is a powerful tool for developing programmable molecular-based technologies that are used in molecular computing, DNA-based sensing devices, DNA-based therapeutics/diagnosis, among others. In the second part, as specialized background, I discuss dynamic DNA structures. All the dynamic DNA structures use physico-chemical interactions for their driving dynamics. I define the meaning of "dynamics" and limit the scope of dynamic structures in this thesis. I describe several typical examples, along their structure and driving interactions.

In chapter two, harnessing intramolecular forces for self-assembling under thermodynamic equilibrium is shown. The design and realization of the one-pot synthesis of multiple-sized molecular rings constructed by shape-variable building blocks is shown. The size of the rings can be tuned by the geometry of the building blocks. A chemical kinetic model is introduced to simulate the formation dynamics of the rings.

In chapter three, harnessing the addition of small molecules for molecular motion and force-directed self-assembly is shown. External hydrophobic molecules introduced into the system modified DNA nanostructures for actuation. The actuation consists of the nanostructure motion from hydrophilic regions to hydrophobic regions. This project provides a conjugation methodology that is used for larger DNA nanostructures at the water/air interface. In this conditions, by reducing the size of DNA nanostructures in the interface, the self-assembly of DNA nanostructures is generated.

In chapter four, harnessing light irradiation for driving phase transitions in DNA hydrogels is shown. I describe the light-driven repeatable control of the sol-gel phase transition of hydrogels made completely of DNA. The physical properties of the DNA hydrogel are assessed by using several methods. Conditions of gelation are investigated based on the molecular structure of component DNA molecules. Future applications are discussed.

In chapter five, harnessing electric fields to control the inter-molecular interactions between DNA molecules is shown. The electric control of the DNA dehybridization modes, namely unzipping and shearing, are investigated in a polymeric hydrogel by using negatively-charged gold nanoparticles. An experimental setup is proposed. Different molecular configurations for the DNA and the gold nanoparticles are tested.

In chapter six, finally, the conclusions among the previous chapters are summarized, including future applications.

1.2 DNA Molecule and Its Properties

1.2.1 DNA

Since the discovery of the molecular structure of DNA (deoxyribonucleic acid or nucleic acid, hereinafter called simply DNA) in 1953 [3], many aspects of DNA have been fully investigated making it, perhaps, the most well-understood biomolecule. From a genetics standpoint, DNA is a fundamental molecule for life because it carries genetic information from parents to offspring. This information-related property is used in diverse research fields, as for example, in cloning of living beings, genome editing [4] or for other technologies. As this thesis belongs to the research field of DNA nanotechnology, my interest is to use the DNA properties to engineer structures. In DNA nanotechnology, researchers widely use synthetic DNA molecules with desired base sequences. Generally speaking, there is no difference between the molecular structure of a natural DNA and a synthetic DNA with the same composing sequences. However, the synthetic DNA strands from two different producing companies may differ depending on the used synthesizing methods involving parameters such as molecular yield.

1.2.2 DNA Backbone

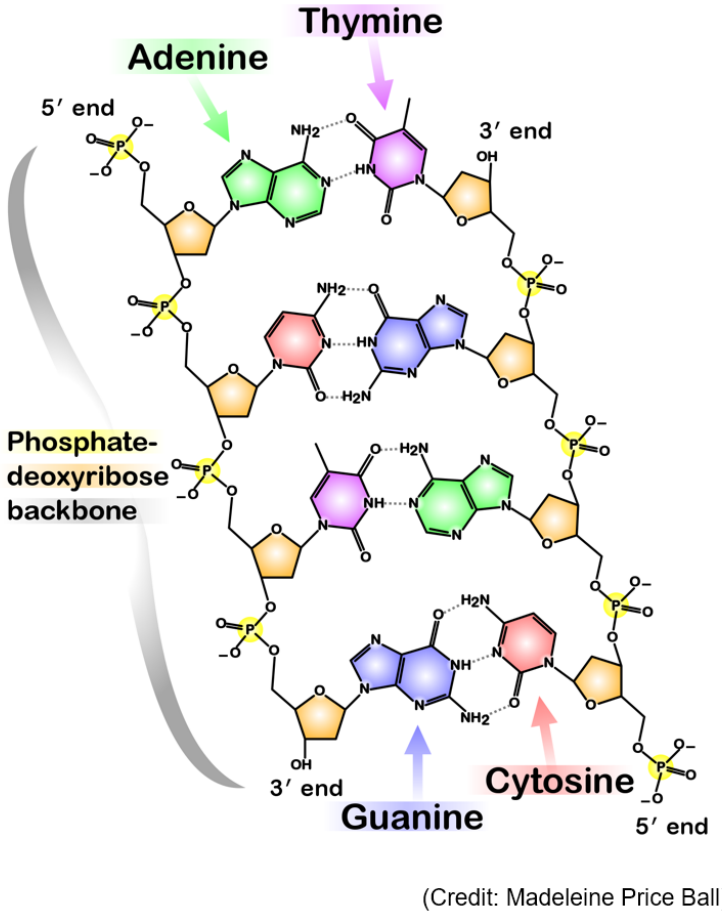

(Credit: Madeleine Price Ball)

Figure 1.1: DNA chemical structure showing the nucleic acid bases.

A single-stranded DNA (ssDNA or DNA strand) is a polymer that has a backbone holding nucleic acid units. The backbone is made of two alternating units covalently joined: a sugar and a nucleobase. The sugar is a deoxyribose, specifically it is monosaccharide and phosphate groups (which are related to phosphoric acid). The nucleobases are sub-units covalently attached

to the sugars. The nucleobases are four, namely Guanine, Adenine, Thymine and Cytosine. In a DNA strand, the molecular structure of both of its ends are different, therefore ends are called 5' and 3' (5' carbon at one sugar, and 3' carbon at another sugar). A direction or orientation is defined from 5' to 3' end. Due to the base-pairing rules, which will be explained later, two ssDNA can join together and assemble into a double-stranded DNA (dsDNA or DNA duplex). In a DNA duplex, while one strand orientation is 5'-3', the other strand orientation is 3'-5'. A scheme of the chemical structure of DNA is shown in Figure 1.1. In the following sections the intrinsic molecular interactions that stabilize DNA duplex structure are described.

1.2.3 Base Paring

In order to form a DNA duplex, the sequences of both forming strands need to be complementary to each other. That is, each kind of nucleobase on one strand make a bond with only one kind of nucleobase on the other strand. The inter-base bond is a hydrogen bond of electrostatic origin, and it is called complementary base pairing or Watson-Crick base pairing (in honor to the discoverers). For example, Adenine (A) bonds only to Thymine (T) with two hydrogen bonds, and Cytosine (C) bonds only to Guanine (G) with three hydrogen bonds (Figure 1.2, left). Two nucleotides making a bond are called base pair. This complementarity pairing is the so-called Watson-Crick base-pairing. Besides the base-pairing, the two strands have opposite directionality;

that is, 5' $\rightarrow$ 3' and 3' $\leftarrow$ 5' as explained above. The B-form of DNA is considered the "standard" DNA helical structure; its inter-base pair distance is 0.32 nm and the helical periodicity is about 1 turn per 10.5 base-pairs (bps), which is 3.5 nm (Figure 1.2, right). Other helical structure is A-form which is commonly found in dehydrated DNA. With these "molecular rules", DNA can be programmed for fabricating some useful structures; however, thermodynamic and mechanical properties and analysis can be taken into account to design more sophisticated structures.

1.2.4 Thermodynamic Properties

The thermodynamic properties of DNA can be accurately predicted to some extend. For example, secondary structures formation and other stable states [5]. A common molecular biology technique for analyzing the thermodynamic stability of a DNA is the melting curve experiment [6]. From the melting curve it it is possible to obtain the melting temperature (T_M) and other parameters such as the free energy.

1.2.5 Mechanical Properties

A DNA strand behaves as flexible and extensible polymer depending on the tensile force applied on it [7]. The flexibility and extensibility of DNA

is due to the molecular structure of the backbone, which allows entropic states. Under tensile conditions the sugars in the ssDNA can have two endo pucker configurations, namely C3' and C2' endo. In a C2' endo configuration the inter-phosphate distance is 0.7 nm [8]. This distance is in the same order range as the inter-base pair distance of dsDNA in B-form (0.32 nm). A DNA duplex, whose nucleotides are all paired, behaves, to put it simply, as a rigid rod according to theory and experiments. The persistence length of DNA is about 50 nm (or approximately 160 nucleotides). The rigidity of double-stranded DNA is the counterpart of the flexibility of single-stranded DNA, and both can be used together for designing DNA nanostructures.

1.2.6 Electrical Properties

DNA has an inherit charge owing to the phosphate ion molecules in the backbone. In a dsDNA, there are roughly two ions, belonging to each strand, per base pair. That is, 2 electrons per 0.34 nm length; in other words, a linear charge of 5.9 e nm^{-1}, where e is the charge of the electron. A surface charge, considering that a dsDNA has a diameter of 2nm, is 0.9 e nm^{-2}. These properties describe the electrical contribution from the structure of DNA, however its behavior is much complex. The response of DNA to electric fields is more surprising to previously predicted. For example, DNA works as an electrical wire, however it is different from a conducting wire used in many modern applications. The charge transport through a DNA wire varies as

the conditions for the system [9]. DNA charge transport has been recently confirmed in nature [10]. Moreover, the DNA structure can be combined with other molecules to realize molecular switches [11].

1.3 Engineering DNA for Fabricating Structures

1.3.1 Static Structures

Static DNA structures are basic constructions. As mentioned in previous section, constructing a static structure involves programming DNA with specific sequences. The molecular design is important in DNA nanotechnology; for example, once structures are self-assembled, they can further self-assemble into high-order structures if required by design. The material to make these structures can solely be DNA or a combination with other molecules. More precisely, structures can be DNA tiles, DNA origamis, DNA hydrogels, and DNA-integrated hydrogels.

DNA tiling and DNA origamis are two general strategies used for designing static structures made solely of DNA, which means only using the base-pairing rules. In DNA tiling, DNA tiles (also called DNA motifs) are used as basic elements for self-assembling larger structures. A DNA tile consists of many DNA duplexes that connect each other by crossover junctions. The crossover junction is naturally found as Holliday junction, which occurs as

intermediate state during the process of genetic recombination in cells (perhaps a Holiday junction is the simplest example of a dynamic structure in thermal fluctuation). The Holliday junction is not fixed and migrates along the strands randomly (Figure 1.3a). When using the junctions as structural components in DNA tiles, junctions must be immobilized in order to make structures with structural stability.

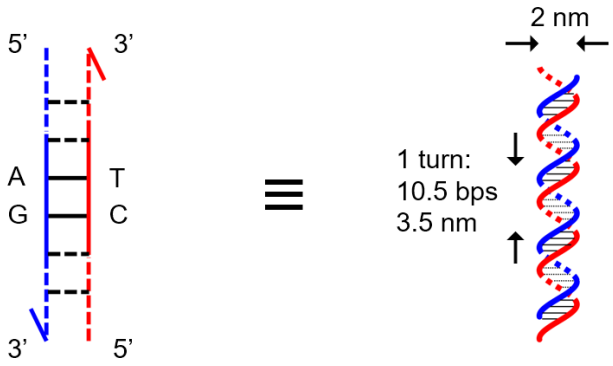

Figure 1.2: DNA duplex. Left: base pairing rules for a DNA duplex. Right: nanometer dimensions of a short DNA duplex.

Immobilization of the Holliday junction is simply done by changing the DNA base sequences composition around the junction (Figure 1.3b). In a DNA tile, two immobilized Holliday junctions defines the shape of the complex (so it is called a double crossover (DX) molecule [12]). Four ends of the helices are decorated with short single-stranded portions called sticky ends, which define connectivity between the tiles. DNA tiles have been widely used as a basic building block for self-assembling 2D crystals [13,14] (Figure 1.3d). The

self-assembly of DNA tiles is sometimes modeled as a process similar to that of crystal growth; namely, monomers (DNA tiles) bind each other to form a nucleate and then grow into a large planar structure. However, more specific interactions between tiles can be introduced through rational design of sticky ends. DNA tiles are mostly used to make periodic 2D patterns with few set of DNA strands at low cost and achieving sizes in the micrometer scale. Contrary to lattices, aperiodic structures would be needed and therefore other different strategies have been applied.

The other strategy is called DNA origami, which is popularly described as the folding of long DNA strands in similar way as the traditional Japanese origami works for paper sheets. Currently, DNA origami is the most powerful technique to assemble nanostructures with determined sizes and shapes [15–17]. This technique is suitable when structures are required in mega Dalton range. As same as DNA tiles, it exploits the specificity of molecular recognition of DNA. A DNA origami is composed of a long circular single-stranded DNA and hundreds of short single-stranded DNAs called a “scaffold” and “staples”, respectively.

In principle, staples fold the scaffold into a desired conformation by hybridization to its complementary section, until the whole structure becomes double-stranded, which is thermodynamically most stable (Figure 1.4). The typical self-assembly protocol for DNA origami requires thermal annealing of

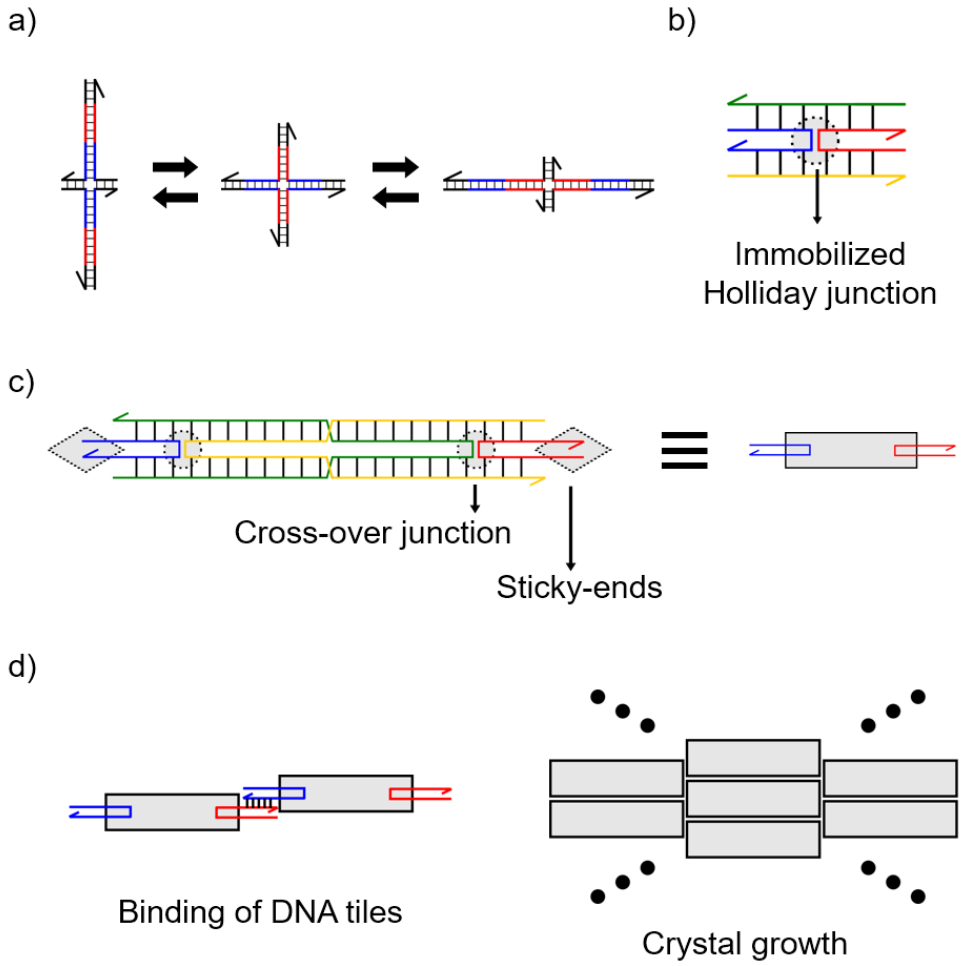

Figure 1.3: Holliday junction is used for self-assembly. (a) Holliday junction is mobile by branch migration. (b) Immobilized holiday junction is the basis for DX tile. (c) DX tile made of two crossovers and four sticky ends. (d) Self-assembled crystal by binding between sticky ends.

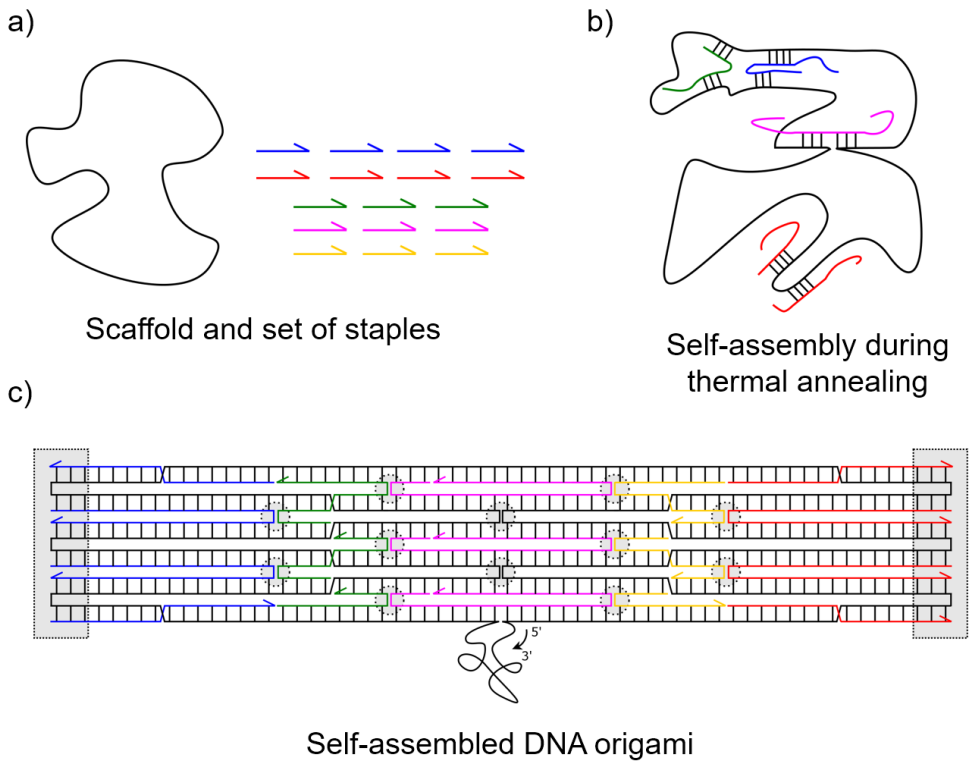

Figure 1.4: DNA origami self-assembly steps. (a) Scaffold and set of staples. Scaffold is usually a 7000 nt long circular strand, and staples are at most 50 nt. (b) As thermal annealing is performed, staples recognize the scaffold and can fix separate sections in the scaffold. (c) Final structure.

a mixture containing the scaffold and the staples. Typical annealing profile usually starts at 95°C, where all the strands exist as single strands, and then decreases gradually to lower temperatures such as 4°C.

As the origami method is general, the used scaffold can be of virtually any long length. For example, it can be as large as ∼51K nucleotides [18], or it can be the most usual scaffold of 7,249 nucleotides (belonging to the DNA of the M13mp18 bacteriophage). On the other hand, the staples are synthetic and have can have diverse nucleotide lengths depending on the particular origami design. Staples usually consisting of less than 50 nucleotides. The

methodology of DNA origami is so general that various ways for routing and arranging the scaffold and staples have been demonstrated to make 2D, 3D and curved nanostructures [19–24]. Furthermore, designing DNA origamis with CAD programs such as caDNAno [25] assists the process of designing DNA nanostructures. On the basis of hybridization of DNA molecules, nucleic acid nanotechnology enables us to rationally design and build various nanostructures and nanodevices. Usually these DNA nanostructures are designed as a thermodynamically stable state, therefore they are intrinsically static [26]. These static DNA nanostructures have been utilized as a building block self-assembled into a platform to immobilize diverse molecules and nanoparticles.

1.3.2 Dynamic Structures and Interactions for Driving Dynamics

In previous section, static DNA structures have been shown however my interest is to design dynamic DNA structures. Dynamic structures are recently getting more attention because they can change their configuration and properties according to applied interactions, as for example, external signals or environmental change. Examples are individual structures that dis-assemble under a signal, group of structures that self-assemble under a force, etc. Some methods for dynamic DNA structures along with their typical examples are reviewed. The material to make these structures can be solely DNA or a combination with other molecules. Structures can be DNA tiles,

DNA origamis, DNA-integrated vesicles, DNA hydrogels, and DNA-integrated hydrogels. Interactions for driving the dynamics are of physical or chemical origin.

A common strategy for building dynamic DNA structures, which is also used by engineers at the macroscopic world, is using moving elements. One typical example of this strategy is using rigid and flexible elements. Rigid elements with particular shapes are connected by joints (or flexible components) to allow certain degrees-of-freedom. Shapes of rigid elements can fit precisely between each other in order to achieve mechanical strength. These properties can be programmed at molecular scale by using DNA nanostructures. Particularly, DNA duplexes and bundles of duplexes can be readily used as stiff (rigid) elements, and DNA strands as flexible elements. Being a polymer, DNA duplex and strands have stiffness and elasticity. DNA stiffness is quantitatively characterized by the persistence length. The DNA elastic properties are predictable to some extend by the free-jointed or worm-like chain models [27]. Under non over-extended conditions, DNA strands are simply regarded as Hookean springs. Building desired structure using the rigid and flexible elements requires trial and error [28–31].

DNA tweezers is a seminal example (2000) of a repeatable actuation of a DNA nanostructure driven solely by DNA molecules; i.e. actuation is driven using the toehold-mediated strand displacement reaction [32–34]. The strand

displacement reaction is perhaps the most extensively used method for base-sequence-specific actuation. It is possible to remove a specific target strand in a DNA duplex by using an invader strand. In this reaction, upon the invader strand binding specifically to the DNA duplex, the target strand is released into solution. The driving force of this spontaneous process is the free energy of the hybridized complexes, where the final duplex is more stable than the initial one before target release. In the DNA tweezers, a short ssDNA segment connecting two dsDNA segments (arms) served as a joint of the tweezers. The closed and open states of the tweezers can be observed by using fluorescence resonance energy transfer (FRET). The tweezers work as a bi-state machine where transition between the states is fueled by additional DNA strands that trigger the toehold-mediated strand-displacement. Transformation from open to close state occurs when a ssDNA called a fuel strand is added. Reversing to the open state is done by adding a complementary strand to the fuel (i.e. anti-fuel). By applying fuel and anti-fuel alternatively, it is able to make a cyclic reaction. Other methods for actuating DNA nanostructures have also been studied including DNA-based single-molecule beacons driven by the presence of Na^+ concentration [35].

Other more recent examples of structures with moving parts are larger DNA-based mechanical mechanisms that undergo conformational transitions along restricted degrees-of-freedom [36]. Rigid and flexible components are DNA bundles and hinges made of DNA loops. The controlled motion along

those degrees-of-freedom is directed by using DNA molecule signals. The same as in the case of the DNA tweezers, the physico-chemical interaction is provided by the signals is DNA base-pairing (hybridization and dehybridization by strand-displacement reactions).

When DNA is used in combination with other molecules (natural or artificial), it is still possible to use the rigid-flexible strategy to fabricate structures with movable parts. In this context, embedding functional molecules is another strategy to achieve dynamic DNA structures. For instance, the folding of a sheet made of DNA origami was driven by (hydrophobic) lipid molecules (cholesterol) decorated on the sheet surface [37]. Incorporation of methylated nucleobases in a DNA nanomotor was used to achieve rotation; B-Z (B and Z structural forms of DNA) transition of methylated bases occurred upon Mg^{2+} concentration change in the environment [38]. Another example is the repeatable assembly/disassembly of hollow DNA capsules made of homogeneous flexible DNA motifs. Motifs connect each other through sticky-ends, where special chemical modifications allow disassembly of the connections upon irradiating light signals [39].

Other more recent example is the random shape-transformations in a soft vesicle [40], where the flexible element is the vesicle and the rigid elements are microtubules interacting with the inner surface of the vesicle. ON-OFF switching is possible by light-inducing DNA reactions that decom-

pose the microtubules/vesicle interactions. In the micro/macro-scale, there are also other attempts to make dynamic DNA structures. One is the shrinking/swelling of DNA-integrated hydrogels, where the rigid and flexible elements are polyacrylamide matrices and cross-linking DNA molecules, respectively [41]. Autonomous methods are also interesting because they do not rely on external interventions. These include DNAzymes and other enzymes that allow a different operations, but usually they need careful consideration of environment parameters such as temperature and ion concentrations [42].

Table 1.1: List of common methods for dynamic DNA structures. For complete review of other methods, the reader is referred to the main text.

METHOD	INTERACTION Applied	STRUCTURE Fabricated	FUNCTION Achieved
0.1	Aptamer (molecular recognition)	DNA origami	Dehybridization (open molecular robot)
0.2	Strand displacement (DNA base-pairing)	DNA tweezers	Dehybridization (open/closed tweezers)
0.3	pH (molecular recognition)	DNA origami	Intramolecular rotation
0.4	Photo-responsive base (light irradiation)	DNA tiles	Dehybridization (reversible)
0.5	Magnetic (plasmonics)	DNA hairpin	Repeatable hybridization/dehybridization
0.6	DNA strand (hairpin)	DNA-integrated hydrogel	Swelling upon hybridization

Applying electric and magnetic fields are other interesting ways to drive dynamic DNA structures. In this category, methods range from harnessing electrically-driven diffusion for molecular computation [43], orientating rotational nanomotors by electric fields [44], controlling the reconfiguration of DNA hairpins by applying magnetic fields [45], and magnetic-driven separation of DNA molecules for artificial self-replication [46]. It is also interesting the employing artificial photo-responsive bases to control hybridization because it is advantageous in two ways [47,48]. First, it does not contaminate the solution environment, and, second, ultra-fast responsiveness was achieved by a self-containing nanostructure [48,49]. In Table 1.1, I show a partial list of the previous exposed examples as a guide.

1.4 Purpose of This Thesis

The main question of this thesis is: "How to apply physico-chemical interactions for novel dynamic DNA structures?". To answer this question, the used method should consider two intrinsically related parameters: the applied interactions, which drives the dynamics, and the structure, where the interaction is applied. These parameters are implemented in molecules. I will give better answer of this question showing four methods in the following chapters. As a brief description of the four methods, I present the following Table 1.2, which shows the physico-chemical interaction, structure and function

of each method.

Table 1.2: Novel methods presented in this thesis. It can be read as "physico-chemical interaction X is applied on structures fabricated with Y to achieve function Z"

METHOD	INTERACTION Applied	STRUCTURE Fabricated	FUNCTION Achieved
1	Mechanical force (molecular)	DNA origami	Self-assembly
2.1	Hydrophobicity	DNA tiles	Separation
2.2	Mechanical force (macro-scale)	DNA origami	Self-assembly
3	UV light	DNA hydrogel	Gel-sol transition
4	Electric	DNA-integrated hydrogel	Decomposition

2

Harnessing Intramolecular Interactions for Self-Assembling Nano-Rings

Contents

2.1 Introduction

Self-assembly is a process where component structures spontaneously join together to form larger structures. The shape of the components is important independently of the scale. In case of microscopic particles, shape is defined in terms of its surface geometry and interaction field around the surface [50,51]. Basically, this interaction field is both the interplay between attractive and repulsive forces. Once the larger structure is assembled, the connection or bonding between components becomes more evident.

The shape of the self-assembly component is static, which were extensively investigated [52–56]. However, macro/micro/nano shapes with dynamic properties have also been used [57–62]. These shapes inspired simulations of the assembly and reconfiguration of ensembles of nanostructures/particles [63–67]. Although these simulations predict notable properties for optics and drug delivery applications, realization of molecular structures with variable shapes is required.

A direct approach to dynamic shapes is engineering structures with movable parts [57,62]. In the macroscale, for example, mechatronic modules had movable parts which allowed defined shape transitions, and therefore diverse configurations were achieved for the target self-assembled structure. However, such controllability is difficult to be achieved at the molecular

scale [68]. Towards solving this challenge, a direct approach is taken by designing building blocks whose moving parts are controlled by intramolecular interactions.

To this purpose, a building block with moving parts is engineered using the DNA origami technique. DNA origami is suitable because it allows to harness the mechanical properties of DNA, as shown by the fabrication of complaint nanostructures [30]. In this chapter, the block with moving parts is referred also as shape-variable building block.

2.2 Novelty

The concept of self-assembling molecular building blocks that can change their shape is new. This concept would offer routes to metamaterials and reconfigurable systems. However, molecular design and implementation is required. In this chapter, I show the shape-variable building blocks made of DNA to answer such requirement. Basically, self-assembling blocks undergo shape transitions along geometrical ranges. This property allows the blocks to assemble into polymorphic nano-rings ranging from 3-mers to 6-mers. In following section, the concept, design, and experimentation of shape-variable building blocks are shown.

2.3 Purpose

The purpose of this research is three-fold. First, to create 2D clusters of DNA nanostructures with weak interaction. Second, to control cluster size by changing shape of component nanostructures. Third, the shape is controlled by intramolecular interactions in the nanostructure. With these purposes, a method is designed and summarized in the following Table 2.1.

Table 2.1: Method presented in this chapter. It can be read as "physico-chemical interaction X is applied on structures fabricated with Y to achieve function Z"

METHOD	INTERACTION Applied	STRUCTURE Fabricated	FUNCTION Achieved
1	Mechanical force (molecular)	DNA origami	Self-assembly

2.4 Design

The concept of shape-variable building blocks (also called monomers) have some characteristics. Monomers are homogeneous. These monomers assembled into closed clusters which have a limited number of mers (that is, x monomers form a x-mer cluster, where $x \leq 6$). The structural characteristics of the monomers are inspired by DNA tiles with a flexible core [58]. Simple case of closed structure [58,69–71] is a nano-ring because components require

two bonding arms. The bonding arms define an angle which is restricted to limited values (Figure 2.1a). The bonding between two monomers is given by shape complementarity, in such a way that they make a *cis* configuration (Figure 2.1b). The monomer angles define the number of monomers in the ring, namely the size of the ring (Figure 2.1c).

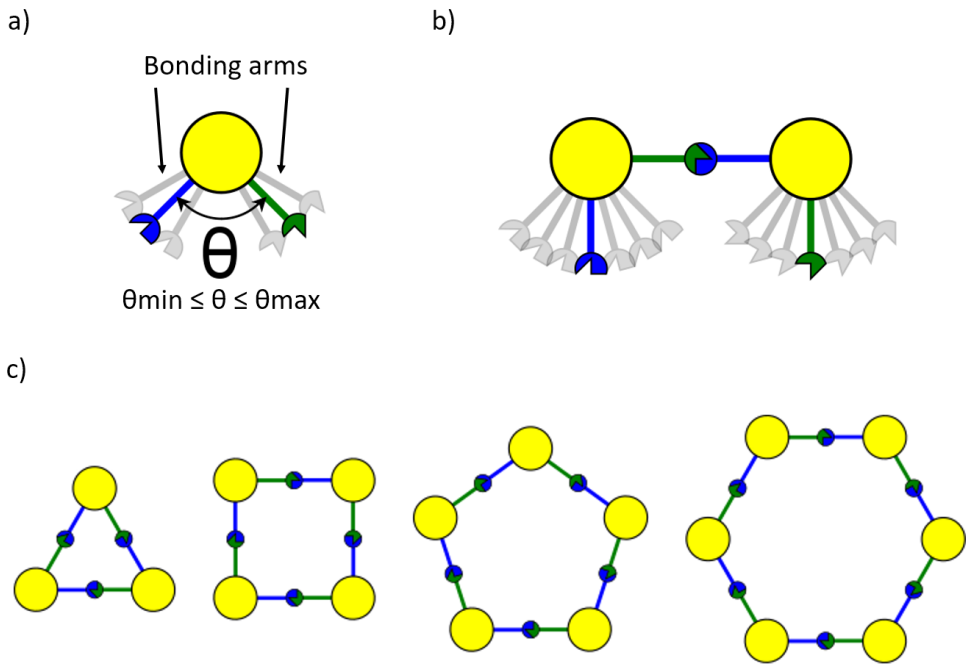

Figure 2.1: Concept of shape-variable monomers. (a) Abstract representation of the monomer with two bonding arms. (b) 2-mer bonding in *cis* configuration. (c) Assembled rings (3-mer to 6-mer).

To implement the concept, some design innovations are implemented with DNA; precisely, the monomer is a DNA origami [15]. For simplicity, the monomer is regarded as having two connected symmetrical pieces, which resemble the bonding arms explained above. Each of the two arm edges allow the geometrical complementarity through stacking interaction of DNA blunt-

ends; the strength of the stacking interaction is programmable and represented in binary code as pioneered by Woo and Rothemund [17]. The monomer has the following particular design in its center:

- Tuneable flexibility at the hinge (enclosed area in Figure 2.1a), which gives degrees-of-freedom to the monomer.

- Contacting edges (Figure 2.1a), which limit the angle between 60° and 120°

In the tuneable flexibility at the hinge, the arms are connected by a single staple strand (precisely speaking is a single phosphate and works as a hinge that allows rotation) and two unpaired DNA segments belonging to the DNA origami scaffold. These DNA segments have two functions. One function is to eliminate undesired degrees-of-freedom such as twisting between arms. The other function is to be entropic springs (spring A and spring B). An entropic spring the one that, when stretched, tend to return to higher entropy states. The length of spring A and B can be exactly adjust by regulating the scaffold, in such a way that loops are formed in the origami (Figure 2.2a, loops are shown in yellow stars); this idea was similarly used for tensegrity structures [31]. For instance, by exchanging the blue-coloured staples in Figure 2.2b, the spring B length is modified. The DNA sequences of the springs should be flexible and should not form any secondary structure. This is done

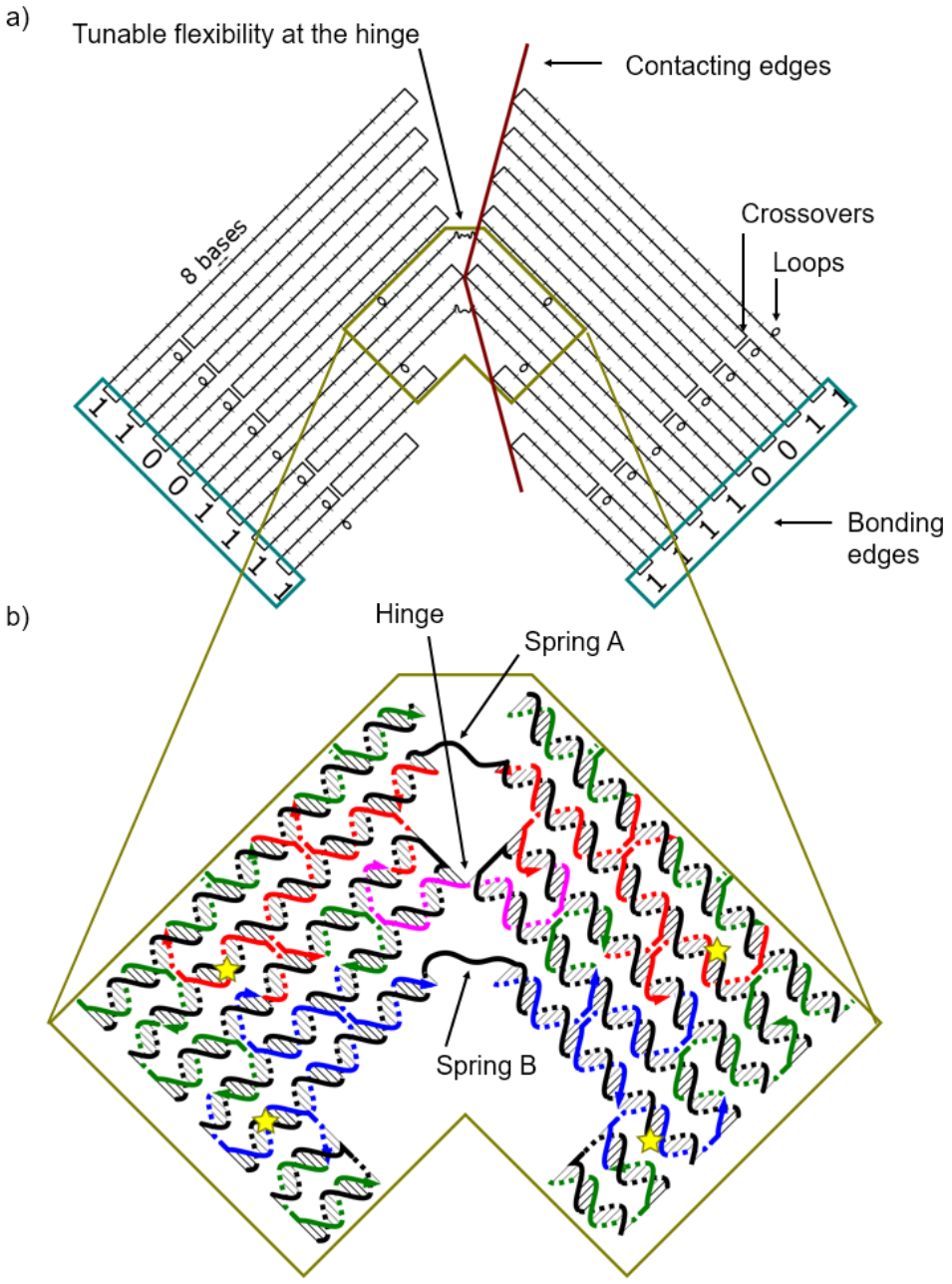

Figure 2.2: DNA origami design. (a) origami scaffold (in black), tuneable flexibility at the hinge (in mustard), contacting edges (in red) and blunt-end stacking codes (in sky-blue). (b) design detail showing staples in colour and the yellow stars indicate the scaffold loop position for tuning springs.

by carefully choosing the sequences along the DNA scaffold, in such a way that five Thymine (TTTTT) are placed in each spring center. This design is equivalent the conceptual shape-variable monomer shown in (Figure 2.3a)

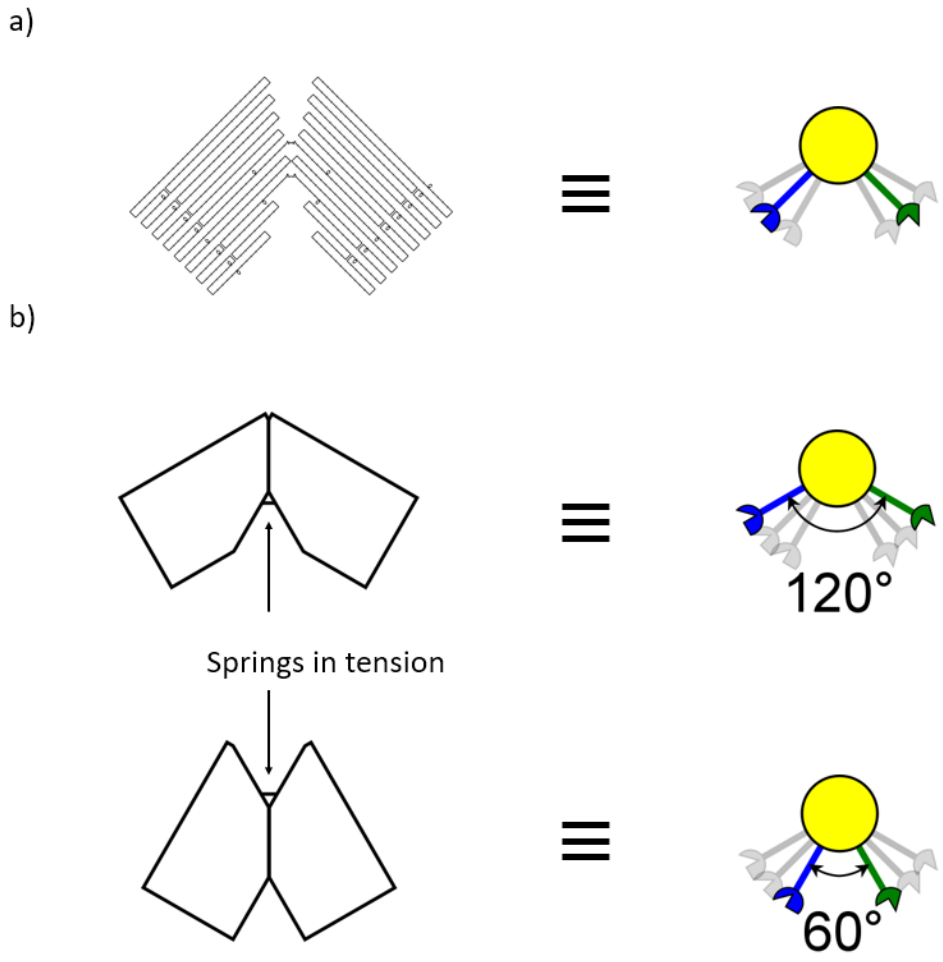

Figure 2.3: DNA origami design and shape-varibale concept. (a) DNA origami and its equivalent shape-variable monomer (b) Origami profile and its correspondent representation for the 60° and 120° configurations.

For simplicity, the notation M(a,b) is defined for the monomer having a and b nucleotides (nt) in each spring A and B, respectively. The tested values of a = 11 nt and b = 8-18 nt; these values are set depending on the

flexibility of the single stranded DNA. The sequences are:

- Spring A = ... T A T T A T T T T T C T T G T ... = a bases.
- Spring B = ... C C T G A T T T T T G A T T T ... = b bases.

Monomers are prepared following the DNA origami preparation protocol in buffer solution. Details of the CAD design (cadnano) are shown in Figure 2.4. Basically, 100 µl DNA origami is made by mixing 2 nM of the scaffold M13mp18 with 75 nM of the staple strands in 40 mM Tris, 20 mM acetic acid, 2 mM EDTA, 12.5 mM Mg acetate (this is called the 1xTAE/Mg2+ buffer solution). The final mixture is maintained at 90 °C for 5 min, then cool down to 4 °C (rate of -1 °C/min). Samples are finally stored at 4 °C. Before atomic force microscopy (AFM) observation, samples are kept at room temperature for at least 4 hours and then used.

Monomers are characterized on mica substrate under the same preparation buffer, which is practically enough to the keep the origami immobilized (Figure 2.5). The protocol consists of the following steps:

1. 2 µl sample is deposited on freshly cleaved mica (1.5 mm diameter, few times with 2 mm diameter) for different deposition times. The usual deposition time for shape-variable monomers is 10 min. The usual deposition time for fixed monomers is 25 min.

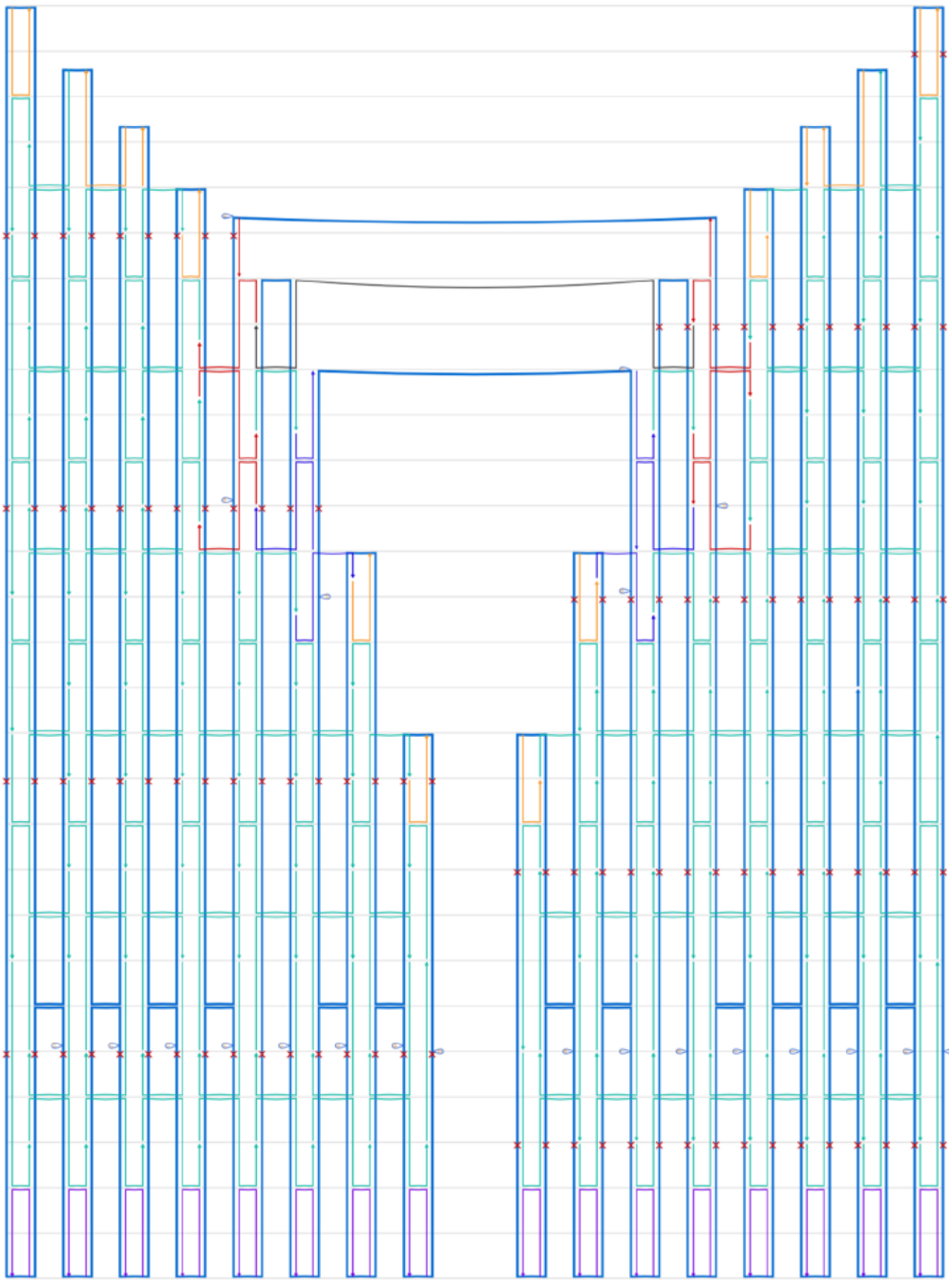

Figure 2.4: DNA origami design made with cadnano.

2. Then samples are rinsed with 10 µl of 1xTAE/Mg^{2+}, leaving a small drop on top of mica.

3. Samples are observed using AFM under 1xTAE/Mg^{2+} buffer.

2.5 Results and Discussion

This section covers the experimental results and discussions. To characterize the monomers and their assembly, atomic force microscopy (AFM; all images are obtained using the High Speed AFM Ando model, except for images with large covering area where the JKP AFM is used) is used. The sample containing the monomers and the assemblies are deposited on a substrate, in this case mica substrate. The used AFM can only be used to observed the nanostructures under solution conditions. The used buffer solution, is the same as the used for preparing the sample, that is 1xTAE/Mg^{2+} buffer solution. AFM images with large covering area show the one-pot polymorphic formation of rings out of M(11,11) with diverse size (Figure 2.6 and 2.7). Rings can be in closed state (Figure 2.8), as well as open state (I do not find closed 6-mer during AFM observations).

The cluster size distribution is defined as the total monomer number contributing to a given cluster. It is calculated by normalizing the number of x-mers, in an open or closed state, in AFM images and multiplying it

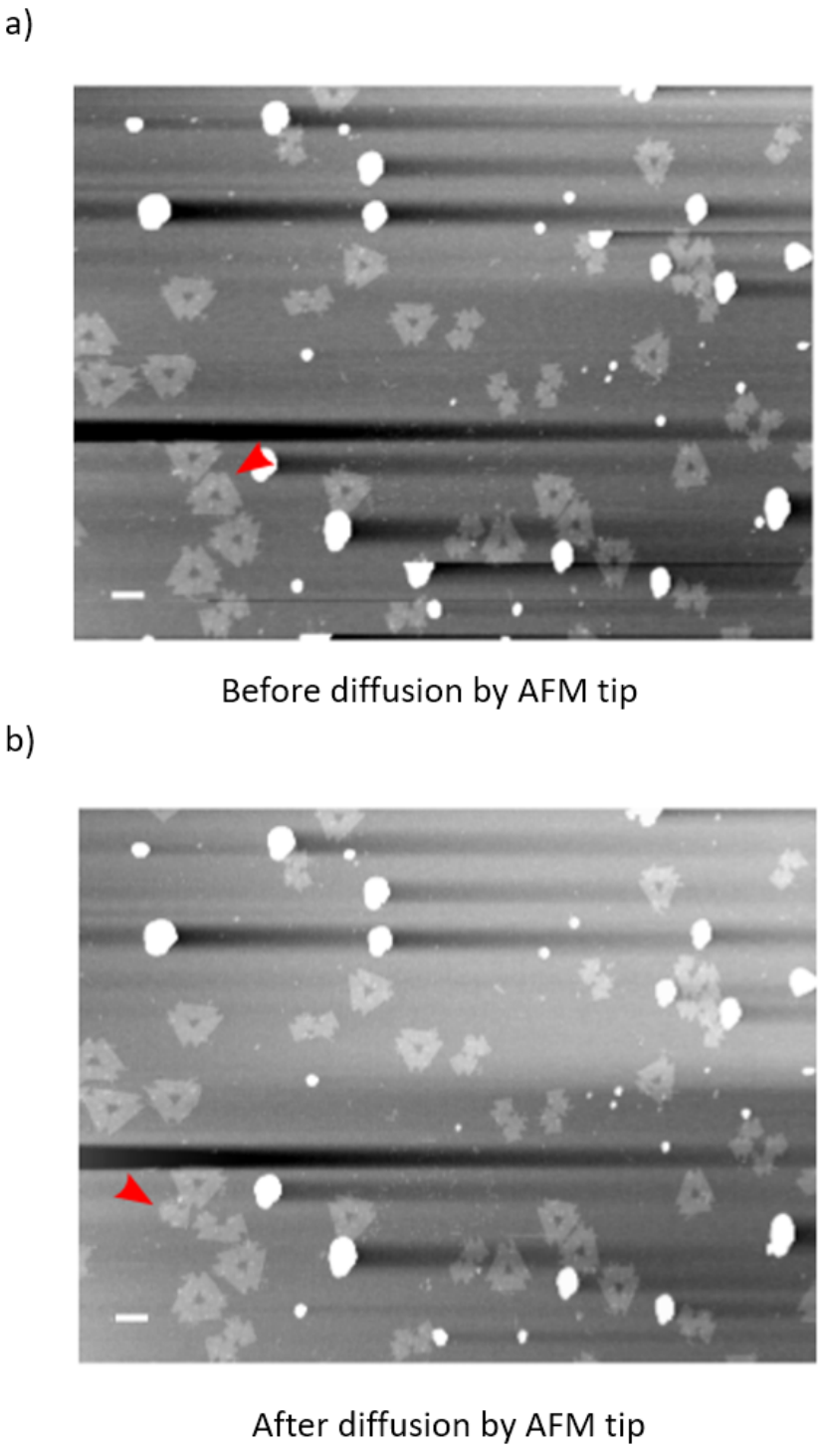

Figure 2.5: Diffusion of monomer on mica surface driven by the AFM. Two consecutive frames under the protocol for AFM observation are (a) before and (b) after. Movement of the monomer is shown in red. Subsequent frames do not show movement of the monomers. Scale bars are 100 nm.

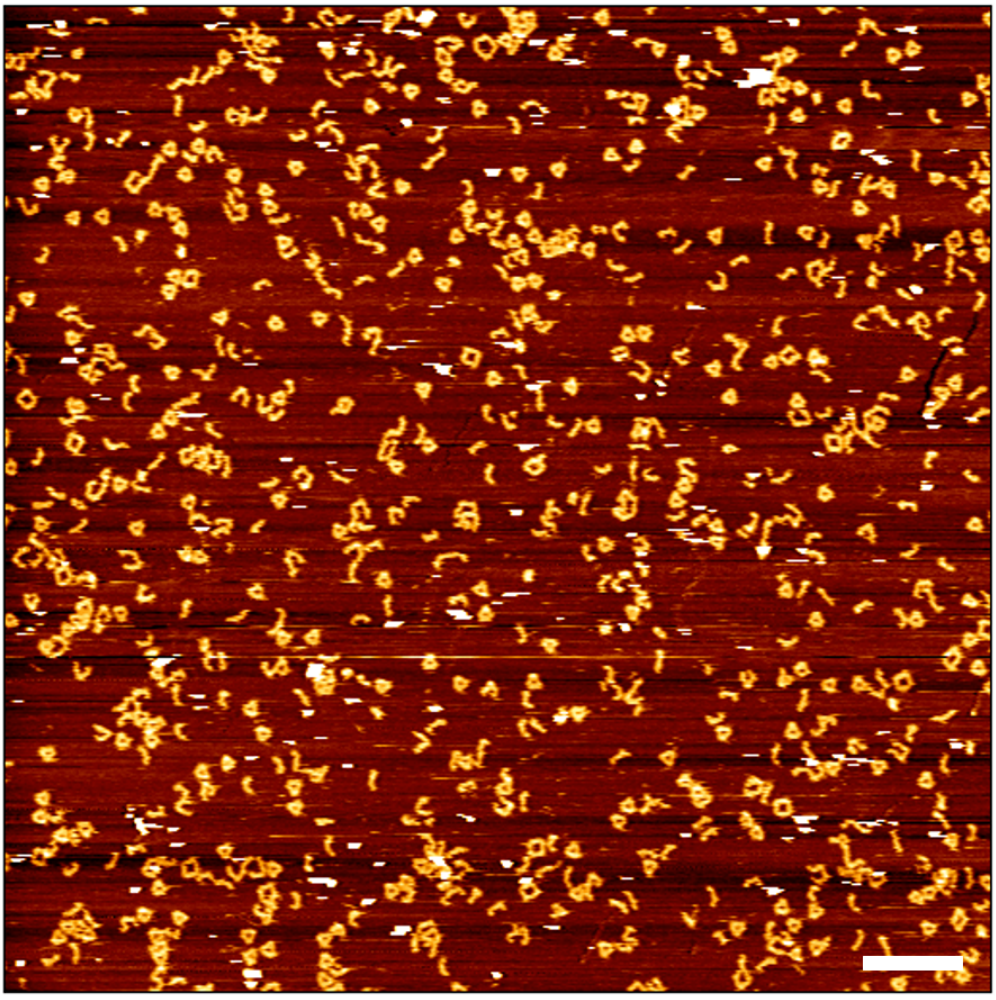

Figure 2.6: Polymorphic rings made of shape-variable monomers M(11,11) as observed by AFM. Scale bar is 1 μm.

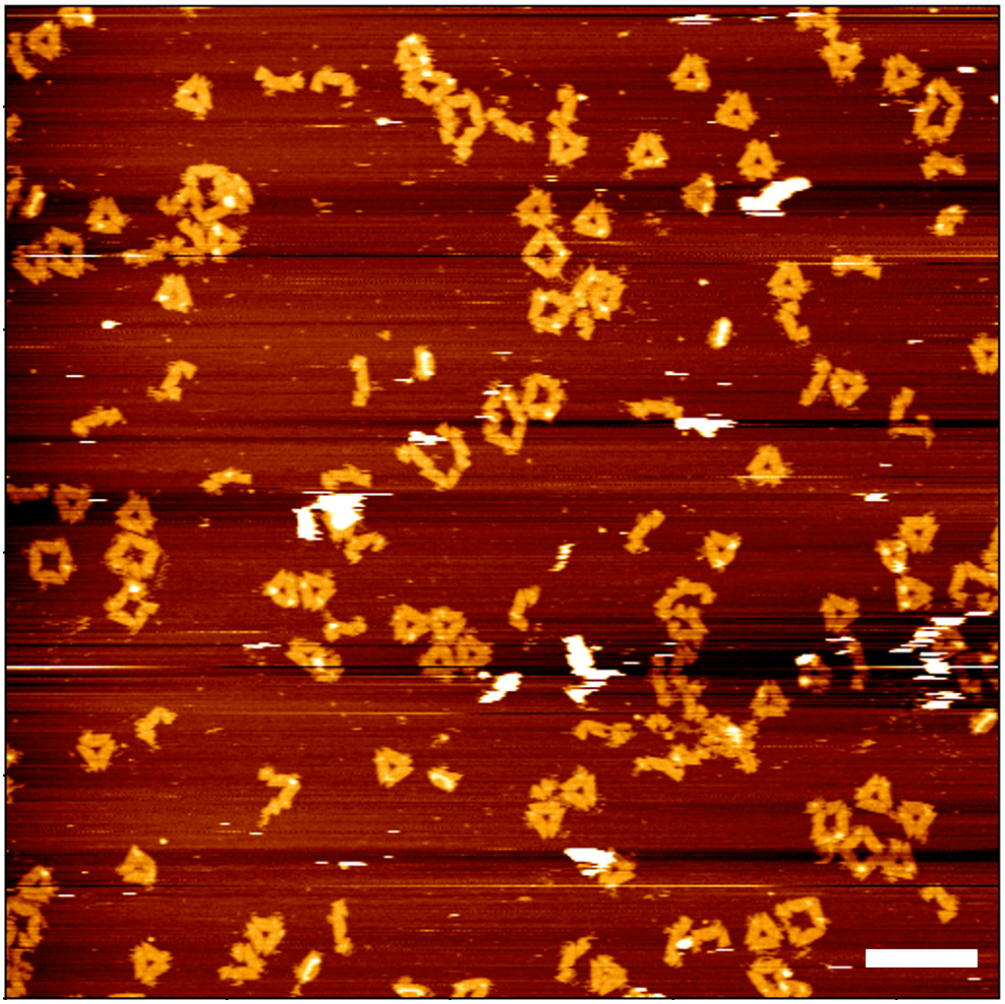

Figure 2.7: Polymorphic rings made of shape-variable monomers M(11,11) as observed by AFM. Scale bar is 500 nm.

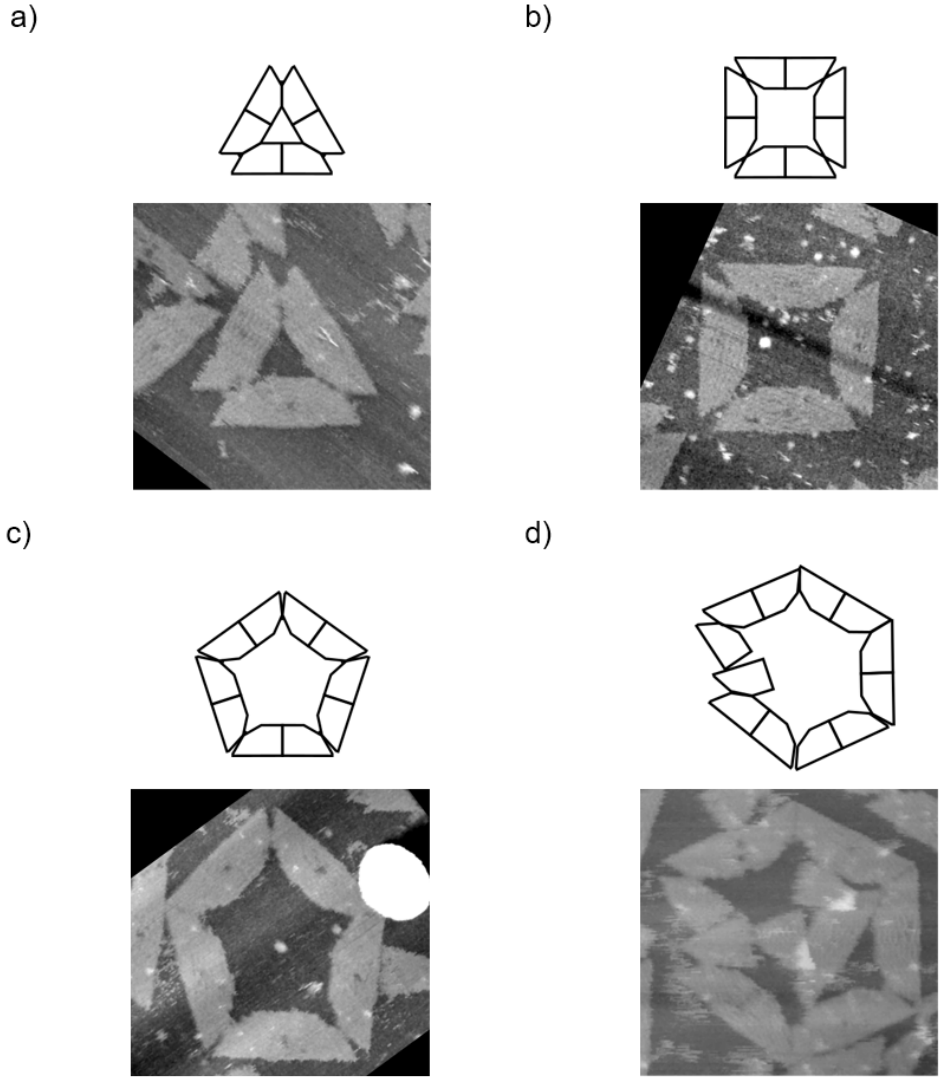

Figure 2.8: Representative rings as obtained from an AFM image such as 2.5. (a) Closed 3-mer. (b) Closed 4-mer. (c) Closed 5-mer. (d) Opened 6-mer.

to monomer number in the x-mer. 1-mers, 2-mers and 3-mers distributions change when tuning spring B to 9 nt or 18 nt (Figure 2.9).

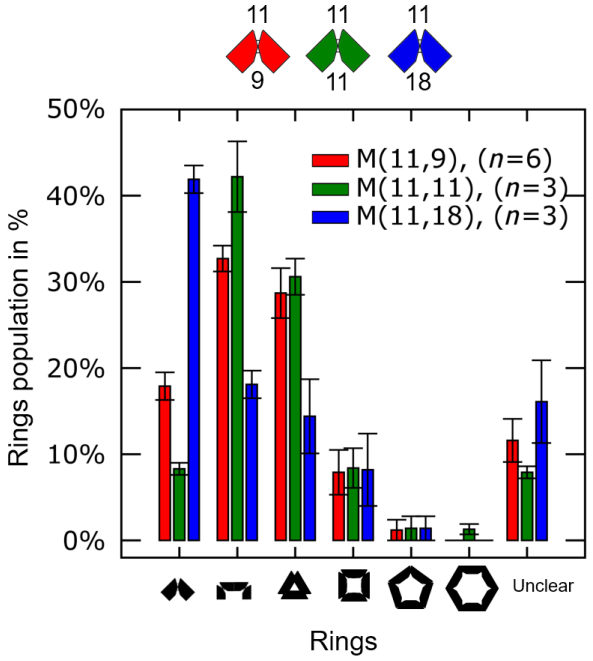

Figure 2.9: Population distribution of monomers contributing to the formation of x−mers for M(11,9), M(11,11) and M(11,18). Error bars indicate the standard error. n indicates the number of analyzed AFM images of 2040 nm x 1680 nm area.

Statistics is used to study the statistical significance for those springs; this is done by calculating the p-values. 1-mer has low distribution for 11 nt (with a $p < 0.01$) and high distribution for 18 nt ($p < 0.01$). 2-mer ($p < 0.01$) and 3-mer ($p < 0.05$) have low distribution for 18 nt. The increment in 1-mer matches the idea that a monomer is more flexible for longer spring B. That is, a more flexible monomer has less probability to connect with other monomers, which leads to less 2-mers and thus less 3-mers. This variation in 2-mers distribution with spring length also agrees with transition state theory, where

the reaction of two particles is described by their relative orientations. Here, although reaction surface area is constant (bonding edge does not change), monomers with longer spring exhibit different energy landscape compared monomers with shorter spring. Increasing spring B to 11 nt increases the closed:open ratio of 4-mers (p = 0.04) (Figure 2.10).

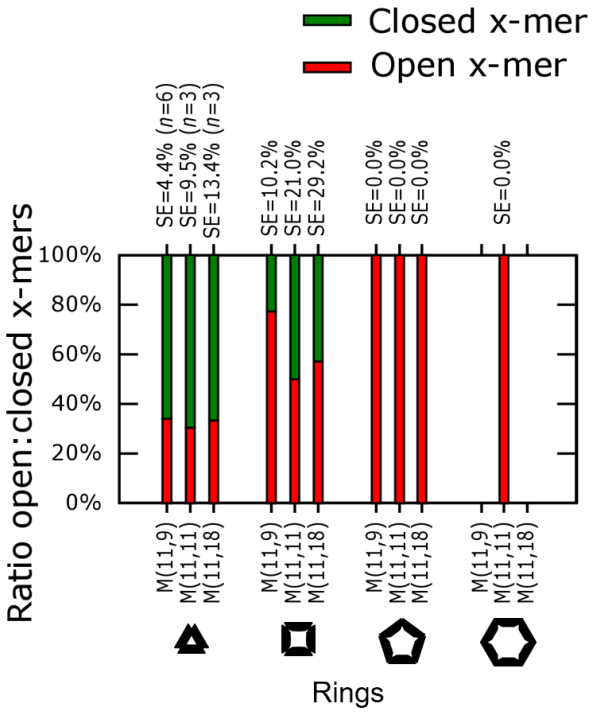

Figure 2.10: Ratio open:closed x-mers for M(11,9), M(11,11) and M(11,18). Error bars indicate the standard error. n indicates the number of analysed AFM images of 2040 nm x 1680 nm.

Some kinetic barriers for the formation of x-mers are shown by the parallel polarity (Figure 2.11a), dislocation and mismatching (Figure 2.11b) of bonds. Closed dimers are also found (Figure 2.11c) and larger clusters (x > 6; Figure 2.11d). The type of ring is identified based on those kinetic

barriers (Figure 2.2, 2.3 and 2.4). By using programmable stacking interactions [17], it is assumed that all the minor grooves make a bond with antiparallel stacking polarity. In the design this polarity ensures *cis* configurations while preventing other bonding configurations. However, it is found that bonds can be formed by mismatching. Figure 2.11a shows stacking bonds with parallel polarity found after deposition on mica. Finding parallel stacking polarity is unexpected. To the best of my knowledge, no other experiment was done to demonstrate stacking through parallel polarity. On the one hand, parallel polarity after deposition on mica may be due to the degrees-of-freedom of the monomer. On the other hand, in the stacking paper, *cis-trans* experiments are done static shapes. A triangle corner needed to fit into a 2-mer for closing the cluster, being only one stacking bond enough for that purpose.

However, two stacking bonds are required for closing cluster out of shape-variable monomers. While one bond has the correct stacking polarity, the other may be kinetically trapped in a parallel polarity due to the inherent degrees-of-freedom. In this work, *trans* configurations are regarded as an indicator of the formation of clusters through the union of two or more open clusters as shown in Figure 2.12, 2.13 and 2.14 (values in the figures indicate average number of events in a deposition area of 2240 nm x 1680 nm). Sometimes it is not clear identifying what kind of cluster is present and are counted as “unclear”.

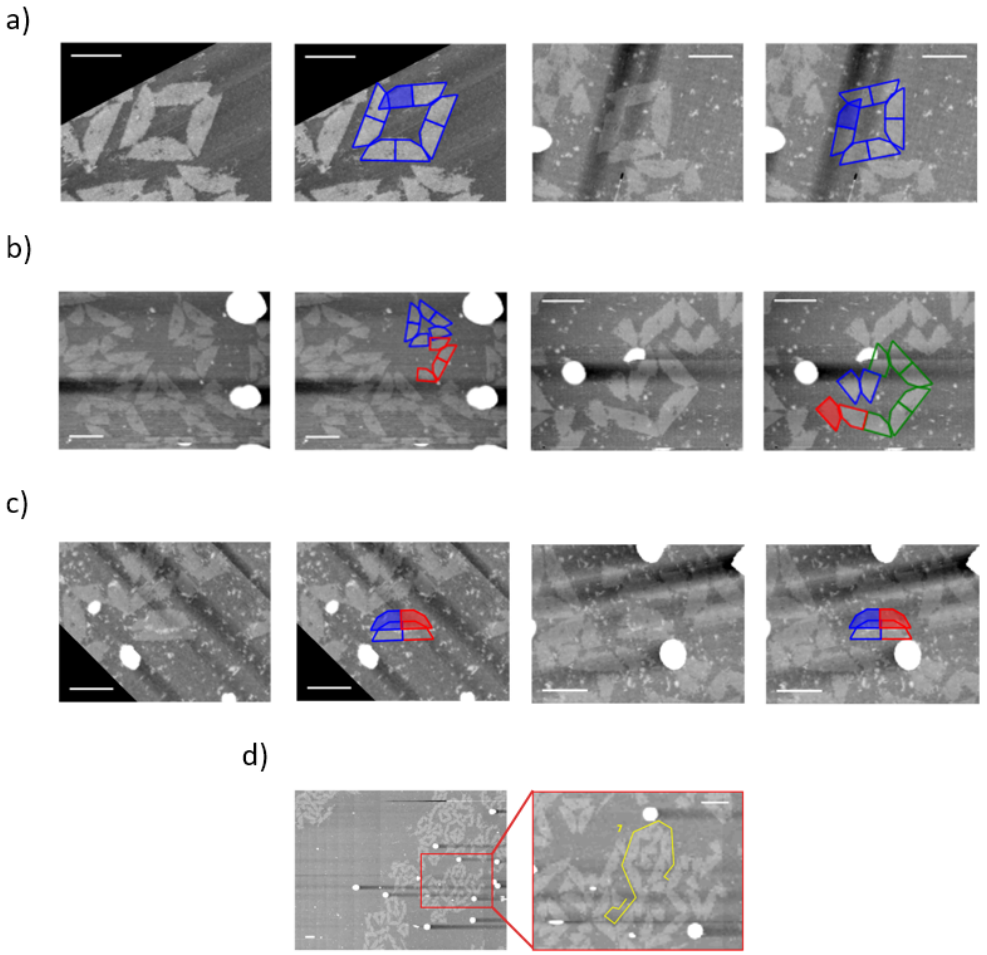

Figure 2.11: Clusters with mismatching. (a) Parallel polarity. (b) Mismatching. (c) Closed dimers. (d) Longer polymers. Scale bar is 100 nm.

Table 2.2: Average number of clusters with mismatching. Clusters are combination of X and Y small sub-clusters. * indicates samples at room temperature for up to one month. Values indicate the average number of occurrences in a AFM image with 2240 nm x 1680 nm.

X+Y	1+2	1+3	1+4	1+5	2+2	2+3	2+4	3+3	3+4	4+5
M(11,18)	1.9	0.6	0.0	0.0	0.0	0.0	0.0	0.0	0.0	0.0
M(11,11)	2.0	0.8	0.0	0.3	0.6	0.1	0.0	0.0	0.1	0.0
M(11,9)	2.6	1.3	0.1	0.0	0.5	0.4	0.1	0.2	0.0	0.1
M(11,9)*	2.3	1.2	0.0	0.0	0.0	0.0	0.0	0.0	0.0	0.0

Table 2.3: Average number of rings with mismatching. Clusters are combination of X, Y and Z small sub-clusters. * indicates samples at room temperature for up to one month. Values indicate the average number of occurrences in a AFM image with 2240 nm x 1680 nm.

X+Y+Z	1+1+1	1+1+2	1+1+3	1+2+2	1+2+3	2+2+3
M(11,18)	0.3	0.0	0.0	0.0	0.0	0.0
M(11,11)	0.0	0.4	0.0	0.1	0.1	0.0
M(11,9)	0.1	0.6	0.1	0.0	0.2	0.1
M(11,9)*	0.0	0.0	0.0	0.0	0.1	0.0

Table 2.4: Average number of rings with mismatching. Clusters are combination of X, Y and Z small sub-clusters. * indicates samples at room temperature for up to one month. Values indicate the average number of occurrences in a AFM image with 2240 nm x 1680 nm.

X+Y+Z+W	1+1+1+1	1+1+2+2
M(11,18)	0.0	0.3
M(11,11)	0.0	0.0
M(11,9)	0.3	0.2
M(11,9)*	0.0	0.0

2.6 Simulation

The dynamic formations of the rings are simulated using a chemical kinetics model. The model is an extension of a pioneering model on dynamical systems done by Hosokawa et al. [72] In the present model, the shape-variable monomer is abstractedly represented by a flexible monomer (Figure 2.12a) instead of the rigid monomers used by Hosokawa. Flexible monomers change their shape randomly between a minimum and maximum angle. Consider a flexible monomer, a second flexible monomer will have different configurations

for approaching the first flexible monomer (Figure 2.12b). The bonding probabilities of the flexible monomer are calculated based on the imposed geometrical restrictions. For example, according to the present experiments, the bonding probabilities for a shape-variable monomer with angles between 60° and 120° are shown in Table 2.5. The results of the simulation are in Figure 2.13. Since this simulation illustrates the time evolution for the formation of the rings, the simulation is compared to experiments in two different conditions: after preparation and after long time at room temperature (up to one month). The results are shown in Figure 2.14. The experimental ring formation is qualitatively represented by the present model. Full details of the simulation model are presented in Appendix A.

Table 2.5: Bonding probabilities for flexible monomer with angles 60° and 120°. X_m and X_l represent two intermediates. For example, m = l = 1 are monomer, but m = l = 2 represents dimers.

m\l	1	2	3	4	5	6
1	0.438	0.375	0.087	0.021	0	-
2		0.076	0.002	0	-	-
3			0	-	-	-
4				-	-	-
5					-	-
6						-

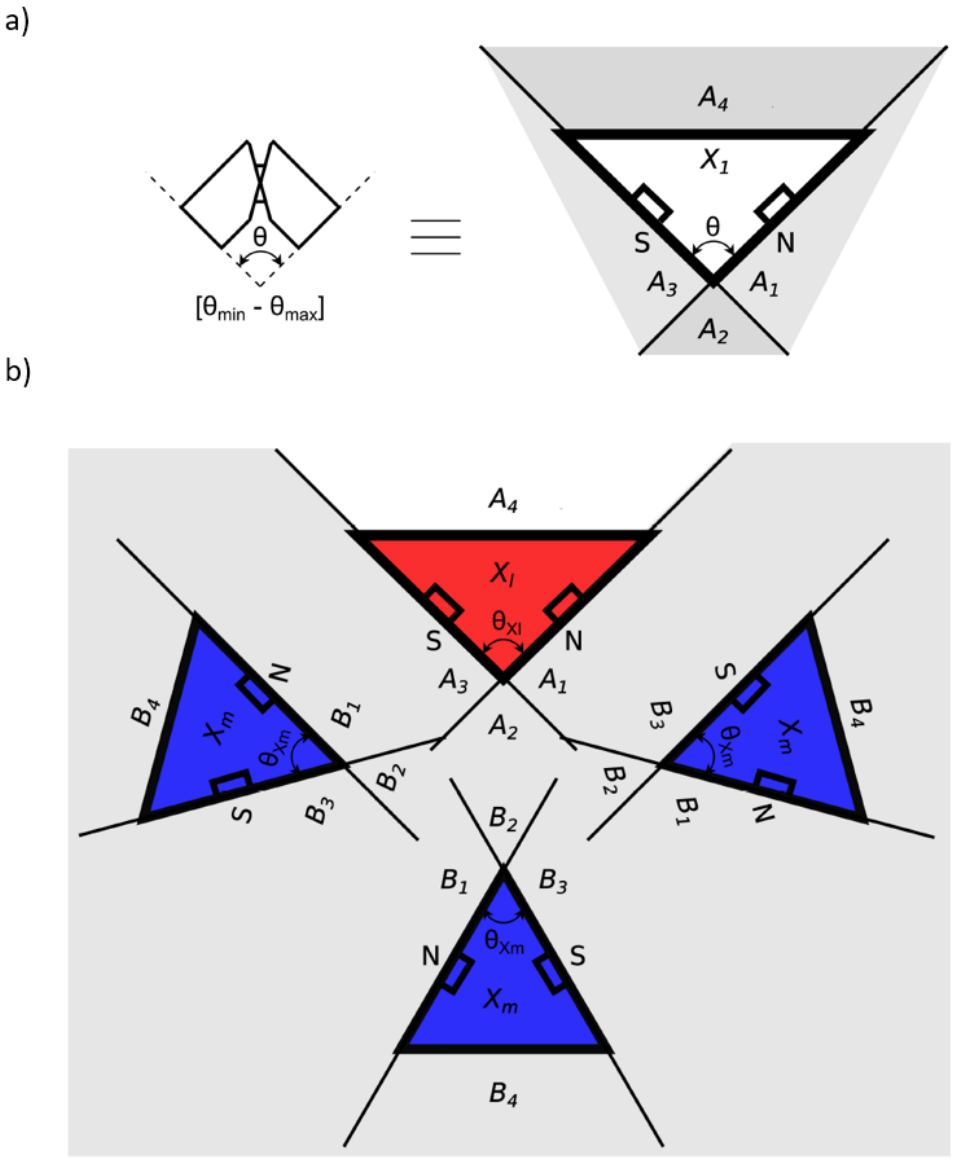

Figure 2.12: Scheme of flexible monomer used for simulation. (a) Shape variable monomer is represented by a flexible monomer. (b) Possible bonding configurations for a flexible monomer interacting with other flexible monomers.

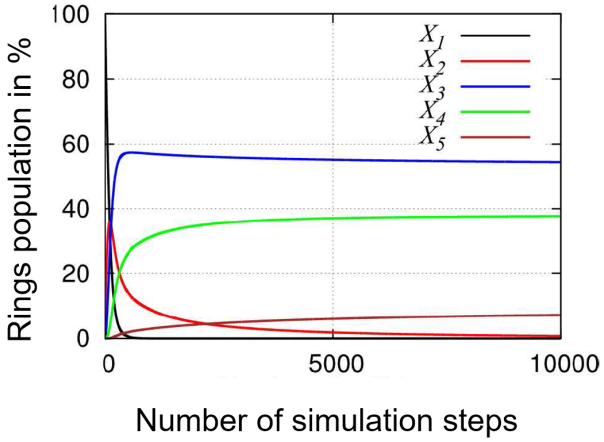

Figure 2.13: Simulation result for flexible monomer with angles 60° and 120°. X-axis is the simulations steps, not the real time.

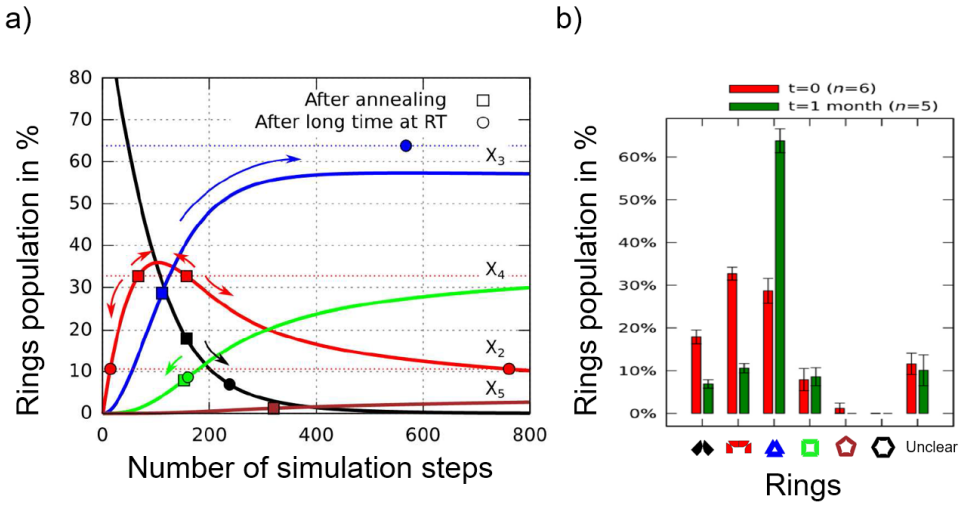

Figure 2.14: Simulation result for flexible monomer with angles 60° and 120°. Results are compared for experiment in two conditions: after preparation (temperature annealing) and after long time at room temperature (up to one month) (a) Same result as in (Figure 2.13) but for time steps up to 800. (b) Experimental distribution.

2.7 Conclusions

Table 2.6: Summary of the method proposed and demonstrated in this chapter

METHOD	INTERACTION Applied	STRUCTURE Fabricated	FUNCTION Achieved
1	Mechanical force (molecular) • Entropic springs • Hinge • Contacting edges	DNA origami • Shape-variable monomers with stacking edges • Using only DNA as building material	Self-assembly • Shape control of monomers using entropic springs • Supra molecular control of rings size by springs

In conclusion, the self-assembly of rings made of shape-variable monomers (flexible monomers) has been studied by experiments and simulation, which makes it the first-time study at the nanoscale. The diameter of the rings can range from 100 nm to 200 nm, which makes them useful as scaffold for long-term experimental investigations such microtubules running in circles [73]. The kinetic model qualitatively represented the ring formation over time. Kinetic barriers were found and large closed rings. The methodology presented is general; this means it is possible to model a monomer with geometrical restrictions (or any other restriction that can be modeled by probabilities). Therefore, it could be extended to simulate the dynamic

formation of polymers with bonds that change change directions.

This work will be referenced for the design of shape-variable monomers in 2D, and will inspire the fabrication of 3D monomers, whose degrees of freedom must be carefully addressed. In the future, the design and construction of reconfigurable rings will be aided by this concept and simulations. This chapter is summarized in Table 2.6.

3

Harnessing Hydrophobic Molecules for Molecular Motion and Force-Directed Self-Assembly

Contents

3.1 Introduction

Nanostructures made of DNA are increasingly used for realizing nanotechnology with molecular precision. This molecular precision is due to the well-defined and characterized structure of single-stranded and double-stranded DNA, which is based on the Watson–Crick base pairing [3]. From one to three-dimensional (1, 2, and 3D) structures can be fabricated by following stablished DNA nanotechnology methods such as DNA origami [15,74,75] and DNA tiles [71]. These methods enable the fabrication of wires [76,77], sensors [35,78] and semiconductors [79].

Structural characterization of DNA nanostructures with tens of nanometric resolution is done with atomic force microscopy (AFM). The core principle that enables observation is the semi-static immobilization of DNA nanostructures on a surface substrate such as mica or silicon wafer. This immobilization is mainly because DNA and the substrates are hydrophilic, and the strong ionic interaction of cations surrounding the DNA nanostructure and the substrate [80]. Particularly, the interaction of lipid-modified DNA nanostructures with hydrophobic surfaces has been recently reported [81–85]. The dynamic motion of hydrophobic nanostructures on hydrophobic substrates suggests application in dynamic positioning of molecular devices and machines [86]. Most of such hydrophobic nanostructures are created by

covalent bonding of lipids (hydrophobic molecules), particularly cholesterol molecules linked to DNA strands. Interestingly, DNA complexation with cationic lipids is an alternative method for creating hydrophobic nanostructures [87,88]. However, a stablished methodology remains challenging since simple in-solution preparation leads to complex aggregation. In this chapter, a methodology for creating hydrophobic DNA nanostructures is reported and extracting them onto hydrophobic regions. This methodology is further shown to expand the available techniques used to self-assemble large scale structures with architectural precision.

Highly architectural components based on DNA can be made for integrated nano/micro devices linking the bottom-up and top-down fabrication strategies [89,90]. The large-scale organization of DNA nanostructure units in solution is relatively straightforward, even though very large structures are restricted by inherit fluctuations and deposition on a substrate can alter the assemblies [17,71,91–96]. To solve this, the self-assembly in the presence of a substrate were reported yielding highly ordered lattices in the micrometer range by temperature annealing [71,97], and by induced-diffusion on mica[98,99] or lipid bilayer [100,101]. However, the yields strongly depends on parameters including concentration [102], temperatures [103], ionic solutions [98,99] and DNA nanostructure [103]. In those methods, nucleation of nanostructures occurs spontaneously which prevents control on the self-assembled product scale. Using Langmuir–Blodgett (LB) films to regulate a wide range of states

at the air–water interface is interesting [104–107]. it is hypothesized that LB films provide sufficient free space for promoting self-assembly of DNA nanostructure units. The LB system enables applying pressures by tuning the macroscopic area of the film (in the range 10–100 cm^2) while retaining the film thickness at the molecular level.

3.2 Novelty

In this work, a methodology for circumventing the self-aggregation of a cationic lipid in-solution and for maintaining the integrity of assembled DNA structures on 2D substrate is proposed and demonstrated. This method is used in two ways.

First, to demonstrate the motion of DNA nanostructures from hydrophilic regions to hydrophobic regions. Transfer of DNA nanostructures is achieved by complexation of the DNA nanostructures with a cationic lipid ($2C12N^+$). This extraction transfer enables structural persistence of the DNA nanostructures, which is not possible by drop-casting. Second, to integrate DNA nanostructure units into a Langmuir–Blodgett (LB) system in order to self-assemble 1D larger nanostructures by reducing the 2D confined space on the air-water interface. The 2D confined medium enables dynamic self-assembly of DNA nanostructures by tuning the macroscopic film area (this is in the range 10–100 cm^2). The LB system allows compression-expansion

cycles. This is done by making a hydrophobic DNA nanostructure that is a DNA origami sheet conjugated with cationic lipids ($2C_{18}N^{+}$).

3.3 Purpose

The purpose of this chapter is three-fold. First, to fabricate a hydrophobic DNA nanostructure. Second, generate a driven motion on substrate. Third, generate a driven motion at the air-water interface. With these purposes, two methods are designed and summarized in the following Table 3.1.

Table 3.1: Methods presented in this chapter. It can be read as "physico-chemical interaction X is applied on structures fabricated with Y to achieve function Z"

METHOD	INTERACTION Applied	STRUCTURE Fabricated	FUNCTION Achieved
2.1	Hydrophobicity	DNA tiles	Separation
2.2	Mechanical force (macro pressure)	DNA origami	Self-assembly

3.4 Design

3.4.1 Design of Hydrophobic DNA Nanostructures

In this chapter, two types of DNA nanostructures are used: a wheel-structured DNA [71] (Figure 3.1a) and a DNA origami sheet[37] (Figure 3.1b). The DNA wheel is made by tile self-assembly [71]. Since it is made out of two complementary DNA strands, it is available in larger quantities (μM) than DNA origami which is composed of a scaffold strand at nM concentrations. The wheel is also suitable for analysis of its mechanical properties. The DNA wheel is prepared as in the original paper of Hamada et al. The DNA origami sheet is prepared according to the original paper of the Simmel group.

Once the DNA nanostructures are assembled, they can be modified with the cationic lipid by following method A and B (Figure 3.2). The method A is the modification of DNA nanostructure deposited in solution (Figure 3.2a). The method B is the modification of the DNA nanostructure on a substrate (Figure 3.2b).

A typical Method A involves mixing an aqueous solution of a cationic lipid (for example, dioctadecyldimethylammonium bromide $2C_18N^+$) (50 μl, 2.1 mM; 2 mol equivalents to DNA phosphate groups) at room temperature with a solution of bare DNA wheels (500 μl, 1 μM) in 1xTAE/Mg^{2+} buffer. Just after mixture a water-insoluble white precipitate is formed. The cationic lipid

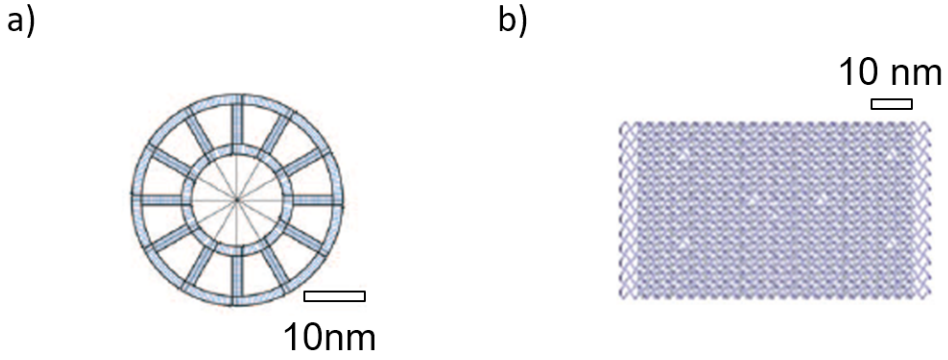

Figure 3.1: DNA nanostructures used in this chapter. (a) DNA wheel used in Hamada et al. [71] (b) DNA origami sheet used in the Simmel group. [37].

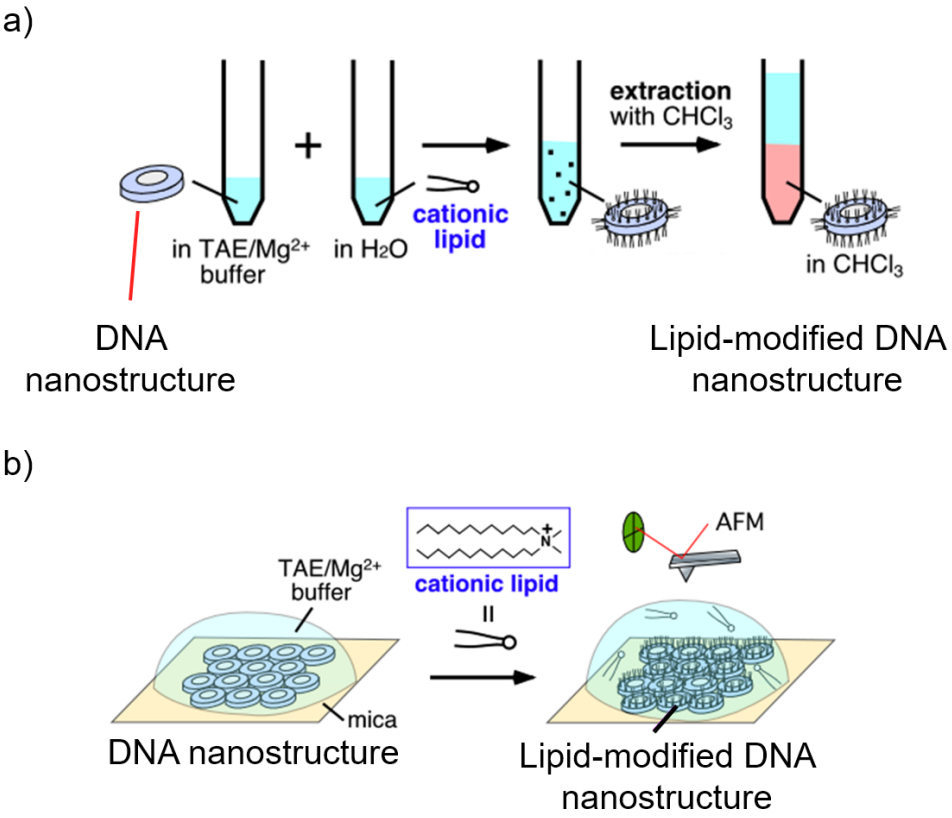

Figure 3.2: Conjugation of DNA nanostructure with cationic lipid. (a) Method A: conjugation in solution. (b) Method B: conjugation on mica.

complexation with DNA wheel is dissolved in an organic solvent (chloroform, $CHCl_3$) (500 µl) to separate modified wheels from bare wheels.

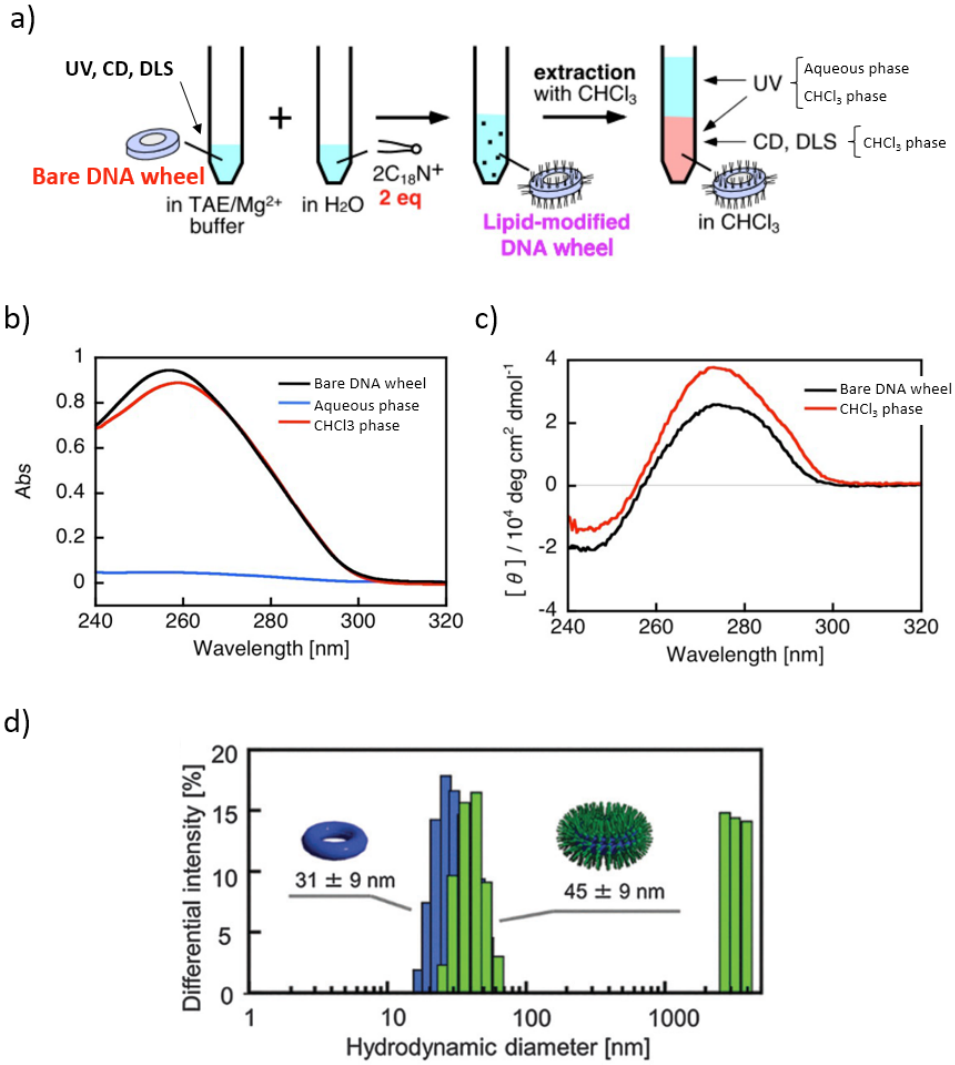

Figure 3.3: Characterization of lipid-modified DNA wheels prepared with the Method B. (a) Scheme of the preparation process and where the measurements are taken. (b) UV absorption (UV) spectroscopy of bare DNA wheel (before preparation), aqueous and $CHCl_3$ phase (after preparation). (c) circular dichroism (CV) spectroscopy of bare DNA wheel and $CHCl_3$ phase. (d) Histograms of hydrodynamic diameters of lipid-modified wheel ($2C_18N^+$) measured by DLS for bare DNA wheel in TAE/Mg^{2+} buffer (in color blue) and lipid–DNA wheel in $CHCl_3$ (in color green).

In order to characterize the properties of the lipid-modified nanostruc-

ture in solution, several properties are characterized as shown in Figure 3.3a. Optical properties are measured using circular dichroism (CD) spectroscopy (J-820, JASCO) and UV absorption (UV) (UV-3600, SHIMADZU). The dimensions of the modified wheel are measured using dynamic light scattering (DLS) (DelsaNano C, Beckman-Coulter). Structural characterization of the wheels is performed using two AFM systems: 1) High-Speed AFM system (HS-AFM) (Nano Live Vision, RIBM) with a silicon nitride cantilever (BLAC10EGS-A2, Olympus) at 50 sec/frame, and 2) AFM system (Nanoscope V, Bruker) with a cantilever for a dynamic force mode (SIDF40, Hitachi High-Tech Science) at 260 sec/frame. First system is used for fast tracking of dynamic events, while the second is used for large scale AFM observation. In the case of the LB system, the Fourier transform-infrared (FT-IR) spectra of cast films using FT-IR spectrometer (Nicolet NEXUS 670 FT-IR) is measured.

The absorbance of the $CHCl_3$ phase at 260 nm is 0.887 (Figure 3.3c, in red color) while the absorbance of the aqueous phase is significantly decreased to 0.046 (in blue color) compared with before extraction (which is 0.932; in black color). The extraction yields are calculated assuming a constant DNA molar extinction coefficient. A CD analysis is done for the modified DNA wheel in $CHCl_3$ solution compared to the bare DNA wheel (Figure 3.3d). The spectrum shows a positive Cotton effect pattern (in color red) similar to B-type of the bare DNA (in black color). The θ value of the positive Cotton effect at 260 nm increases for the modified wheel. The same trend is usual in A-type

DNA spectrum; this suggests the modified wheel may be dehydrated due to $CHCl_3$.

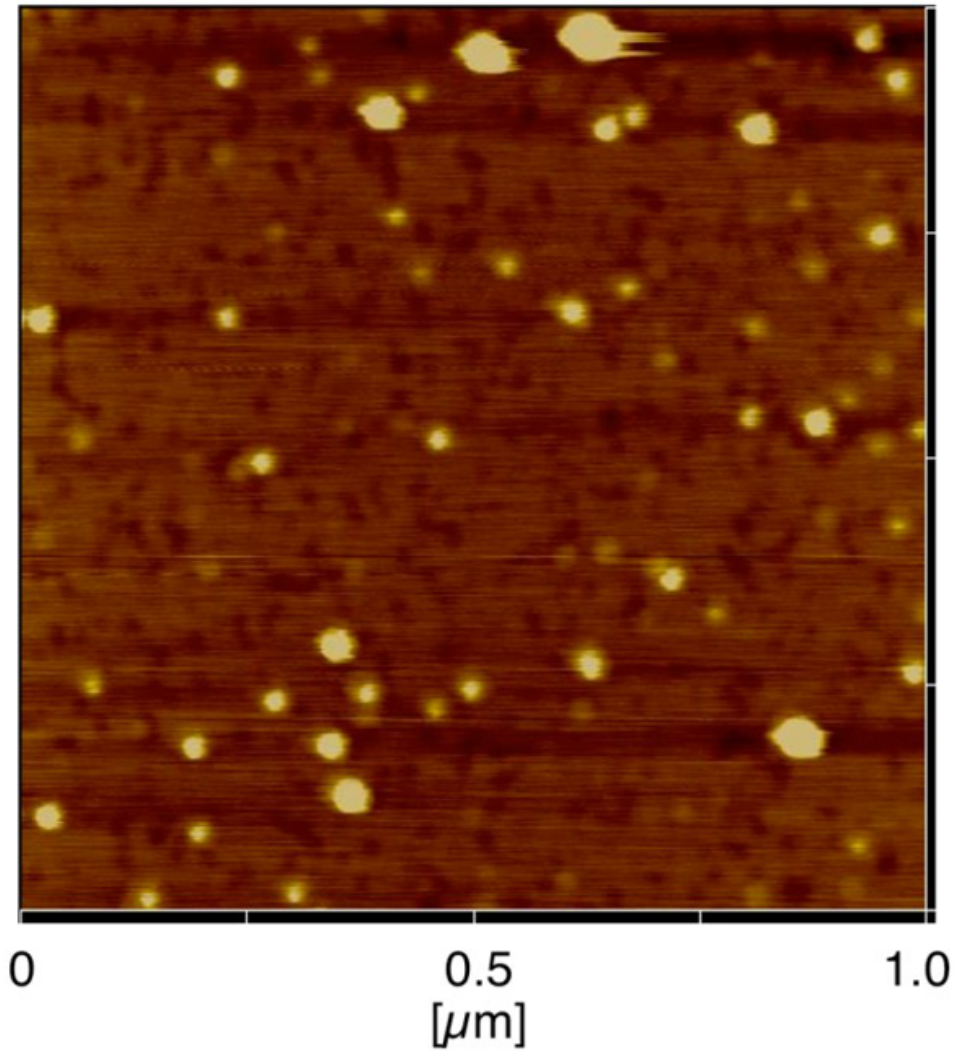

Figure 3.4: Drop casting on mica of the modified wheels as prepared in Method A.

By using DLS, the hydrodynamic diameters of bare wheels are analyzed (10 μM in TAE/Mg^{2+}), modified wheel (10 μM in $CHCl_3$) and $2C_{18}N^+$ vesicles (10 mM in water). Since the shape of the wheel is disk-like with a thickness

of 1.5 nm, the hydrodynamic diameter must be smaller than the geometrical diameter of a wheel (40 nm). Peaks at 45 ± 9 nm and larger size (>2000 nm) are observed for the Method A (Figure 3.3d, in green color). This indicates aggregates of modified wheels when comparing with peaks due to vesicles of lipid alone (174 ± 82 nm) (data not shown). In summary, the diameter of the wheels increased from 31 ± 9 nm to 45 ± 9 nm after lipid modification ($2C_{18}N+$). +). This data suggests that modified wheels can be mono-dispersed in solution (10 mM wheel). Drop casting on mica can-not simply be used for extracting modified wheels, as shown by aggregations in AFM images (Figure 3.4) [108]. To avoid aggregation, Method B is adopted, which is in-situ modification of wheels deposited on mica.

HS-AFM is used to confirm the wheel structure before and after addition of cationic lipid (didodecyldimethylammonium bromide; $2C_{12}N^+$) (Figure 3.5). Hereinafter, experiments with wheels are done using the smaller cationic lipid ($2C_{12}N^+$) to avoid dissolution of the lipid. Bare wheels have characteristic delicate framework in their interior (Figure 5a and 6a) which becomes rough when modified by the lipid (Figure 3.5a). Modified wheels have a 3.0 nm height (Figure 3.5b), which is 1.5 nm (comparable to $2C_{12}N^+$ length [109]) higher than bare wheels whose height is 1.5 nm (Figure 6c). This high increment is comparable to an interdigitated bilayer made of cationic lipid, which is plausible [110].

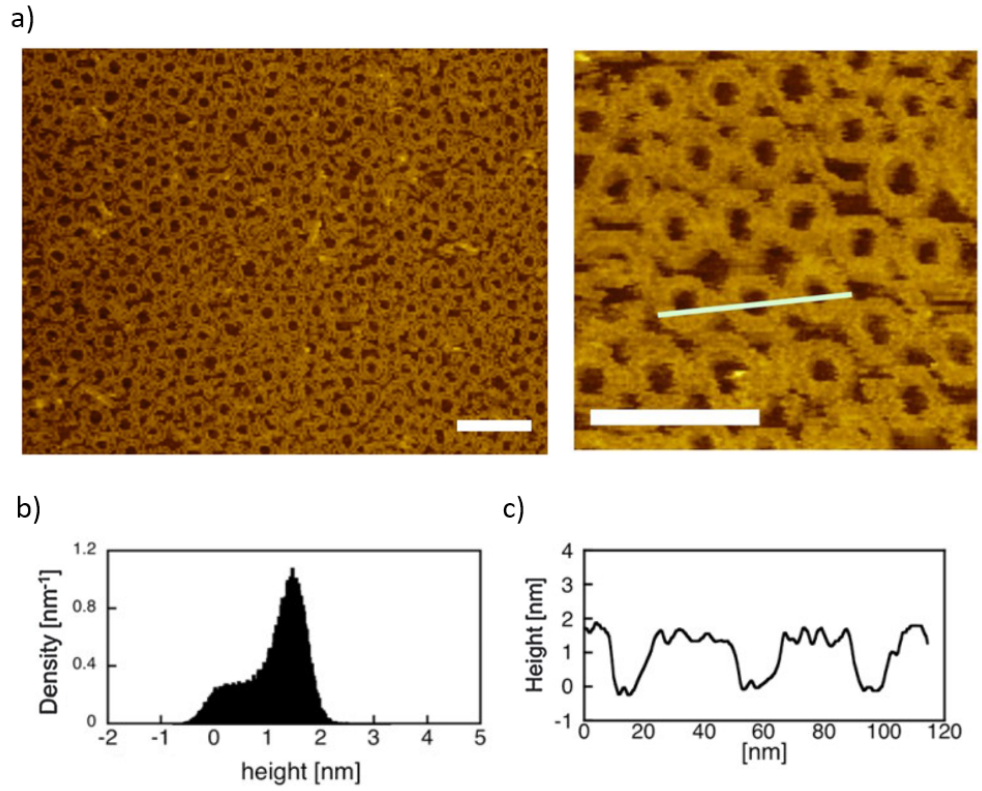

Figure 3.5: Lipid-modification of DNA wheel on mica surface. (a) Left: Representative AFM image of bare wheel and modified wheel on mica surface. Right: inset of a modified wheel (indicated by black dot lines) enclosed in a white box. Scale bars are 50 nm. (b) Height distributions of left image in a. (c) Height profile of the white line in left image in a.

3.4.2 Design of LB Films with Hydrophobic DNA Nanostructures

The design of hydrophobic DNA nanostructures is essential for integrating DNA nanotechnology and Langmuir–Blodgett (LB) systems. LB films are prepared incorporating hydrophobic DNA nanostructures. As bare DNA nanostructure, a DNA origami reported by the Simmel group is used [37]. This origami is a twist-corrected single-layered sheet and is made using same sequences and preparation as the original paper.

The shape of the sheet is rectangular with theoretical dimensions: 90

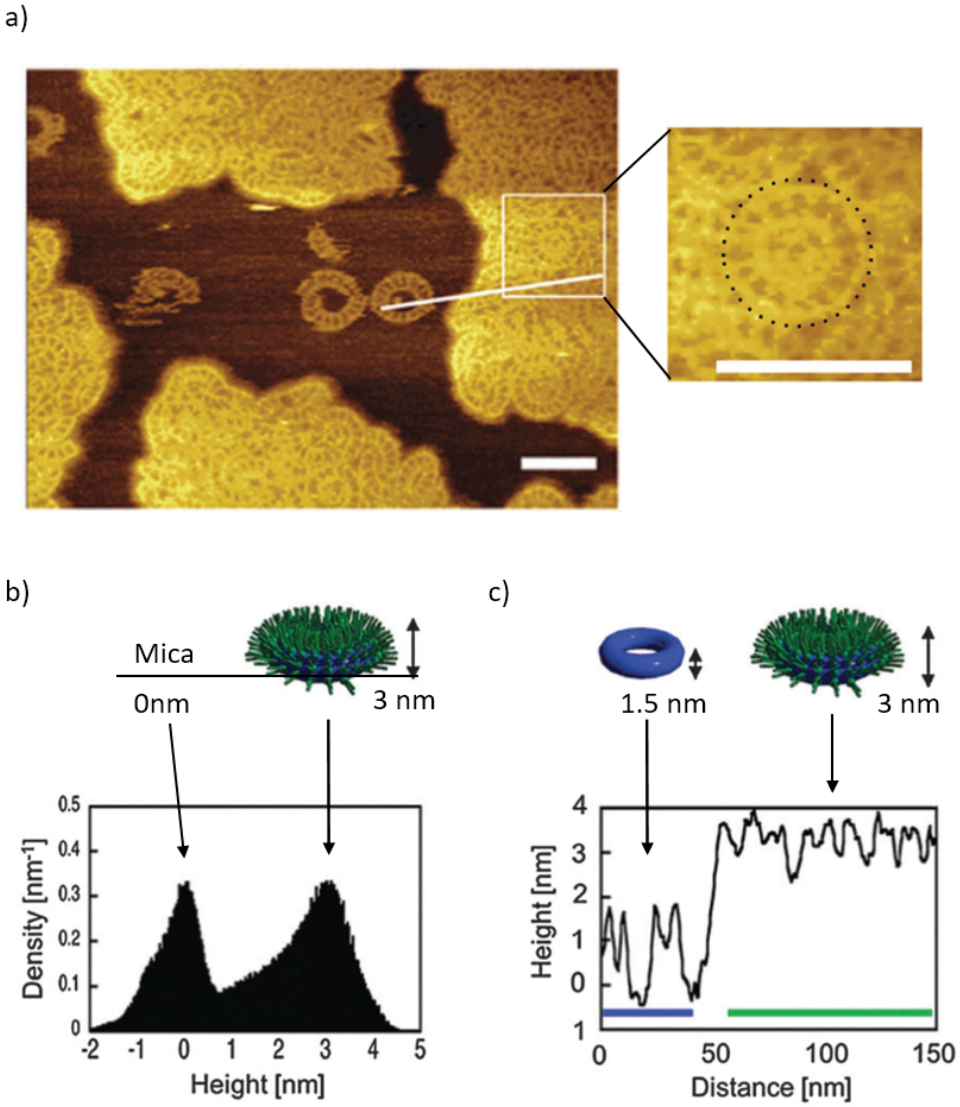

Figure 3.6: AFM image of bare DNA wheel on mica surface. (a) Left: representative image. Right: Inset of a section. (b) Density distribution of wheels of the left image in a. (c) Height distribution of the line profile of the right image in a.

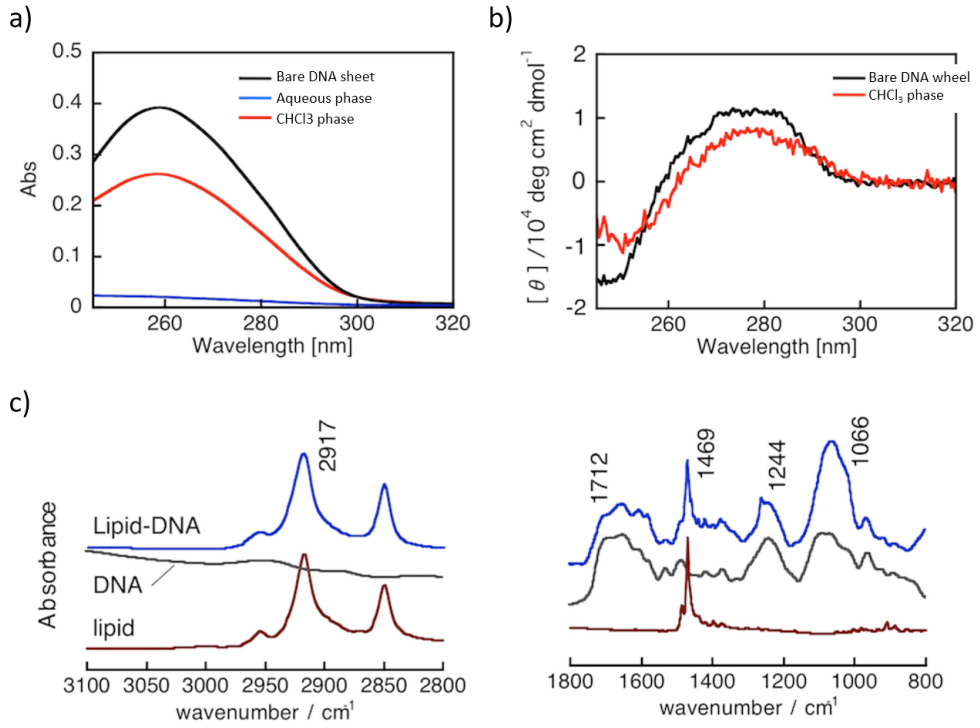

Figure 3.7: AFM image of bare DNA wheel on mica surface. (a) Left: representative image. Right: Inset of a section. (b) Density distribution of wheels of the left image in a. (c) Height distribution of the line profile of the right image in a.

nm x 65 nm. This sheet is modified with a cationic lipid (dioctadecyldimethylammonium bromide, $2C_{18}N^{+}$; 1 mol equivalent to DNA phosphate groups) by following the Method A. UV, CD and FT-IR are measured for the formed complex. UV measurement at 260 nm of the CHCl3 phase containing modified sheets has 0.263 (Figure 3.7a, in red color). The UV at 260 nm of the aqueous phase decreased to 0.021 (Figure 3.7a, in blue color), which indicates that. UV at 260nm of bare sheets is 0.392 (Figure 3.7a, in black color). By assuming a constant DNA molar extinction coefficient, the extraction yield is 67%. According to CD measurements, the modified sheets maintain DNA helicity (Figure 3.7b). Fourier transform infrared (FT-IR) measurements of the film show complex formation of lipid with DNA. FT-R confirms retention

of stacked base-pair structure (Figure 3.7c).

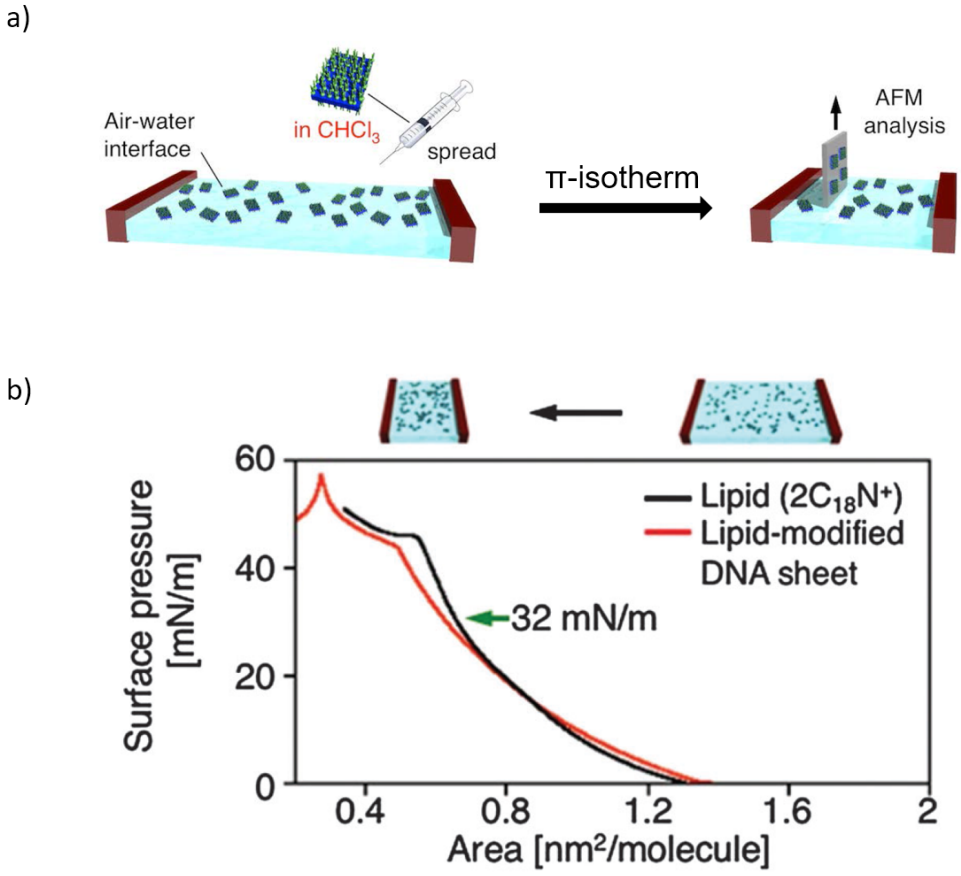

Figure 3.8: Method to create a LB film made of hydrophobic DNA nanostructures. (a) Scheme for the preparation of LB film made of lipid-modified DNA sheets. (b) (a) Surface pressure isotherms of DNA origami sheets (red) and a lipid ($2C_18N^+$; black).

After confirming the modification, a LB film is prepared with the modified sheet. DNA sheets in $CHCl_3$ are spread on the air–water interface (Figure 3.8a, left). In the interface, the space containing the DNA sheets is compressed to form a LB film (Figure 3.8). The π–A isotherm indicates the formation of a stable monolayer with a collapse pressure of ca. 43 mN m^{-1} (Figure 3.8b)). The lipid density on the DNA sheet side is theoretically 0.53

nm^2 per molecule, which agrees with the LB film collapsing. This agreement suggest that the long alkyl chains of the lipids are perpendicular towards the air phase. The compressed LB film of DNA sheets is transferred at 32 mN m^{-1} to a mica for AFM observation (scheme in Figure 3.8a, right). The structure of the modified sheet is preserved as shown by approximately 100 nm x 70 nm dimensions in AFM observation under dry conditions (Figure 3.9). This suggests that lipid modification do not cause the sheet disintegration after dissolution in CHCl3, and that the air–water interface allow the hydrophobic nanostructures to disperse homogeneously. This monolayer made of hydrophobic nanostructures is formed on pure water in which bare DNA nanostructures disintegrate [111]. After lipid-modification (Method A), the sheet increases its height from 0.8 nm to 1.2 nm (Figure 3.9) in dry condition. The sheet thickness is smaller than the single-layered DNA origami in liquid phase (1.5 nm). This may be due to dehydration.

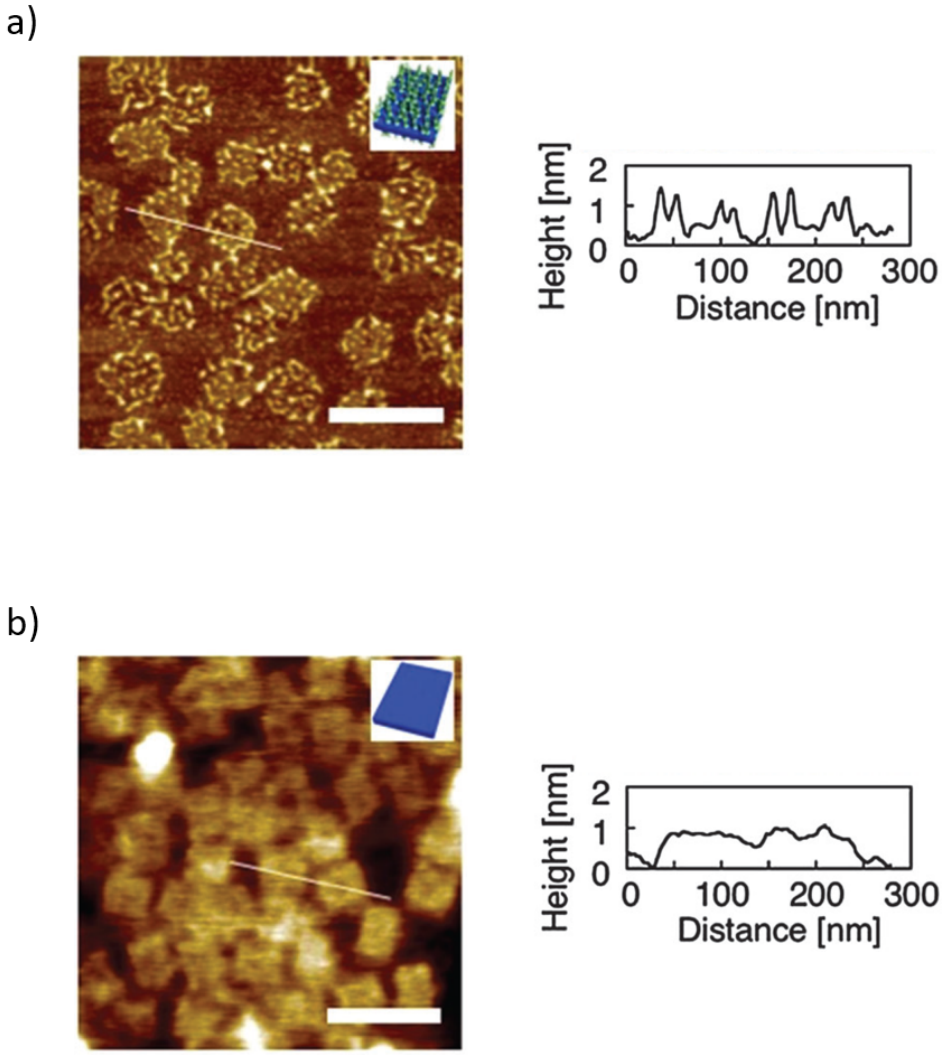

Figure 3.9: Representative AFM images. (a) modified DNA sheets (left) and line profile (right). (b) bare DNA sheets (left) and line profile (right).

3.5 Results and Discussion

In previous section, the design of the hydrophobic DNA nanostructure is shown for two purposes. First, the motion of hydrophobic nanostructures from one hydrophilic to hydrophobic regions. Second, the pressure-directed self-assembly of hydrophobic nanostructures at the water air interface.

3.5.1 Motion of Hydrophobic DNA Nanostructures

The concept of the motion is shown in the scheme in Figure 3.10. To demonstrate motion of hydrophobic DNA nanostructures, a patterned 2D substrate is fabricated [112]. The patterning procedure is shown in Figure 3.11a. The 2D substrate with hydrophobic regions is prepared by treating with an alkyl (C_{18}) silane. Untreated regions remain hydrophilic (SiOH) (Figure 3.11b).

Bare DNA wheel prefer the hydrophilic substrates (Figure 3.12a), while not depositing in hydrophobic substrates (Figure 3.12b). When using the patterned substrate, wheels deposit only in the hydrophilic region (Figure 13, left). After adding the cationic lipid on the patterned 2D substrate, DNA wheel modification starts and resulting modified wheels transfer onto hydrophobic regions (Figure 3.13, right). This motion (lipid-assisted transfer) using 2D surfaces is analogous to 3D-extraction using organic solvents. This process

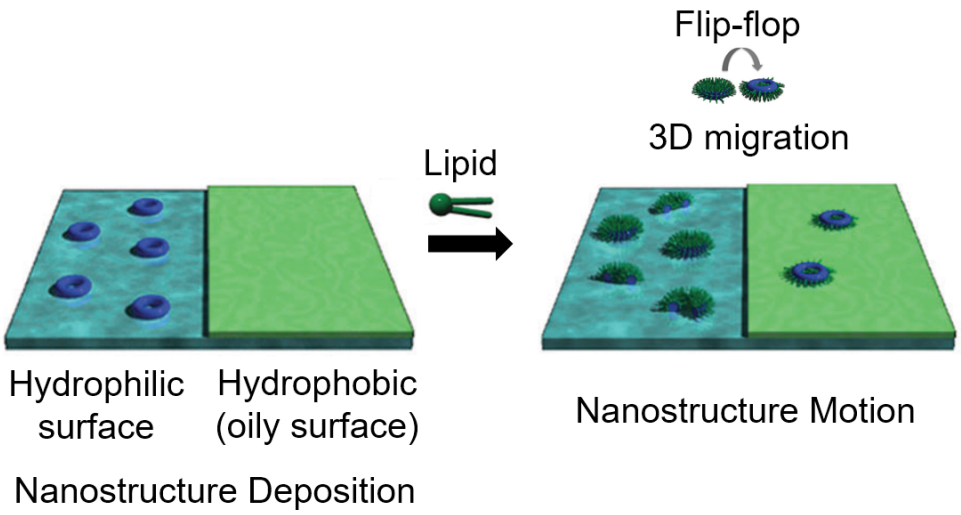

Figure 3.10: Concept for the motion of a hydrophobic nanostructure. The nanostructure is deposit on the hydrophilic region. After addition of the cationic, the lipid modifies the nanostructure making it hydrophobic. The hydrophobic nanostructure migrates onto the hydrophobic region.

resulted in up to 30% transfer of wheels, despite the strong immobilization on the hydrophilic by divalent magnesium ions [80].

During AFM observations closed wheels and wheels with opened structure are observed in the hydrophobic and hydrophilic region (Figure 3.14a). The number of closed and opened wheels are counted before and during lipid-modification. In the hydrophilic region, after lipid-modification, closed wheels reduces from 65% to 34% (Figure 14b), maybe due to stress caused by complexation by the cationic lipid. In the hydrophobic region, the ratio of closed wheels (68%) is comparable to the initial of bare wheel in hydrophilic region, indicating that the modified DNA is extracted to hydrophobic region due to complexation with the cationic lipid. This transfer process maintains pristine wheel structures, which do not aggregate, and are immobilized trough

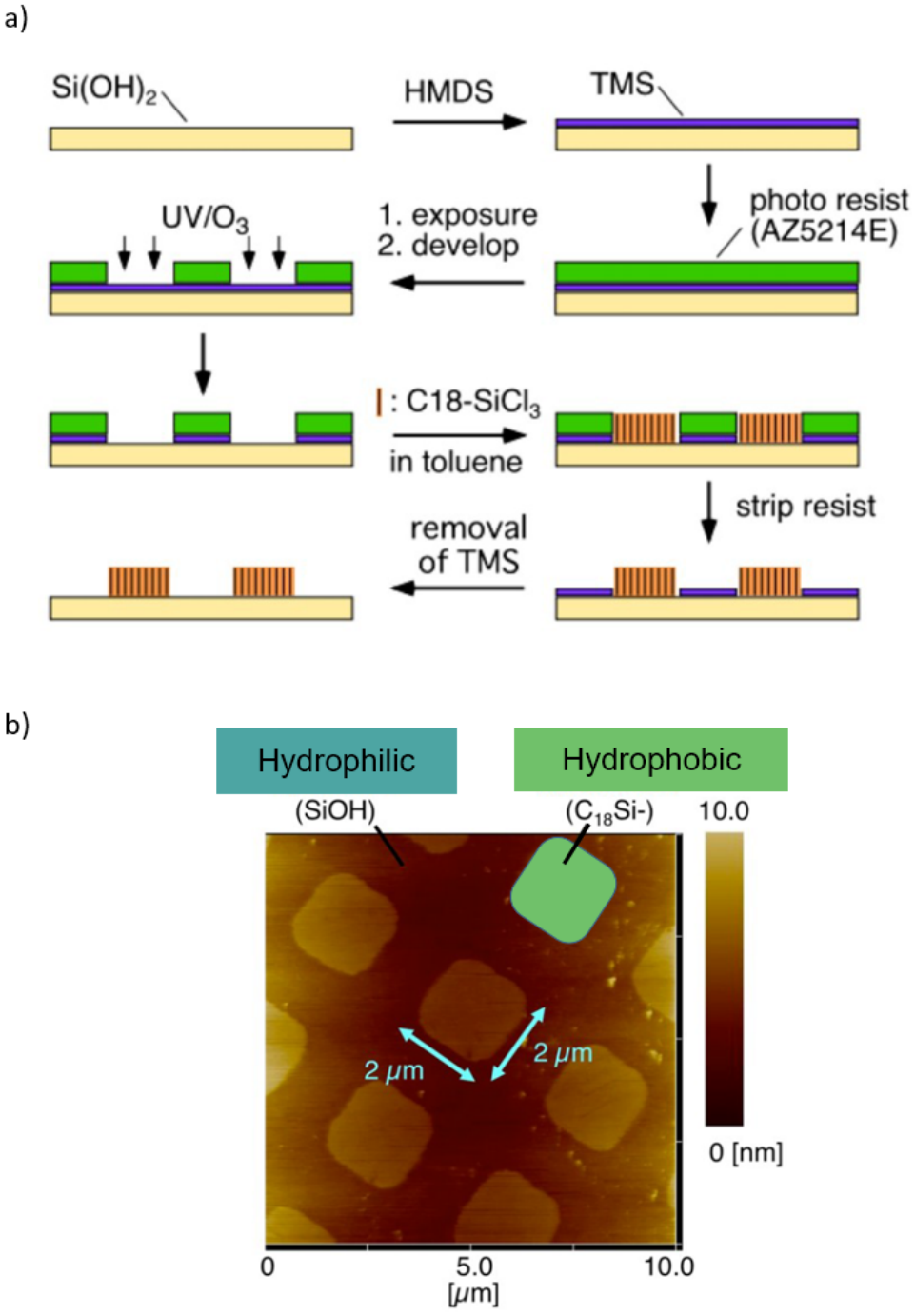

Figure 3.11: Patterning of silicon wafer. (a) Scheme of the patterning procedure for alkylsilane (C_18) on SiO_2 wafer. (b) AFM image in air phase of C_{18}-patterned SiO_2 wafer substrate (using Nanoscope V, Bruker). Frame rate: 260 sec/frame.

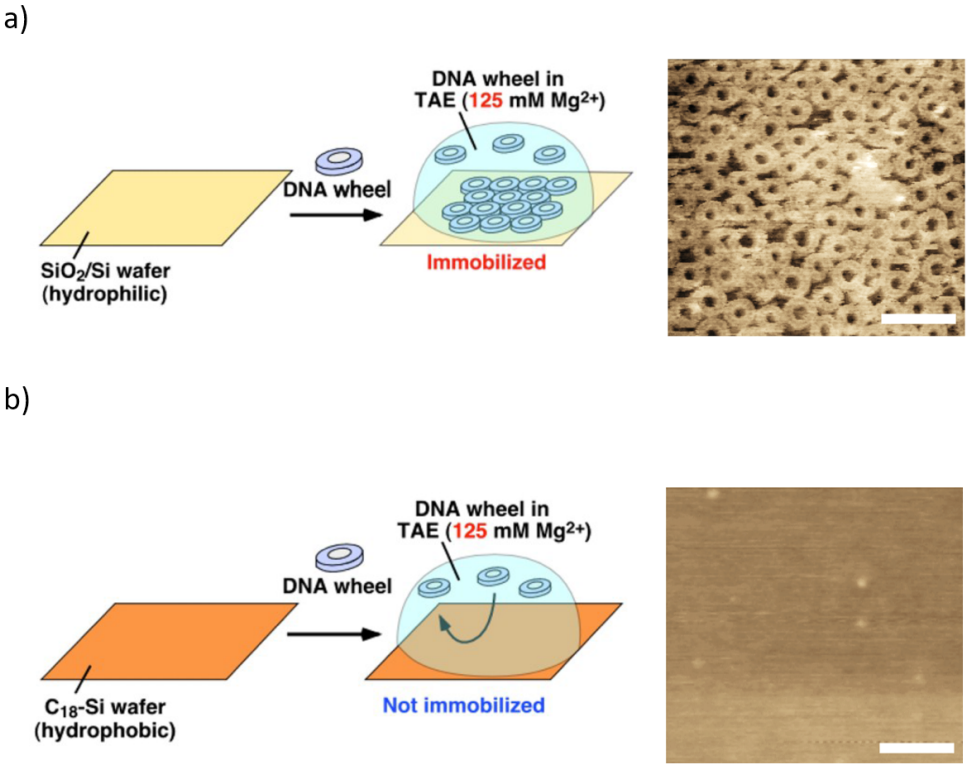

Figure 3.12: Scheme and representative images of AFM observation. (a) Deposition of bare DNA wheel on SiOH. (b) Octadecylsilyl coated substrate. Scale bars: 100 nm.

hydrophobic interactions between alkyl chains on the hydrophobic substrate.

The density distribution of DNA wheels is calculated as a function of wheel distances from the hydrophilic/hydrophobic borderline (Figure 3.15a). If a modified wheel moves to the hydrophobic regions by mere 2D diffusion, wheels density should decrease for longer distances from the borderline [113]. However, the behavior seems to be combined (Figure 3.15b). No simple distance dependency is found for the whole observation time, but the density increases suddenly after 9 min of adding lipid (Figure 3.15c). This effect indicates that wheel transfer is governed by 3D transfer through solution, involving wheels migrating to solution and later absorption onto the hydrophobic region. This

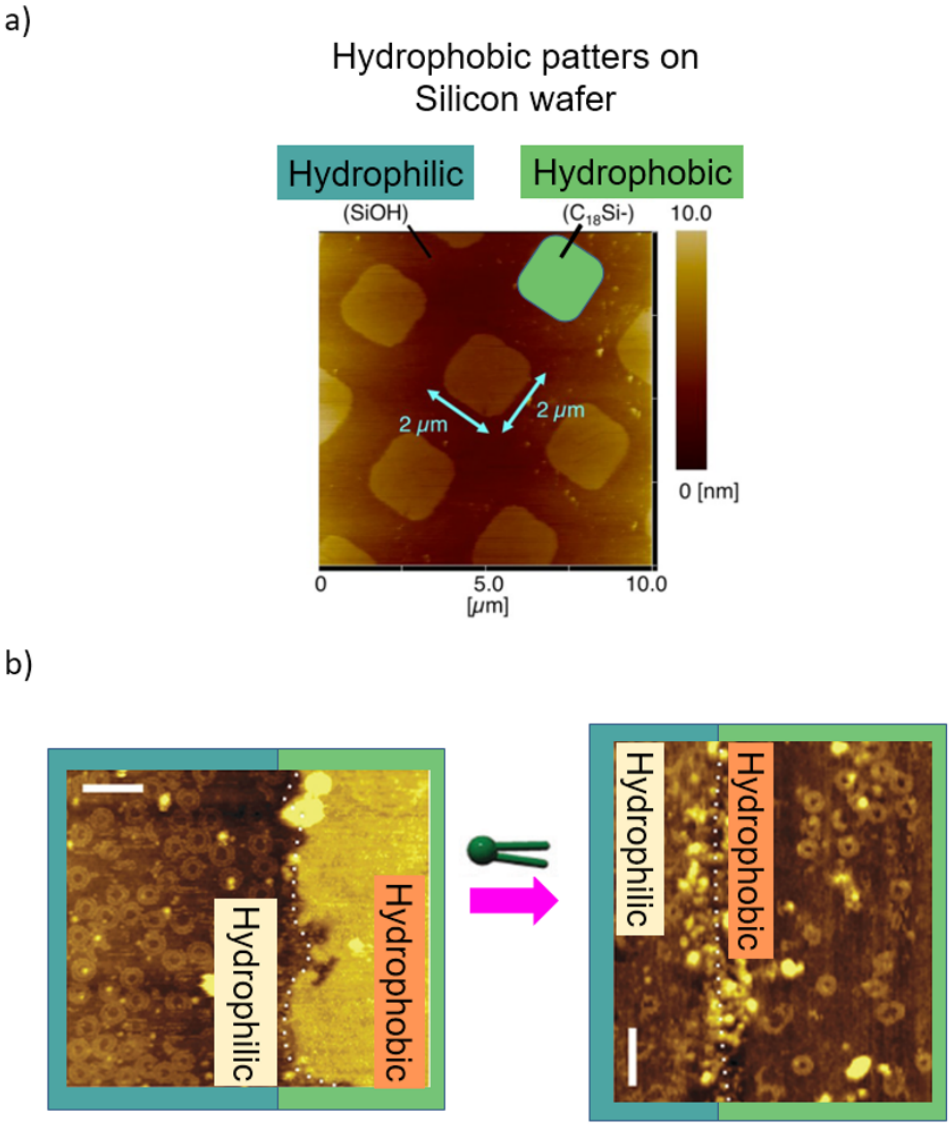

Figure 3.13: Representative AFM images of motion of a hydrophobic nanostructure. Left: before adding cationic lipid. Right: after adding cationic lipid. Hydrophobic nanostructures move onto the hydrophobic region after adding lipid. Scales bars are 100 nm.

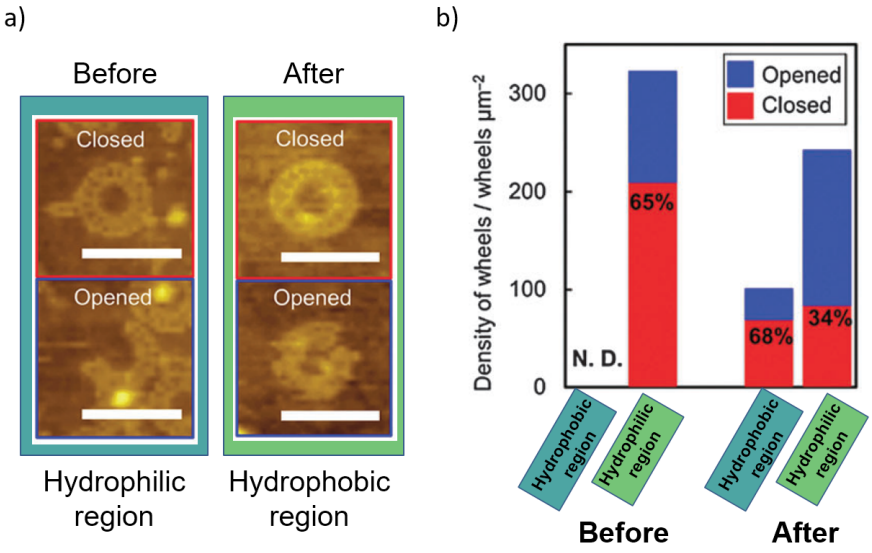

Figure 3.14: Open and closed structures of wheels. (a) Wheels before and after the addition of cationic lipid. (b) Wheels density in hydrophilic and hydrophobic regions before and after adding cationic lipid.

3D transfer is also confirmed by a suggested wheel inversion (flip–flop) on to the hydrophobic region. The flip-flop mechanism agrees with the height of modified wheels (1.5 nm) on hydrophobic region (C_{18}) (Figure 3.16b). This height is the same as the bare wheel thickness (Figure 3.16c) suggesting interdigitation of wheel lipids with C_{18} alkyl chains [114]. From Figure 3.15b, the diffusion coefficient constant (D) of the modified wheels in the hydrophobic region is D = 0.7 ± 0.9 nm^2 s^{-1}, which is 6 orders of magnitude smaller than for cholesterol-modified DNA origami [81,85]. This smaller diffusion agrees with a larger number of anchors provided by the cationic lipid.

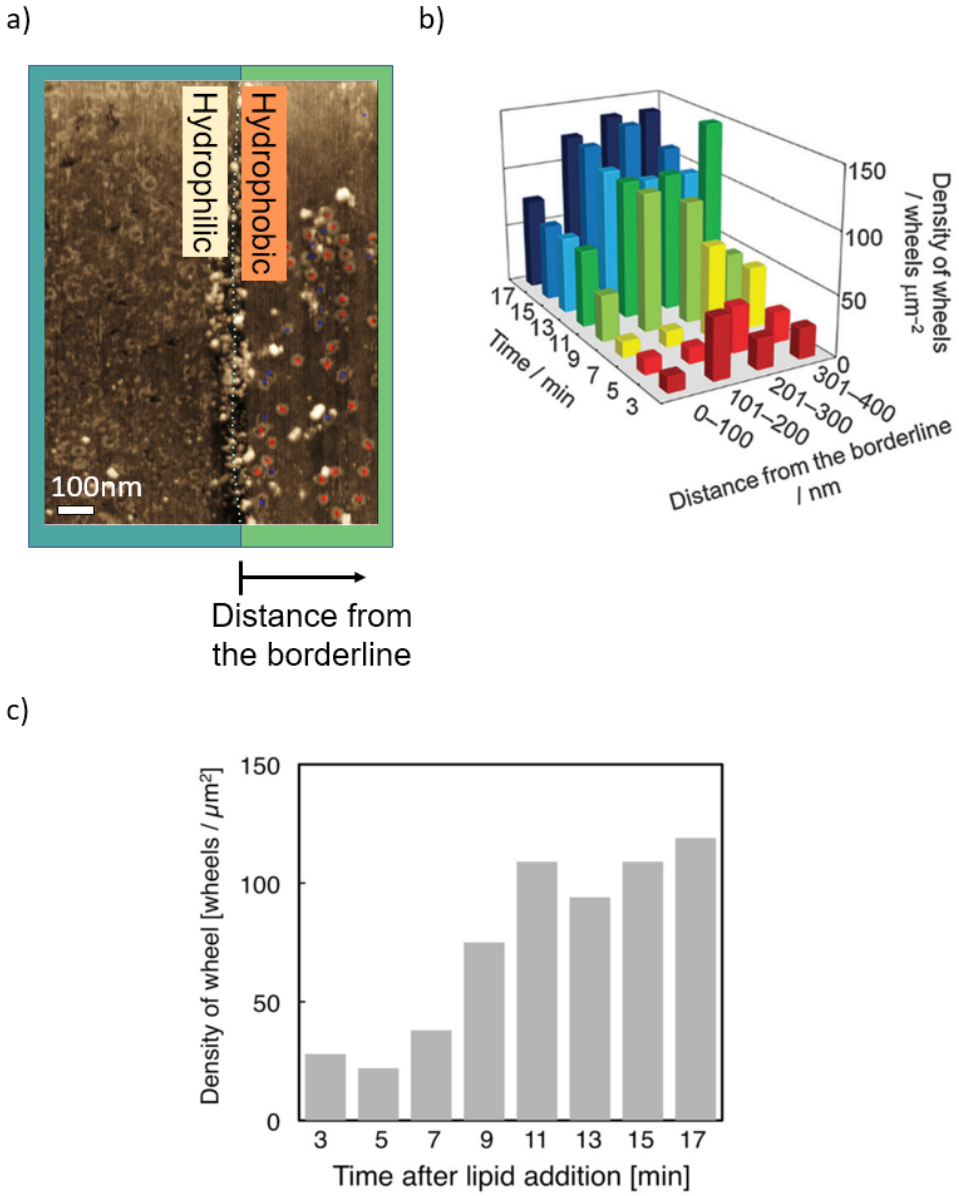

Figure 3.15: Quantification of wheels. (a) Closed and opened wheels in red and blue, respectively. Image was taken after 22 minutes of adding the cationic lipid. (b) The wheel density (wheels μm^{-2}) is calculated as a function of time and space (distance from the borderline interface between the hydrophobic and hydrophilic regions). (c) Averaged density of modified wheel on hydrophobic region (0-400 nm from the borderline) after adding lipid ($2C_{12}N^+$).

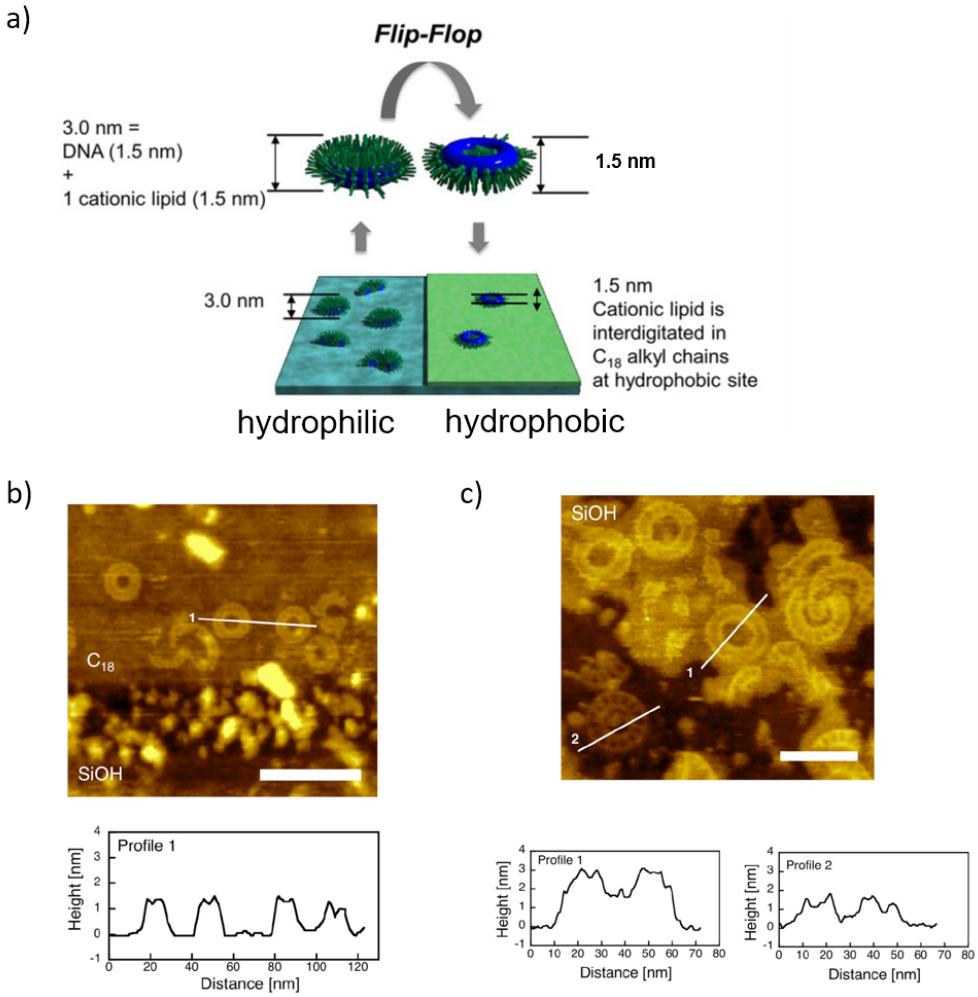

Figure 3.16: Modified wheels and characterization. (a) Scheme of the flip-flop mechanism. Heights are shown. (b) Representative image of modified wheels and profile distribution on a hydrophobic region. (c) Representative image of wheels and profile distribution on silicon wafer substrate after adding cationic lipid.

3.5.2 Pressure-Directed 1D Self-Assembly at the Air-Water Interface

A LB film monolayer of modified sheets is prepared as discussed in the Design section of this chapter (Design of Langmuir–Blodgett films made of hydrophobic DNA nanostructures). Our aim is to dynamically control the monolayer morphology by directly perturbing the monolayer confined space (Figure 3.17). Diverse modes of pressure perturbation can be applied to the LB system. In the present case, dynamic pressure changes are applied through compression/expansion processes. The applied pressure range is from 3 to 30 mN m^{-1} (Figure 3.18), which must follow the π-A isotherm.

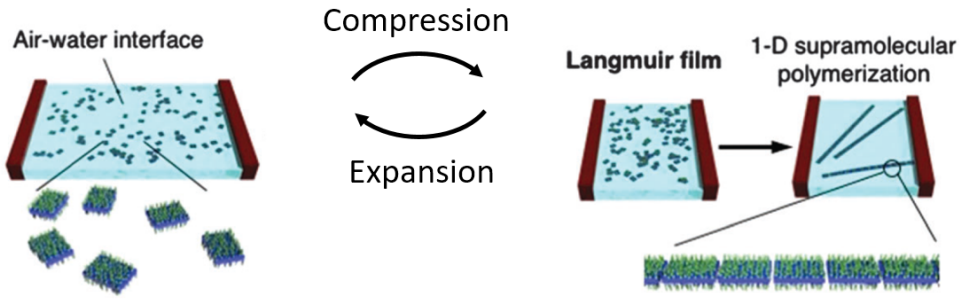

Figure 3.17: Scheme for the dynamic control of the air-water interface area.

The result of compression/expansion cycles is the gradual self-assembly from a state of isolated modified sheets (Figure 3.18a) to larger 1D assemblies (Figure 3.18c). This compression/expansion is the main factor for the observed 1D assemblies because simple stationary compression (for 30 min) at low (3 mN m^{-1}) or high (30 mN m^{-1}) retain modified sheets in isolated form (Figure

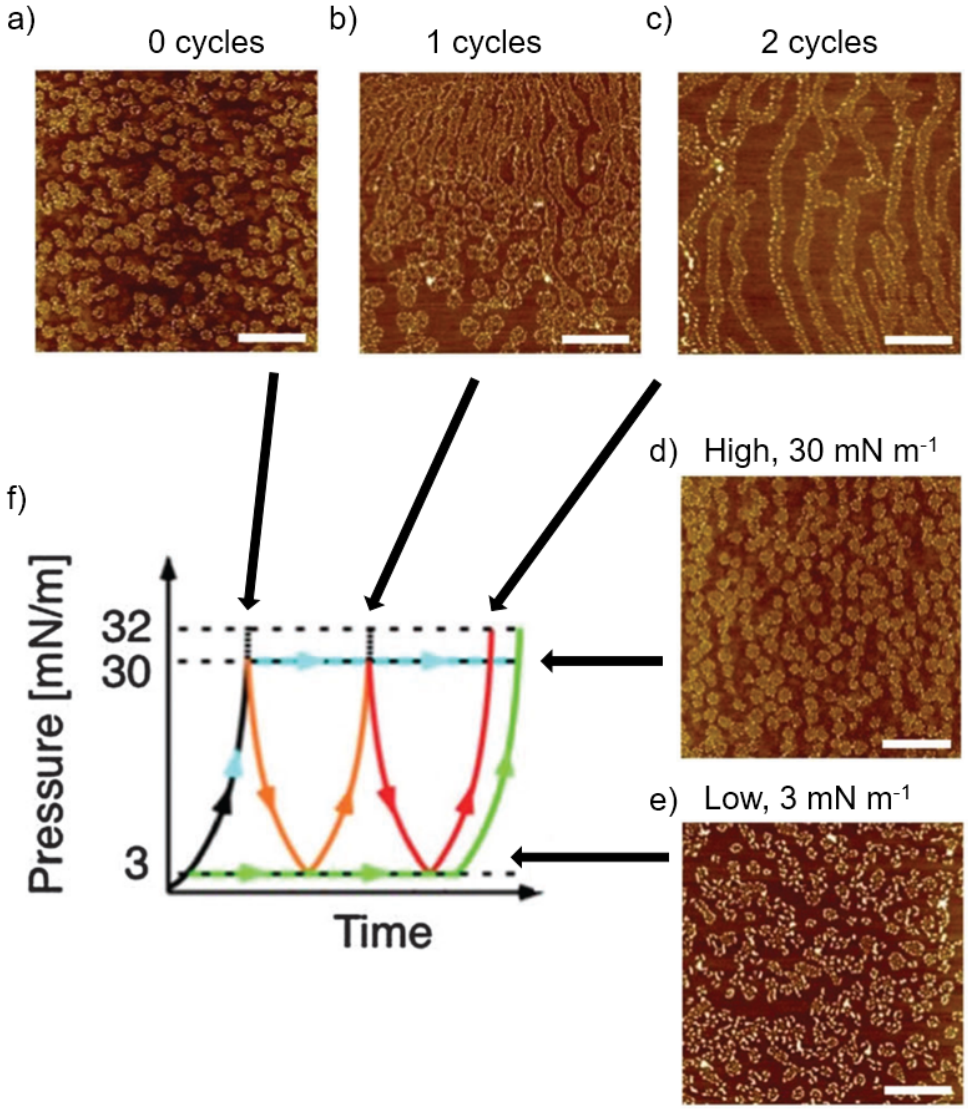

Figure 3.18: Dynamic control of the hydrophobic sheet monolayer conformation at the air-water interface applied through pressure. (a) 0 cycles. (b) 1 cycle. (c) 2 cycles of compression/expansion. (d) High pressure 30 mN m^{-1}. (e) Low pressure 3 mN m^{-1}. (f) Applied pressure over time for the cases in a, b, c, d and e.

3.18d-e). Increasing the cycles (up to 10 times) also promotes formation of 1D assemblies (data only shown in the original article [115]). While cycles with higher pressure (between 30 and 40 mN m^{-1}) generate no significant difference compared to normal cycles. A quantitative analysis of the structures after compression/expansion cycles is done. The number of isolated modified sheets per surface area is analyzed. After 1 cycle, the number decreases from 61 to 19 sheets per mm^2. After 2 cycles, the number decreases to 0.4 sheets per mm^2 (Figure 3.19a). The length of the 1D assemblies made of DNA sheets increases by increasing the compression/expansion cycles.

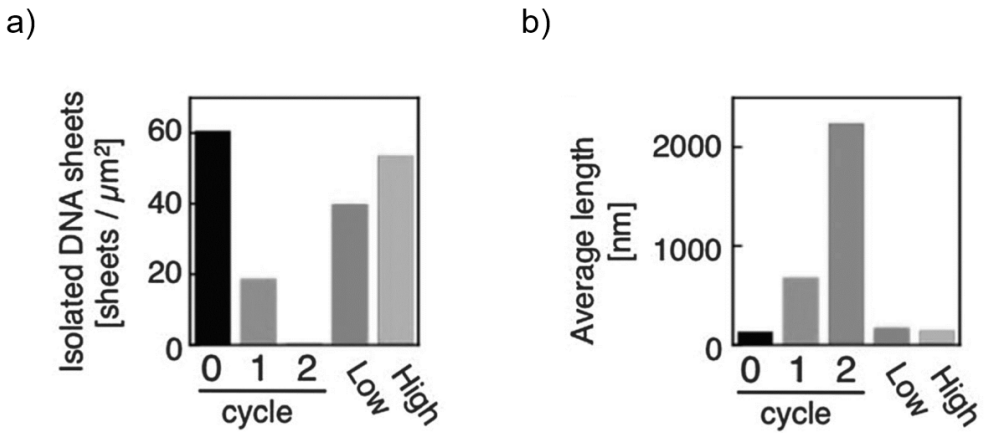

Figure 3.19: Quantitative analysis for the compression/expansion cycles. (a) Isolated hydrophobic DNA sheets that remains after compression/expansion cycles. (b) Average length of 1D assemblies made of hydrophobic DNA sheets after compression/expansion cycles.

The aspect ratios of the length (L) versus height (H) and width (W) (Figure 20a) of the 1D assemblies are calculated. The L:W and L:H are 17 and 15 (Figure 3.20b) times larger than the one for a single modified sheet,

respectively. W:H ratios are constant, which indicates that the thickness of a single sheet is maintained at molecular level. This supports the role of the 2D confined space at the air–water interface preventing 3D aggregates.

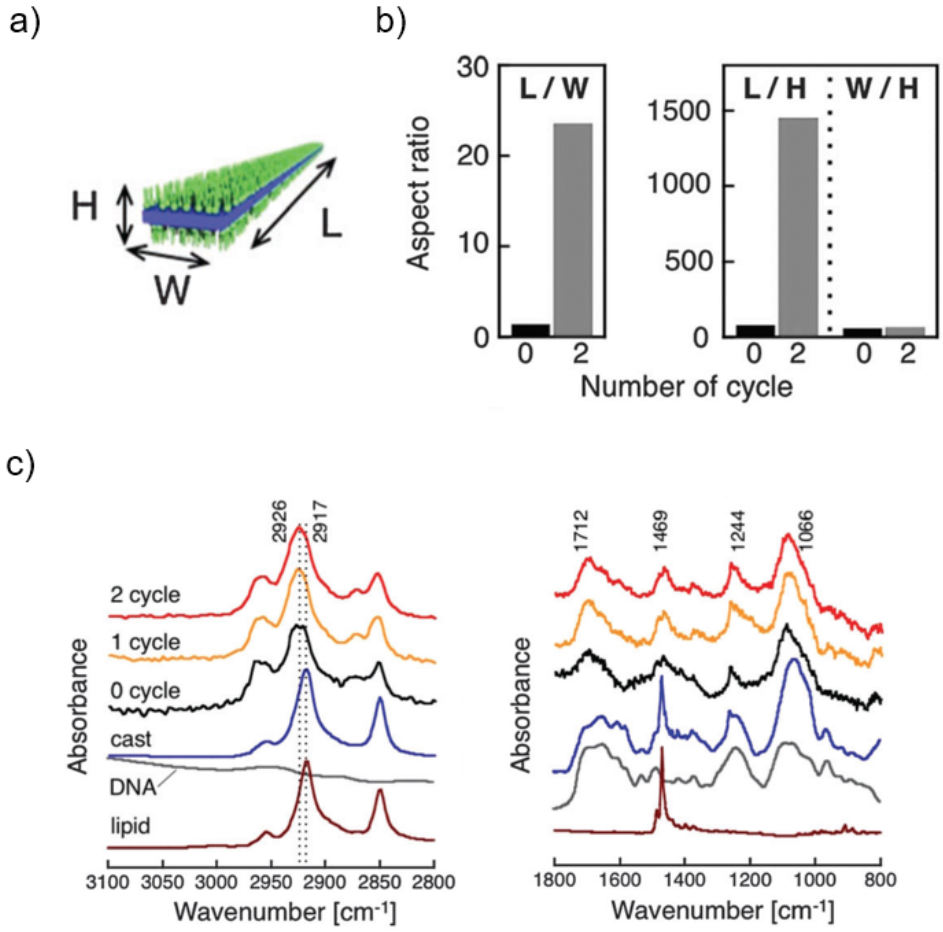

Figure 3.20: Characterization of the modified DNA nanostructure sheet. (a) Scheme of the modified sheet with length (L), height (H) and width (W). (b) Aspect ratios of the 1D assemblies for 0 and 2 compression/expansion cycles.

FT-IR of LB films indicates that the structure remains almost intact during pressure perturbation (Figure 3.20b). The C=O band, at 1712 cm_1, of stacked base pairs is maintained [116]. This strongly indicates that the sheet

DNA helices persist in the 1D assembly. On the one hand, the persistence of the CH_2 band of the LB films (2926 cm_1) shows amorphous packed state of the lipids. On the other hand, cast films of hydrophobic sheet shows the CH2 band at 2917 cm_1, which suggests a crystalline packing structure (Figure 3.20c) [117]. In summary, the supra-molecular 1D assembly of DNA sheets is achieved by a dynamic process on the 2D air-water interface.

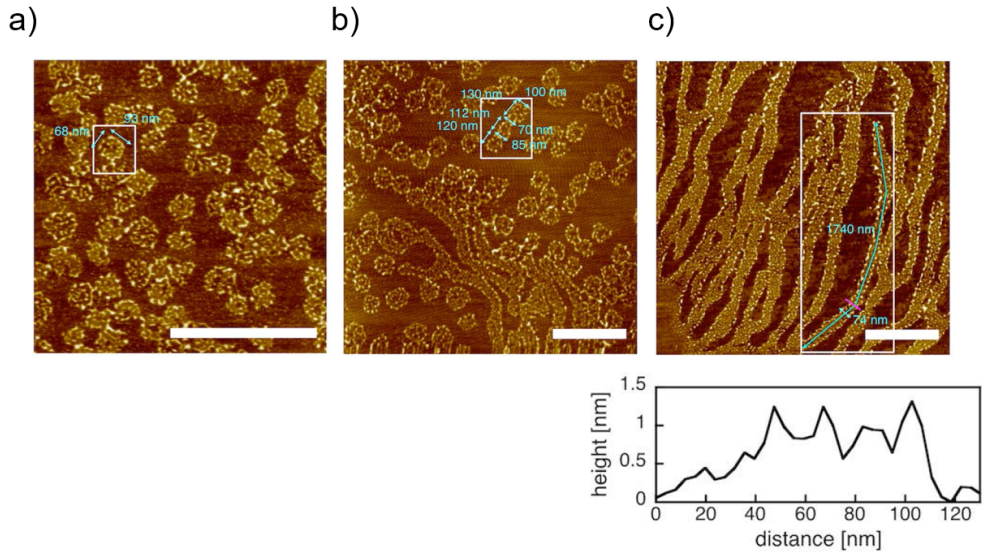

Figure 3.21: Detail of the nanostructures formed by compression/expansion cycles. Representative AFM images after 0 (a), 1 (b) and 2 (c) compression/expansion cycles.

This selective 1D assembly may be due to the non-specific random hybridization of unpaired loops (32 bases) on the DNA sheet shorter side. These loops have an electrostatic charge and are placed on the sheet for preventing aggregation of sheets [37]. After complexation with the cationic lipid, the loop balances its net charge. Therefore, lipid-modified loops may interact

each other making non-specific base pairings. Furthermore, hydrogen bonding may be promoted at the air-water interface [118,119], which may promote DNA sheet connections through the loops. This speculation is supported, by the shorter side connection of the 1D assembly (Figure 3.21). Importantly, the dynamic compression–expansion perturbation procedure was essential in the induction of supramolecular 1-D polymerization of lipid-modified DNA sheets. Thus, fusion occurs by balancing the condensing effect of compression at higher pressure (which facilitates base pairing) with a greater fluidity at lower pressure (which promotes the reorganization of the DNA sheets.

3.6 Conclusions

For the first-time, it has been demonstrated the in-situ lipid-modification of DNA nanostructures deposited on a substrate. DNA nanostructures became hydrophobic with its structural properties preserved, as it was shown by the present diverse experimental confirmations. In addition to the in-situ modification, an in-solution modification has been confirmed too.

By using the demonstrated in-situ lipid-modification, I have developed an extraction method of DNA nanostructures from 2D surface to another 2D surface by 3D migration. Substantial extraction was obtained after 10 min of injecting the lipid. A novel flip-flop mechanism for the nanostructure was observed, which is a first-time physical insight in DNA nanotechnology. In

the future, by using this technique, researchers will make sophisticated DNA devices deposited on hydrophilic surfaces, and transfer them to hydrophobic surfaces. Precise alignment of DNA nanostructures can be designed and fabricated using special architected surface patterns with nano-metric precision. This developments will lead towards a nanoarchitectonics [120] with complex DNA nanostructures.

By using the present demonstrated in-solution method, I have made for the first-time a LB-film made of hydrophobic DNA nanostructures at the air–water interface. By applying pressure, hydrophobic nanostructures underwent supra molecular anisotropic self-assembly (1D self-assembly) due to nonspecific hybridization of the loops surrounding the DNA nanostructure. The 1D self-assembly was controlled up to 2 μm after two compression/expansion cycles. 1D self-assembly is showed, but a 2D self-assembly at the air-water interface can be induced by distributing the DNA nanostructure loops along appropriate directions. Furthermore, by harnessing the non-specify interaction of the loops, it may be possible to design a dynamic self-assembly [121][122]; i.e. self-assemble when applying pressure, and dis-assemble in the absence of it. In the future, by carefully balancing hydrophilicity and hydrophobicity, 3D DNA structures with motions will be actuated by macroscopic pressure (applied by "hand") at the air–water interface.

This chapter is summarized in the following Table 3.2.

Table 3.2: Summary of the method proposed and demonstrated in this chapter.

METHOD	INTERACTION Applied	STRUCTURE Fabricated	FUNCTION Achieved
2.1	Hydrophobicity • Between hydrophobic molecule and hydrophobic pattern	DNA wheel • Simple DNA nanostructure with wheel shape (a delicate frame is visible) • Electric repulsion between DNA duplexes is minimized	• Structure becomes hydrophobic • Molecular separation (extraction): motion from 2D, to 3D solution, and eventually to 2D surface
2.2	Mechanical force (macro pressure) • By pressure (macro-force) controlling confined space at air-water interface • Random base-pairing between origami units	DNA origami sheet • A flat DNA origami with crowded DNA duplexes	Self-assembly • Hydrophobic structure float at the air-water interface • Pressure-controlled 2D distribution • Length depends on number of cycles

4

Harnessing Light Irradiation for Phase Transitions in DNA Hydrogel

Contents

4.1 Introduction

DNA nanotechnology makes possible the fabrication of nanometer to millimeter scale structures [123–128], for example, millimeter scale hydrogels integrating DNA molecules [129–136]. There are two types of these hydrogels. One is fully made of DNA molecules [125], and the other is made of polymers which structural rigidity is mediate by DNA [130–132]. The former, which is of particular interest to this chapter, is made of DNA motifs hybridizing at their sticky-ends. Since these gels are purely made of DNA, the component DNA molecules can be chemically functionalized in diverse ways for making useful devices [133–136]. However, these hydrogels may lack structural rigidity or require high concentrations of monomers for gelation (mM range). To improve the mechanical stability of the hydrogel, their DNA network may be ligated [125] at the expense of generating molecular waste products in the hydrogel. Ligation leads to a covalently linked network that is not reversible preventing gel-sol transition, which may serve for drug release. Using photo-responsive artificial bases is an alternative route to provide ligation without generating waste products. They allow speedy and efficient reversibility [137–139], and they have been applied in DNA devices [136,138], with the exception of hydrogels fully made of DNA.

4.2 Novelty

A DNA hydrogel is designed and it can, under photo-irradiation, undergo repeatable gel-sol/sol-gel phase transitions. The hydrogel is made of specially designed DNA motifs binding each other. The binding can be activated or deactivated by photo-irradiation leading to the phase transitions. The conditions for gelation and solation (such conditions include DNA concentration, DNA dimensions, diffusion coefficients), and the structural characteristics of this DNA hydrogel are carefully studied by diverse proposed experiments.

4.3 Purpose

The purpose of this chapter is two-fold. First, to make a DNA hydrogel with reversible bonds. Second, to externally control the phase transitions of the hydrogel. With these purposes, a method is designed and summarized in the following Table 4.1.

Table 4.1: Method presented in this chapter. It can be read as "physico-chemical interaction X is applied on structures fabricated with Y to achieve function Z"

METHOD	INTERACTION	STRUCTURE	FUNCTION
	Applied	Fabricated	Achieved
3	UV light	DNA hydrogel	Gel-sol phase transition

4.4 Design

The motif design is based on a reported X-shaped motif for hydrogels [125,140]. To make a DNA hydrogel, diverse motifs designs are tested looking for the optimized motif size. A motif with general dimensions is represented by Xxx-Yyy-Zzz, where xx is the sticky end length in nucleotides, yy is the arm length, and zz is the unpaired bases number (Figure 4.1).

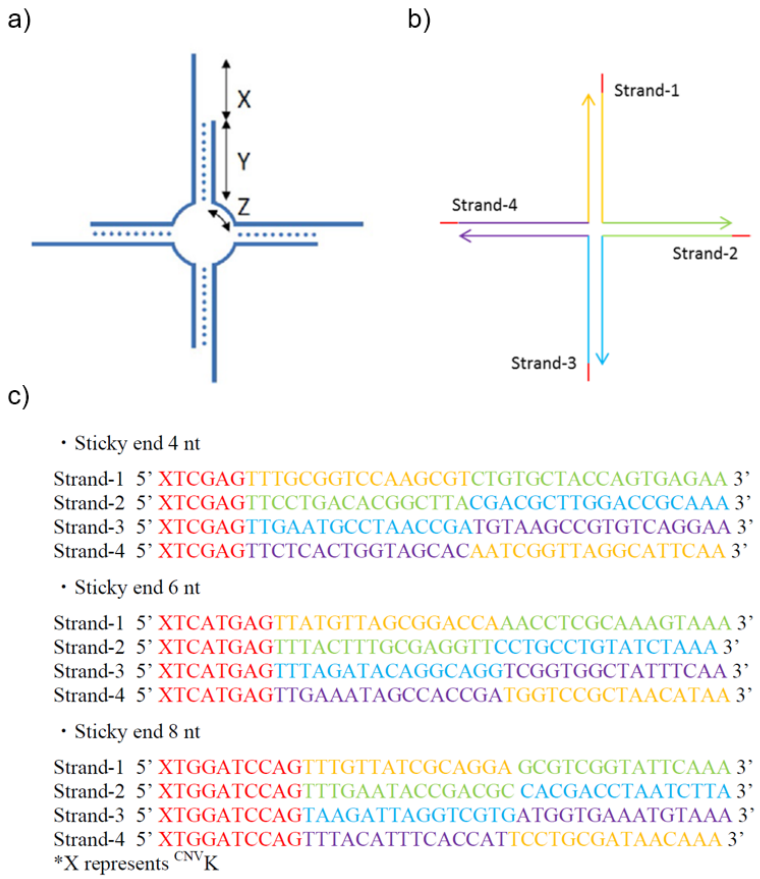

Figure 4.1: X-motifs that self-assemble into a DNA hydrogel. (a) X-motif as represented by Xxx-Yyy-Zzz, where xx is the sticky-end length in nucleotides, yy is the arm length, and zz is the unpaired bases number. (b-c) X-motif showing the strands and corresponding DNA sequences in color.

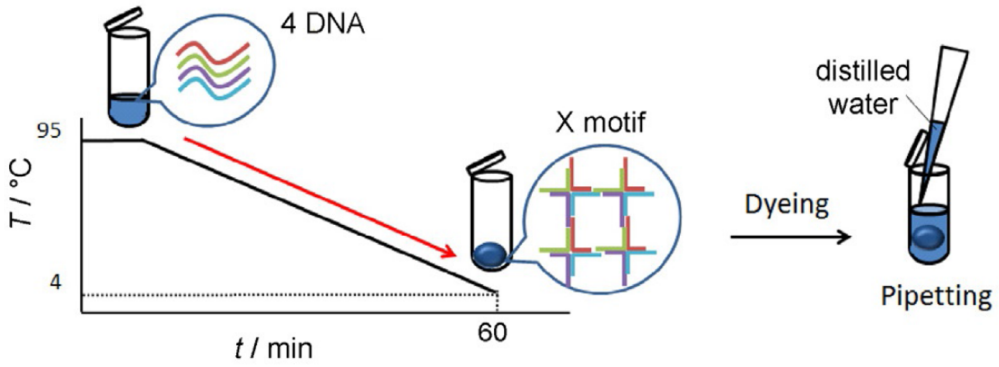

Figure 4.2: Scheme of the dying method used to prove the gelation of the DNA hydrogel.

DNA sequences are show in Figure 4.1b-c. Unmodified DNA is synthetized by Eurofins Genomics, while ^{CNV}K-modified DNA is purchased from Nihon Gene Research Laboratories (Sendai, Japan) and Tsukuba Oligo Service Co (Ibaraki, Japan). Hydrogels are prepared by annealing DNA in Tris (10 mM, pH 8.0) with EDTA (1 mM), and NaCl (50 mM) as shown in Figure 4.2.

For photo-responsive experiments, UV light is from a light emitter (MAX-303 xenon light). The light emitter has 340 and 360 nm filters (Asahi Spectra, Tokyo, Japan). The 360 nm filter is chosen as the closest to the wave length 366 nm. The trajectory (due to Brownian motion) of fluorescent beads (ThermoFisher Scientific, Catalog No.: F8811) is measured by total internal reflection fluorescence microscopy (TIRF) using microscope (IX71 ARC EVA microscope, Olympus). The beads are diluted (1:200) from the original stock.

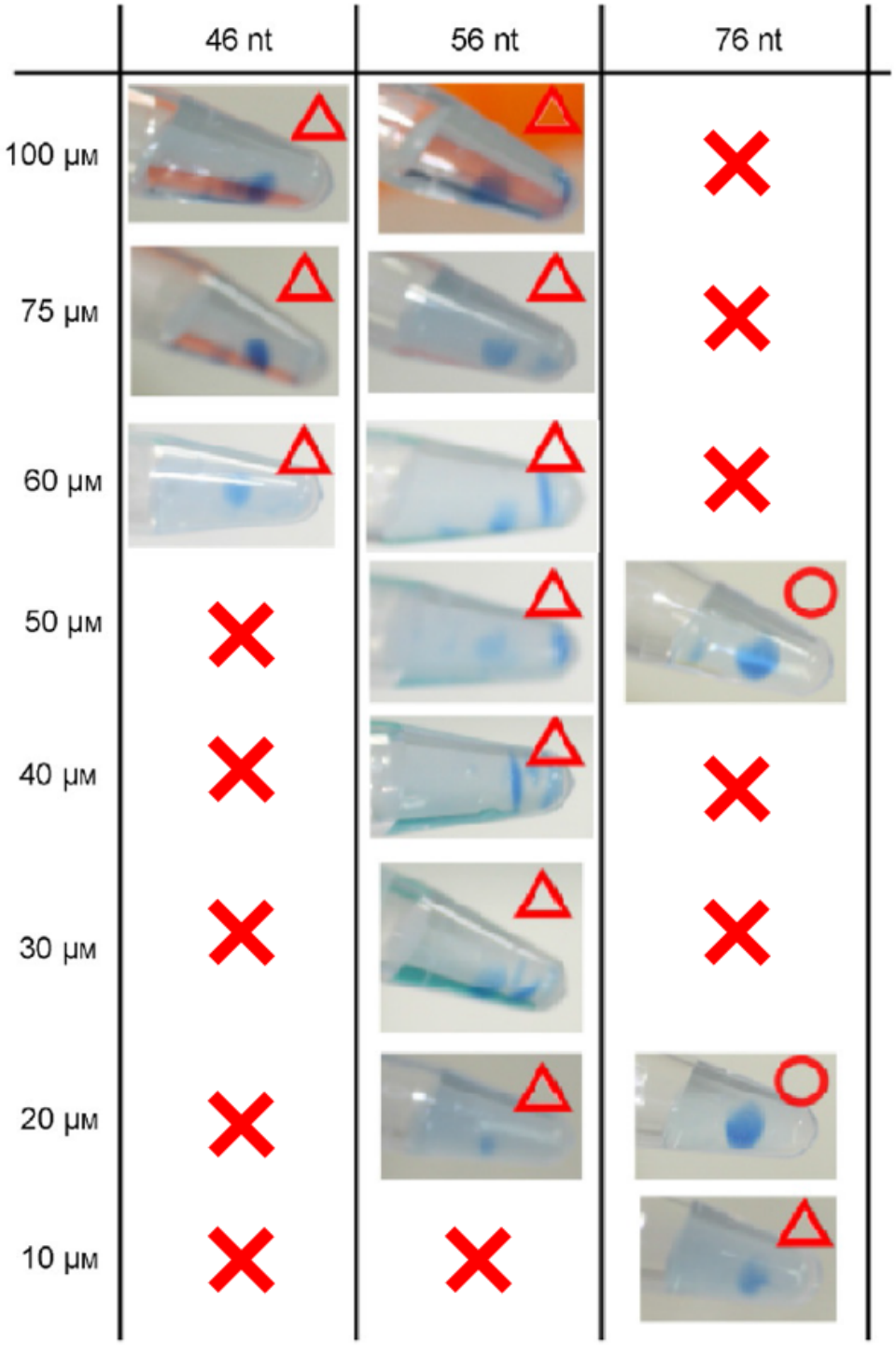

Figure 4.3: Motif arm test for the dyeing method shown in Figure 4.2. Motif has no photo-responsive base. Gelation is if the dyed hydrogel remains as a lump when surrounded by excess water. If the lump dissolves, it is said the hydrogel gelation is not possible. Motifs are X8YyyZ4 where the tested yy is 17, 27, and 37. In the figure, circle means that gelation is confirmed, △ triangle means gel is formed but broken by inserting surrounding water, X means gel is dissolved.

To find the motif dimensions that generates a hydrogel at the lowest concentrations, it is tested under the dyeing method diverse motif designs without photo-responsive bases. The dying method scheme is shown in Figure 4.2. This method requires using a loading buffer (Takara Bio, Japan) for dying the hydrogel, and then immerse it into an excess amount of water. To guarantee inter-motif connections at room temperature, the sticky-end length is set to 8 nt (= xx). Inserting short flexible linker such as 4 nt (= zz) at the junction lowers the minimum required concentration (according to data not shown). Motifs with three different arm lengths (= yy) are tested at various concentrations (Figure 4.3). A longer arm length forms a gel at 20 mM, which is ten times lower than the concentration required by the X-motif (X4Y14Z0) [125].

The photo-responsive artificial base is placed at the sticky-ends of the motifs to allow dissociation of inter-motif binding. Different types of DNA with photo-responsive molecules were reported. For example, p-CVP (p-carbamoylvinyl phenol nucleoside) [137], ^{CNV}K (3-cyanovinylcarbazole) [138,139], azobenzene [136]. p-CVP and ^{CNV}K are used as cross-linkers. Azobenzenes are used as intercalator.

^{CNV}K is used as photo-responsive base, in this chapter, because it is ultra-fast, photo-reversible, highly specific to pyrimidine bases (Cytosine and Thymine), and has non-distorting structural properties [141]. ^{CNV}K is

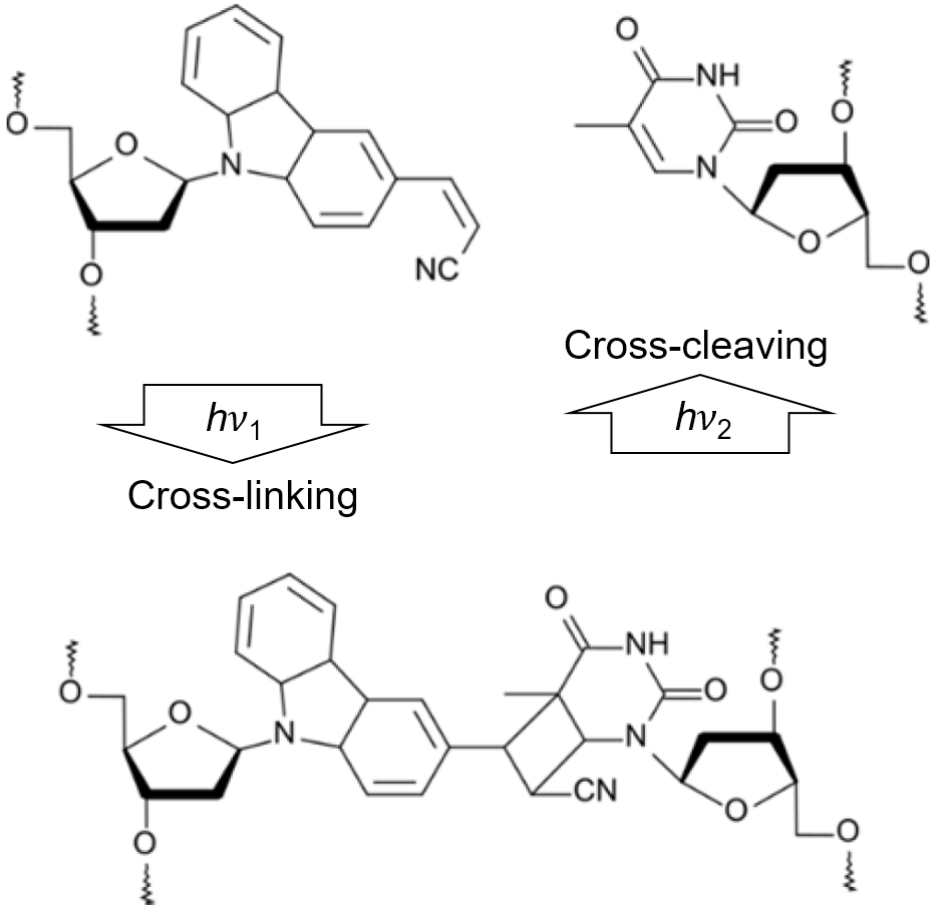

Figure 4.4: ^{CNV}K photo-responsive base cross-link and cleave Thymine in response to light frequencies.

used to photo-crosslink with (or cleave from) an adjacent Thymine base in a complementary sticky-end.

Ultraviolet (UV) irradiation at two different wavelengths are used (Figure 4.4). Finally, a motif design with photo-responsive bases is given in Figure 4.5a. Gelation (photo cross-linking) is achieved under 366 nm UV for 5 minutes at 48°C, and solation (photo cross-cleaving) is achieved under 340 nm UV for 15 minutes at 45°C (Figure 4.5b). The application times and temperatures are optimized as shown for 125 µM X6Y16Z0 (Figure 4.6).

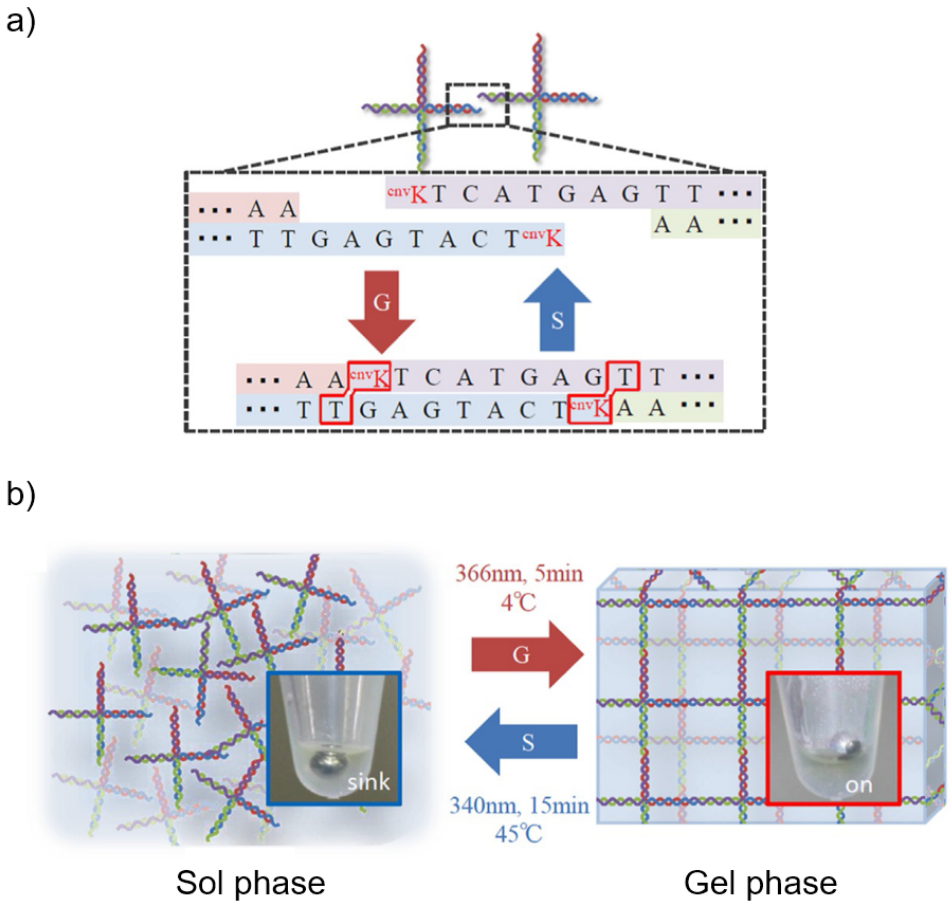

Figure 4.5: Gel-sol phase transitions. (a) X-motif with incorporated ^{CNV}K photo-responsive base. (b) Sol-gel phase transition under 366 nm (4°C, 5min), and gel-sol phase transition under 340 nm (45°C, 15min).

The time influence on irradiation is analyzed for both gelation and solation (Figure 4.6a-b). The diffusion coefficient of the 0.2 µm fluorescence micro beads trapped in the samples is measured using TIRF. The beads are diluted (1:200) from the original stock. Results indicate that at least 1 minute and 2 seconds of irradiation are required for gelation and solation, respectively. The temperature dependence for solation is tested (Figure 4.6c). Result shows no solation at 4°C but for 37°C; therefore, 45°C is enough for solation. The diffusion coefficient of the beads in polyacrylamide-bis solution and its

hydrogel is tested control experiment (Figure 4.6d). Solution is a mixture of 9.7 % Acrylamide and 0.33 % BIS (final concentration) in 1xTBE buffer. The diffusion coefficient in the polyacrylamide-bis hydrogel and its solution are comparable for DNA hydrogel gel and sol phase.

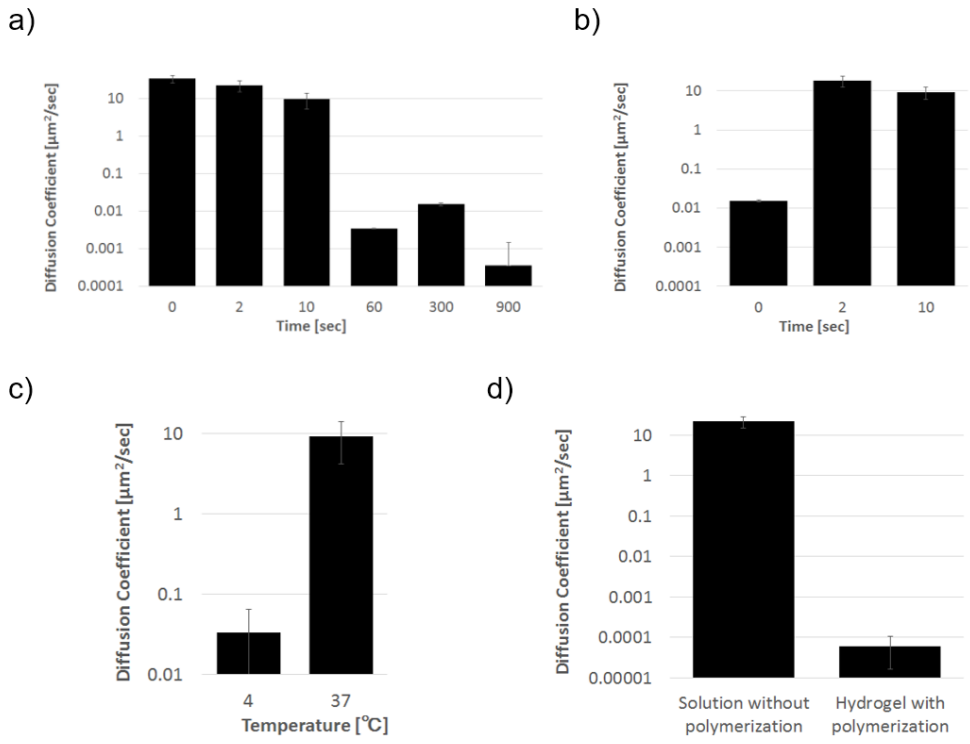

Figure 4.6: Diffusion coefficient of 0.2 μm fluorescence microbeads trapped in the samples. (a) Time influence for sol-gel transition. (b) Time influence for gel-sol transition. (c) Temperature influence for solation. (d) Control experiments. a, b, c and d are in logarithmic scale.

4.5 Results and Discussion

The gel–sol transitions are tested using the steel ball test for 500 mM motifs with photo-responsive bases and with three different sticky-end lengths

(xx = 4, 6, 8) (Figure 4.7). The steel ball is a binary test where the ball is included into the sample, and if the ball stays on top (sinks) it is verified the quality of the sample as gel; if the steel ball sinks, it is confirmed that the sample is a sol. xx = 6 shows the most stable transitions among the results. xx = 8 shows gel formation but it fails returning to solution phase. 40 µM X6Y34Z4 with photo-responsive bases shows repeatable gel–sol transitions. Therefore, it is concluded that 40 µM is the lowest concentration for reversible gel-sol transitions.

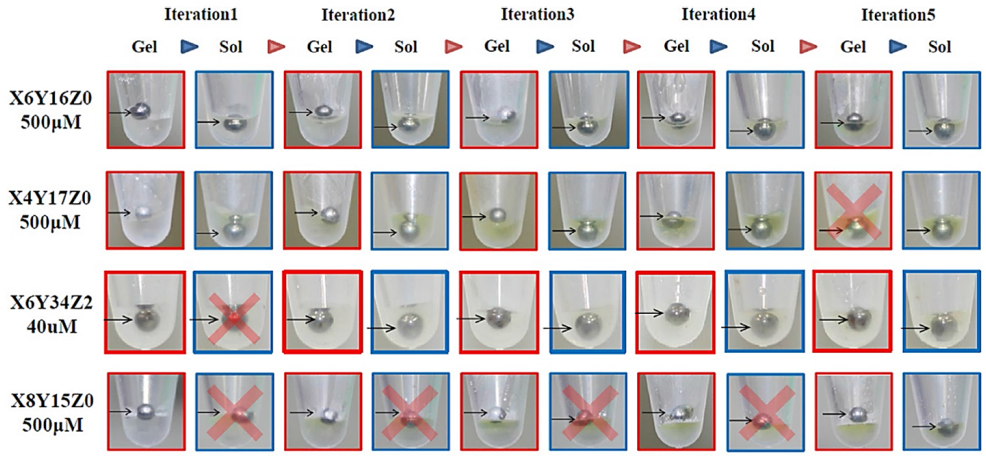

Figure 4.7: ^{CNV}K photo-responsive base cross-link and cleave Thymine in response to light frequencies.

In order to characterize the hydrogel mechanical properties, the "swelling degree" ratio is calculated. To calculate this ratio, the hydrogel weight variation under both wet and dry conditions are measured. 5 µl DNA hydrogel is put in liquid nitrogen (1 min) and it is dried in a freeze-dry chamber (for 24 h). The weight is measured in this dry state. Then 200 µl buffer is

added to the sample, and incubated for 24 h to allow swelling. The weight is measured in this swelling state. Swelling degree is defined by the Equation 4.1:

$$\text{Swelling degree in percentage} = \frac{M_s}{M_d} \tag{4.1}$$

where M_s and M_d are the swelling and the dry state weight, respectively. In Table 4.2, the swelling degrees of motifs with arms xx = 4, 6, 8 are shown.

Table 4.2: Swelling degree for two different concentrations and three motif sticky-ends.

Swelling degree in percentage			
	xx		
motif concentration	4 nt	6 nt	8 nt
0.5 mM	1.5 x 10^3	1.9 x 10^3	2.0 x 10^3
1 mM	1.5 x 10^3	1.9 x 10^3	2.0 x 10^3

The diffusion coefficients [142,143] for the gel and sol phase are also measured by entrapping fluorescent beads (0.2 μm diameter) in the hydrogel (Figures 4.8). The Brownian motion of the bead is observed by TIRF microscopy. Diffusion coefficients are calculated by following bead trajectories using a tracker package in Fiji image processing software. The larges variation is for the motif with xx = 6 nt arm (maximum difference 0.5 $\mu m^2 s^{-1}$). The variation decreases when increasing the number of gel-sol transitions iterations.

Although the diffusion coefficient change is smaller for xx = 4 nt, the difference increases after five cycles. Diffusion coefficient is almost zero for the motif with sticky-end xx = 8 nt.

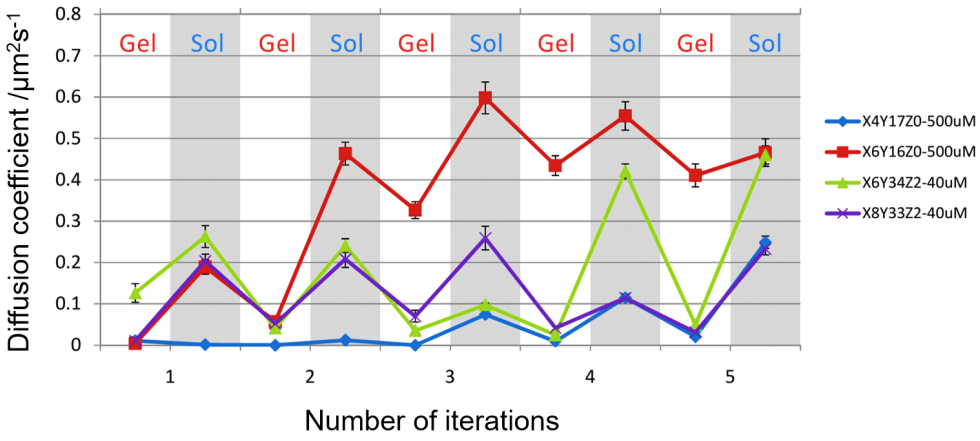

Figure 4.8: Diffusion coefficient of 0.2 μm diameter fluorescence beads in DNA hydrogels vs the number of iterations. The motif has sticky-ends xx with 4, 6, or 8 nt: X4Y17Z0 500 μM, X6Y16Z0 500 μM, X6Y34Z2 40 μM, X8Y33Z2 40 μM. Error bars represent standard deviation (n=30).

4.6 Conclusions

For the first time, a novel DNA hydrogel (completely made of DNA molecules) with designed phase transition properties based on reversible photo reaction (UV irradiation at different wavelengths) was implemented. Different configurations and concentrations were tested, and suitable conditions for gelation were found; i.e. the minimum DNA motif concentration is as low as 40 μM. Gel-sol transitions were observed for at least 5 cycles. The physical

properties of the hydrogel were assessed by using the swelling degree and diffusion coefficient of entrapped beads.

In the future, the proposed photo-responsive hydrogel will be useful as medical device in applications including drug delivery and molecular diagnostics by delivering sensing molecules in cells. The reversible gel–sol transition will be utilized as a mechanical actuator in biochemical-mechanical devices, i.e. molecular robots [68].

This chapter is summarized with the following Table 4.3.

Table 4.3: Summary of the method proposed and demonstrated in this chapter.

METHOD	INTERACTION Applied	STRUCTURE Fabricated	FUNCTION Achieved
3	UV light (Photo irradiation) • UV light at two different frequencies • Photo-responsive base conformation change	DNA origami • Simple DNA motifs with sticky ends • Sticky ends have photo-responsive base	Self-assembly • Control 3D conformation of DNA motifs: sol-gel • Fast response: at least 10 sec (sol-gel) and 2 sec (gel-sol) • Repeatable transitions: at least 5 times

5

Harnessing Electrophoresed Nanoparticle for DNA Dehybridization

Contents

5.1 Introduction

In previous chapters, DNA nanotechnology was used for fabricating several materials including, in increasing size, DNA tiles, DNA origami, hydrophobic DNA nanostructures, and DNA hydrogels (fully composed of DNA molecules) and DNA-integrated hydrogels [123]. All these structures are composed of hybridized DNA molecules. Control of hybridization and, its reverse, dehybridization reactions is fundamental for realizing useful DNA devices based on DNA nanostructures; for example, molecular computing devices [144–146] and drug delivery materials.

The most widely-used method to control DNA hybridization is a simple temperature annealing. In case of DNA dehybridization control, it is not so simple but it can be the toehold-mediated strand displacement reaction can be implemented [32]. Basically, in this reaction, a target DNA strand in a DNA duplex is displaced by an external DNA strand. An advantage of this reaction is its sequence-specificity which provides reliability and robustness. A disadvantage is that generated molecular waste may interfere with the system's function [147]. On the other hand, other method such as tensile force control of DNA dehybridization [148] maintains a waste-free environment. A tensile force on a DNA duplex can cause two effects depending on where the force is applied. Basically, the force can be applied perpendicular (unzipping of DNA duplex) or

parallel (shearing of DNA duplex) to the DNA duplex axis. The most common example of unzipping is when DNA helicase unzips parental DNA during cellular replication [149], and shearing can be used in molecular sensors [150]. Applied force magnitude is also important for the dehybridization dynamics; for example, a common parameter in tensile dehybridization is the critical force, which is defined as the force that gives 50% of dehybridized duplexes [151]. Also it is well-known that the critical force for unzipping has smaller magnitude than the shearing one [152]. Moreover both forces reach a plateau when the DNA lengths are sufficiently long (more than 25 bps in the case of shearing) [153].

Diverse studies have been performed in the theoretical arena about the tensile dehybridization. Among them, the most interesting one is the simulation platform developed at Oxford University. Recently, by using this simulator, Ouldridge and coworkers claimed that the critical force for dehybridizing short DNA duplexes depends on the observation time (or application time, hereinafter) [151]. In other words, the applied force is not an issue for sufficiently long application times. To the best of my knowledge such a claim has not been confirmed experimentally; therefore, the proposed system in this chapter may be the first confirmation. One interesting way to generate tensile force is by using external force fields. External force fields have been already applied in single molecule experiments for studying the extension and dehybridization dynamics of DNA duplexes. External force fields are, for

example, optical trapping fields [154], magnetic field [152], and gravitational field [155]. A third type of force field is the electric field [156], which is not frequently used for generating tensile dehybridization force but for electric-driven dehybridization.

Hydrogels are 3D materials that have plenty applications such as electrophoresis, which is a common method for molecular separation based on electrical forces on charged molecules. A standard electrophoresis hydrogel is polyacrylamide-bis which has a neutral charge. The hydrogel structure, i.e. its porosity, allows diffusion of molecules of diverse sizes [157]. Moreover, the mechanical strength and stretching of hydrogels can be enhanced as, for example, polyacrylamide matrix with alginate chains [158]. The hydrogel structure also allows chemical conjugation with functional molecules; for example, DNA molecules can be chemically conjugated to polyacrylamide-bis hydrogels [159]. In addition to electrophoresis, other applications include controlled drug release [160,161] and tissue/robot interface for heart failure treatment [162]. In DNA nanotechnology, hydrogels incorporating DNA devices [163] were used for molecular computations including edge detection [144], cellular automata simulations [145] and reaction-diffusion generated patterns [146].

Two dehybridization electric control methods have been demonstrated for detecting single nucleotide polymorphism [156,164]. In the first method,

Sosnowski and coworkers anchored DNA duplexes in the polymeric network of a 1 μm-thick agarose hydrogel, which is placed over nanofabricated Pt electrodes. DNA strands were released from the hydrogel when electric current is applied through the electrodes. Based on the applied electric current, the electric field was estimated to be orders of magnitude lower than the required theoretical value. Therefore, the authors suggested that pH change in combination with electric field contributed to dehybridization. In the second method by the Bartlett's group [164], DNA duplexes were directly anchored to the surface of a gold electrode. When the gold electrode was driven negative, DNA strands were released from the electrode. It was suggested that dehybridization was due to the electrical repulsion between the electrical double layer of the electrode and the negatively-charged DNA. However, the same group recently refuted this hypothesis suggesting a new mechanism related to the electronic states of the DNA when borrowing electrons from the electrode [165]. Therefore, understanding the underlying molecular mechanisms for dehybridization under electric field requires further investigation.

5.2 Novelty

In this chapter, a new method for electric control of dehybridization modes (unzipping and shearing) of DNA strands captured (hybridized) by DNA-integrated hydrogel (hereinafter called simply hydrogel) is presented. Tensile

force on the DNA duplex is applied by electrophoresing gold nanoparticles. The tensile force is generated by applying an electrophoretic pulling force on negatively-charged nanoparticles attached to the DNA strand. For this purpose, negatively-charged gold nanoparticles (GNPs) [166–168] are used. To apply voltages, the DNA duplexes are immobilized in a hydrogel segment inside a capillary placed inside a silicon chamber. DNA duplexes are located some centimeters far away from the electrodes, to eliminate the electrical double layer effect due to the electrical electrodes. Under electric field (25 V cm^{-1}), DNA strands captured to DNA-integrated hydrogel are pulled by the GNPs. This is similar to pulling DNA duplexes in single-molecule studies by micromanipulation (for example, optical tweezers [154]), but in our case manipulation is done in hydrogels and dehybridization is massively in parallel. Over time, dehybridized DNA strands are gradually released from hydrogel. Moreover, this system avoids undesired increments in pH and temperature.

5.3 Purpose

The purpose of this chapter is two-fold. First, to find an experimental system for applying voltages (in the order of 100V) without significant increments of temperature and pH. Second, to dehybridize the duplex by applying electric field. With these purposes, a method is designed and summarized in the Table 5.1.

Table 5.1: Method presented in this chapter. It can be read as "physico-chemical interaction X is applied on structures fabricated with Y to achieve function Z"

METHOD	INTERACTION Applied	STRUCTURE Fabricated	FUNCTION Achieved
4	Electric	DNA-integrated hydrogel	Decomposition (Dehybridization)

5.4 Design

The notation Un-GNPd and Sn-GNPd are used for simplicity, where U/S stand for the Unzipping/Shearing configuration (Figure 5.3a and b). Unzipping samples are prepared when GNP is attached at the 3 end of the U strand, and Shearing samples are prepared when GNP is attached at the 5' end of the S strand.

In Un-GNPd and Sn-GNPd, the letter n indicates the number of nucleotides that can be captured (hybridized). d after GNP shows gold size in nm. 15, 20, 25, 30 and 49 nucleotides (nt) are tested. GNPs with diameters of 5 and 10 nm.

DNA strands (HPLC purified from Eurofins Genomics) are functionalized with GNP (Tanaka company, Japan); this modification is hereinafter called DNA-GNPs. After arrival, DNA strands are dissolved in water water. Two types of GNPs coated with citrate acid are used (5 nm and 10 nm). GNPs are passivated with Bis(p-sulfonatophenyl)phenylphosphine dihydrate

dipotassium (BSPP) salt. For passivation, 250 μl of GNPs and 50 μl of BSPP solution (50 mg/ml in water) are mixed in a micrutube. A total of 6 microtubes are heated at 50°C for 30 min using a thermocycler (Eppendorf Mastercycler personal). Under 20,000 G at 4°C for 2 h, all microtubes are centrifuged in centrifuging machine (Kubota 3780). Supernatant is discarded carefully, and remained gold on the bottom becomes the stock gold solution. Thiol-modified DNA (50 μM) is mixed with 100 μM TCEP, and incubated at room temperature for 1 hour. This mixture gives a final DNA concentration of 40 μM.

To prepare 10 μl of DNA-GNPs, the GNPs stock is diluted to a final volume containing 1 mg/mL BSPP, 1xTBE, 200 mM NaCl, and 4 μl water. Once prepared, it is added 1 μl of deprotected thiol-modified DNA (26 μM) to the mixture. The final mixture is pipetted many times (at least 3 times) until the solution becomes homogeneous at simple sight. For 1 hour, the mixture sample is heated at 50°C. Then, the mixture is stored at room temperature. Characterization using 2% agarose gel electrophoresis (5 V per 4 cm, 1.25 V cm^{-1} for 15min) for DNA-GNP5 and DNA-GNP10 are shown in Figure 5.1. This gel electrophoresis confirms that each GNP modifies only a single DNA strand.

Prepared DNA-GNPs are introduced into a capillary containing a DNA-integrated hydrogel, which is a hydrogel with covalently anchored DNA

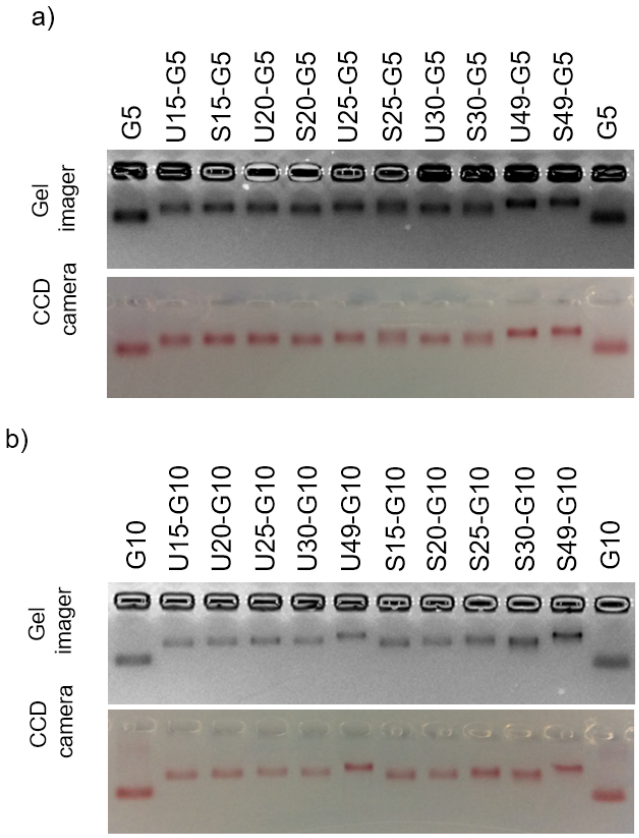

Figure 5.1: 2% gel electrophoresis assay for both two DNA-GNP of different diameters. a) 5nm and b) 10nm GNP. Gel imager uses white EPI light source and 530/28 filter.

strands. The hydrogel is a 3% polyacrylamide (3.3% acrylamide:bis). The anchored DNA strand is 50 nt long and it is hereinafter referred as anchor. Anchor DNA is complementary to DNA-GNP.

Anchor is linked to the hydrogel via a 5' end acrydite chemical modification. The anchor concentration in the hydrogel is 1 μM. In such a concentration, there is approximately one DNA anchor molecule in a cube with 120 nm side. This cube is at least 24 times or 12 times bigger than the 5nm or 10 nm GNP diameter, respectively; therefore, the DNA-GNP must be captured by only one DNA anchor. The hydrogel is put in a 3 cm-long glass capillary with 1

mm/1.5 mm inner/outer diameters (Figure 5.2).

The DNA strand in the DNA-integrated hydrogel is complementary to DNA-GNP. 0.5 µl of DNA-GNPs, which are mixed in a final volume containing 8% sucrose in water, are injecting into the capillary using a micropipette. DNA-GNPs can not enter inside the hydrogel but are trapped over the hydrogel due to the sucrose molecules. The capillary is placed into a vertical chamber with platinum (Pt) electrodes separated 4 cm. 5V are applied for 2 hours, which is sufficient for the DNA-GNP to be captured by the DNA-integrated hydrogel.

For the modification of U and S with GNP, a single thiol molecule is used. In case of U, the thiol is modified in its 3' in the C3 Carbon; while in case of S, it is modified in its 5' in the C6 Carbon. Molecular structures of 3' thiol and 5' thiol with protection are shown in Figure 5.4a and 5.4b, respectively. Connection between the GNP-thiol and the complementary sequences of the U/S strands is done through two Thymine bases (TT).

GNP are colloids with a visible reddish color, that makes them a suitable colorimetric label detection inside the capillary using a CCD camera (canon EOS Kiss X7) (Figure 5.5) [157]. The CCD camera is coupled to an optical microscope stage to magnify the region including the DNA-GNPs captured by the hydrogel. To provide a uniform background for CCD recording, a 1 mm thick polytetrafluoroethylene (PTFE) white sheet is used as background

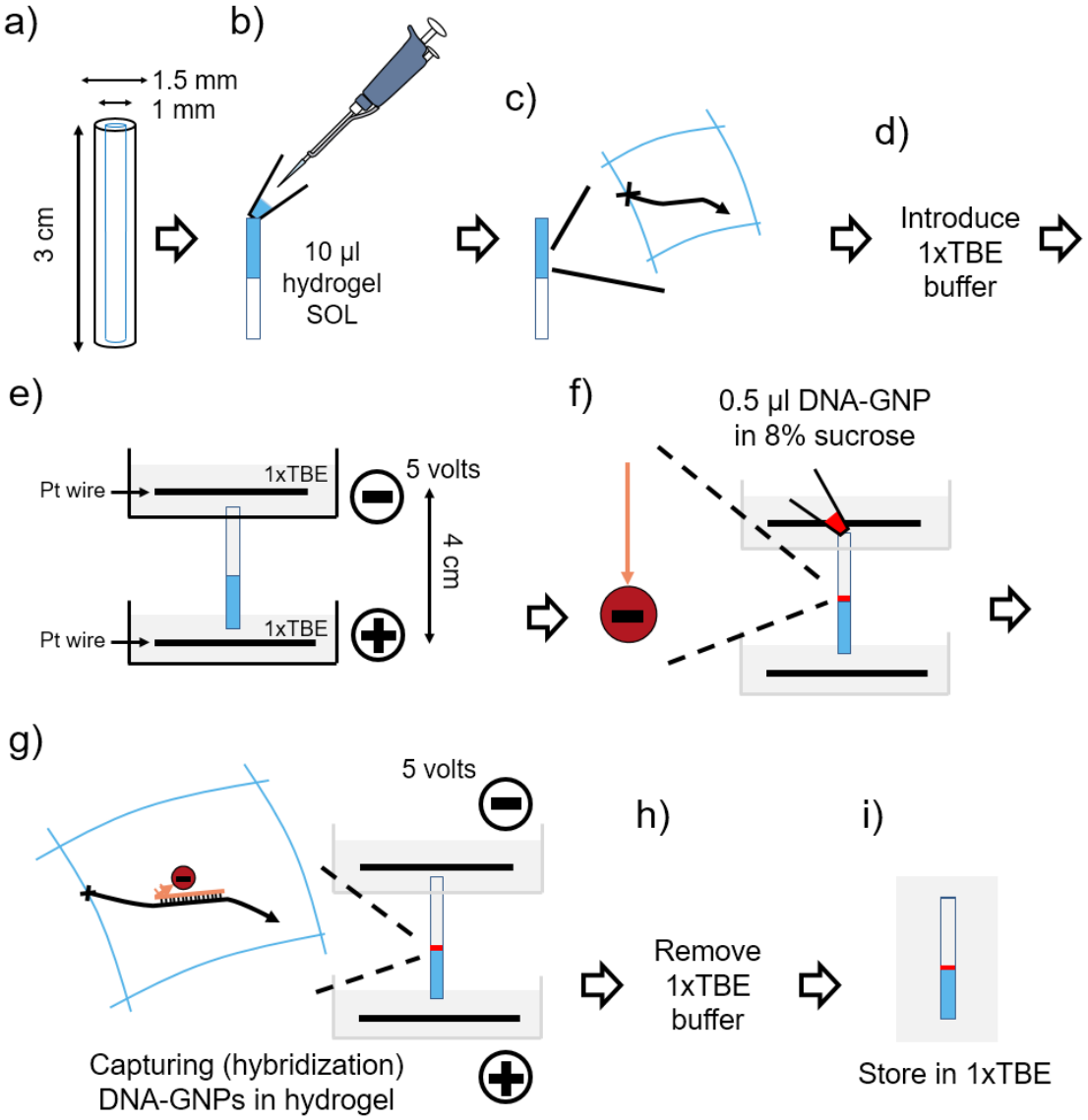

Figure 5.2: Scheme of the preparation of capillary with DNA-integrated hydrogel and captured DNA-GNPs. a) Glass capillary tube with 1.5 mm and 1 mm for outer and inner diameters, respectively. b) 10 µl of DNA-integrated hydrogel in sol state is introduced inside the capillary for gelation. c) DNA-integrated hydrogel gelates inside the capillary for 1 hour. d) After gelation 1xTBE buffer solution is introduced to fill the capillary. e) Capillary is placed in vertical silicon chamber, and 5 volts are applied for 30 min. f) 0.5 µl DNA-GNP in 8% sucrose are introduced into the capillary. g) 5 volts for 2 hours are applied along the capillary to make the DNA-GNP get inside and be captured by the hydrogel. h) Capillary is taken out of the chamber, and 1xTBE buffer solution is replaced by new 1xTBE buffer solution. i) Capillary is stored in 1xTBE buffer solution.

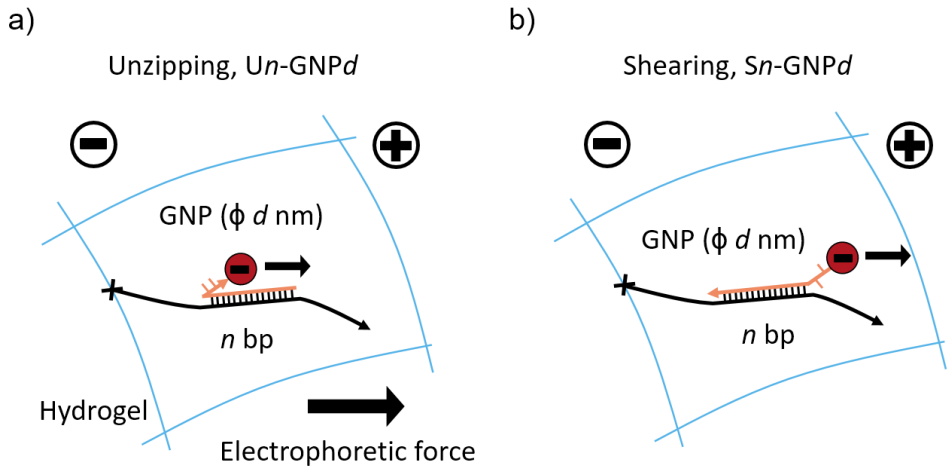

Figure 5.3: DNA dehybridization by electrophoresing negatively-charged gold nanoparticles. DNA-GNPs captured by hydrogel in unzipping a) or shearing b) configuration is achieved by using two different DNA-GNPs

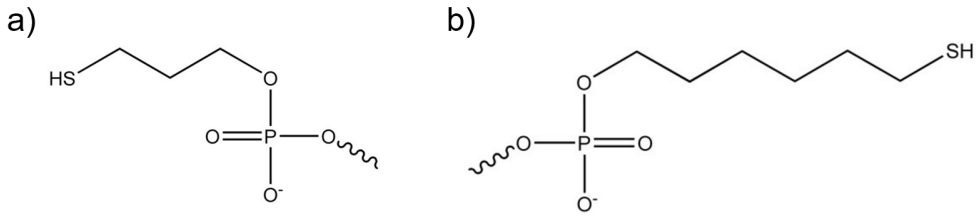

Figure 5.4: Thiol modifications for a) 3' and b) 5'.

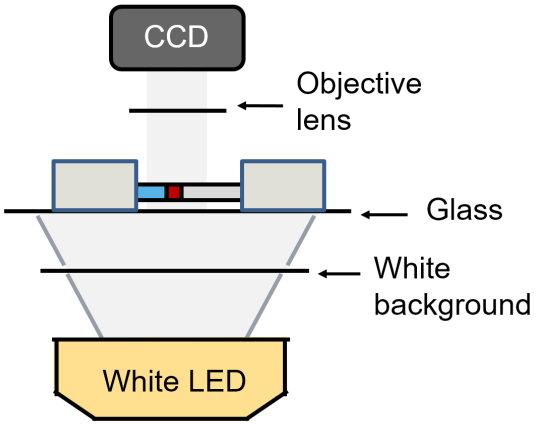

Figure 5.5: CCD recording setup for the dehybridization time evolution.

illuminated by white LED array. CCD recording is done at 30 frame per second. Recording time is done for a total time of 12 min; that is, 10 min of voltage application (20 V, 60 V, 80 V, 100 V), and 1 min before and 1 min after voltage application. The hybridization ratio is calculated by analyzing the time evolution (decrease) of the average reddish intensity in a fixed area.

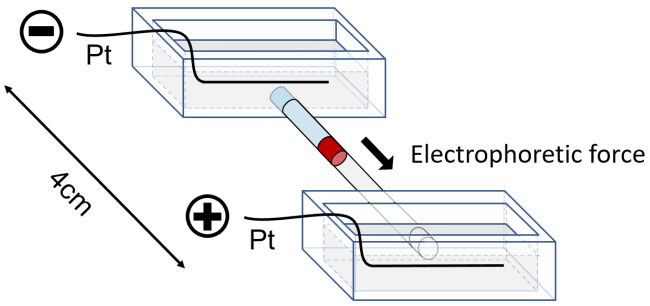

Figure 5.6: Experimental setup for voltage experiments. Glass capillary with DNA-GNP is inserted into the horizontal silicon chamber.

A silicon chamber is made for voltage application through the capillary axis (Figure 5.6). Basically, the chamber is two silicon compartments that works as buffer reservoirs for 1xTBE buffer solution (pH 8.5). To apply voltages, two 0.2 mm diameter Pt wires are introduced as electrodes. After inserting the capillary between the two compartments, Pt electrodes have a separation interval of 4 cm. Each Pt electrode is connected to the opposing poles of a regulated DC power source (DC160-7.2 from NF corp, Japan), whose ripple noise is below 12 mV. One half of the capillary is filled with the hydrogel and the other half with the buffer solution. The hydrogel is placed at the negative side. pH recordings are carried on near electrodes by using an

electrode (Micro ToupH electrode 9618S-10D) connected to a pH meter device (Horiba D-54). Temperature recordings are taken on the external surface of the capillary, at its middle point, by using a Type-K thermocouple (Fluke 80PK-1 Bead Probe, fast response, 260 °C maximum temperature) connected to a data logger (T&D MCR-4TC). Electrical currents on the capillary-hydrogel-buffer-electrode system are calculated by using the voltage drops in a shunt resistor (1.2 Ohm).

The resulting phenomena of applying voltages (electric fields) in a solution medium belongs to the electrokinetics , particularly electrophoresis in a hydrogel. Commom parameters associated with any electrokinetic phenomena are pH change and Joule heating (temperature rise). pH change and temperature rise have checked in the present experiments, and they are negligible. A description of the parameters is provided as follows. First, DNA duplexes may be sensitive to pH changes which are originated on the Pt electrode. In the present case, DNA duplexes are located approximately 1.8 cm and 2 cm far away from the negative and positive electrode, respectively. This distance prevents interaction of the generated ions with the DNA duplexes, which is confirmed by the low pH change before and after voltage application for both electrodes (± 0.2). Second, temperature increment (due to Joule heating) may destabilize the duplex when this is comparable with the DNA melting temperature [6]. The temperature on the outer surface of the capillary (at the middle point) is measured while applying voltage. For 100 V, the maximum

temperature rise at the steady state is as much as 2 °C (80% reached within 2 min. Figure 5.7). The shape of the measured temperature profile agrees with more accurate experiments using fluorescent molecules [169]. Third, the electric current through the hydrogel is measured using a shunt resistor in series with the chamber. For 100 V, the electric current density is approximately 0.3 fA/nm^2 (considering the inner capillary diameter of 1 mm).

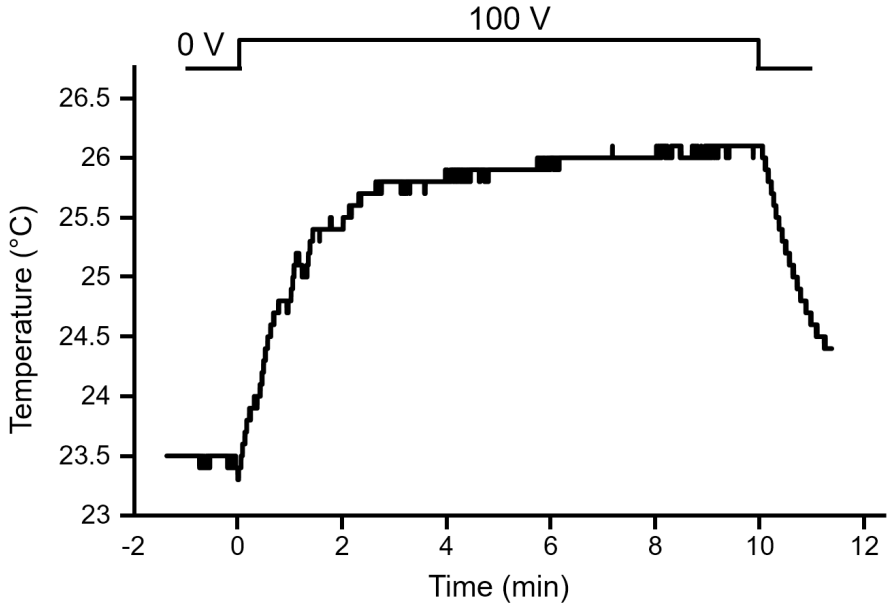

Figure 5.7: Representative plot of the measured temperature on the outer surface of the capillary axis under 100V.

5.5 Results and Discussion

A representative result for U15-GNP5 under 100 V is shown in Figure 5.9). The time-evolution of the hybridization ratio (HR; related with the dehybridization ratio by following DH = 1 - HR) of U15-GNP5 under 100 V

(electric field of 25 V cm^{-1}) is calculated for 10 min (a representative result is shown in Figure 5.10). The calculation is done by recoding a fixed area including the DNA-GNPs, and then processing the color intensity corresponding to the reddish color (Figure 5.8).

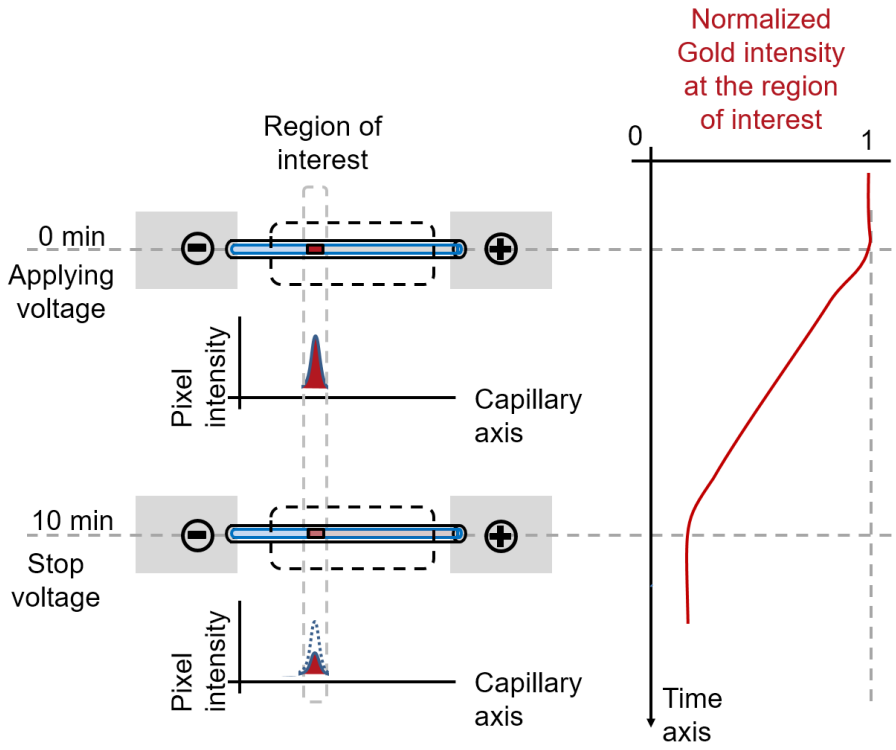

Figure 5.8: Scheme of the calculation of hybridization ratio by analysis of the red intensity corresponding to DNA-GNP.

The HR over time shows a gradual dehybridization or release from the hydrogel to buffer solution. DR over time can be represented by rates assuming a linear fitting. For example, DR of U15-GNP5 (0.067 min^{-1}) is 3 times faster than the rate of S15-GNP5 (0.023 min^{-1}) (Figure 5.10). The difference between the dehybridization of U15-GNP5 and S15-GNP5 is expected, because shearing configuration is known to be stronger than the

unzipping configuration according to other methods [152].

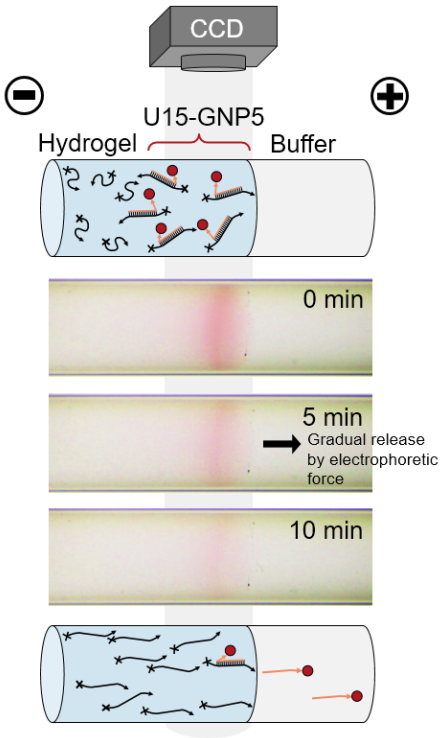

Figure 5.9: Representative capillary experiment using U15-GNP5 under 100 V.

Unzipping and shearing 15nt are tested under different voltages (Figure 5.11a and 5.11b, respectively) using a 5 nm GNP (U15-GNP5 and S15-GNP5). The results show that the HR over time depends on the applied voltage for both unzipping and shearing. By using the same data, the time development of the HR as a function of voltage is shown in Figure 5.12c-d. In the unzipping case (Figure 5.12a), there is the existence of a critical voltage, which is defined as the voltage that gives 50% of DNA dehybridization. This critical voltage depends on the application time. For example, for an application time of 10 min, the critical voltage is 80V. This plot also shows that critical voltages

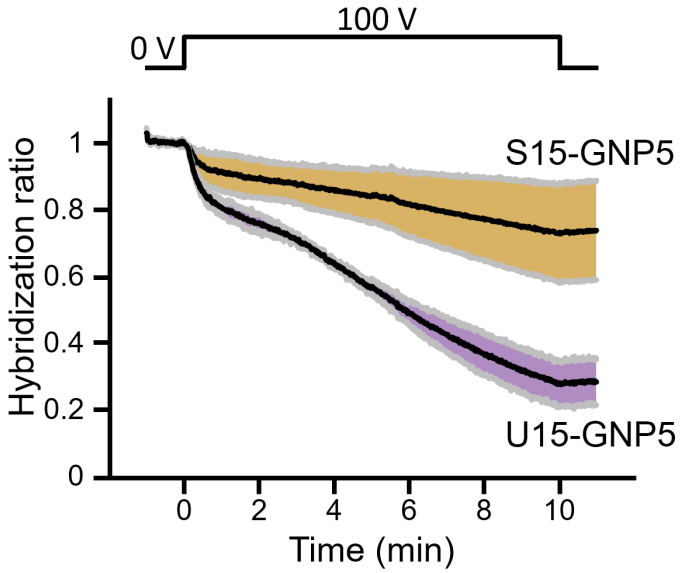

Figure 5.10: Representative capillary hybridization ratio using U15-GNP5 and S15-GNP5.

lower than 80 V are possible for longer application times (> 10 min). The case of shearing is different (Figure 5.12b). There is no significant dehybridization compared with unzipping.

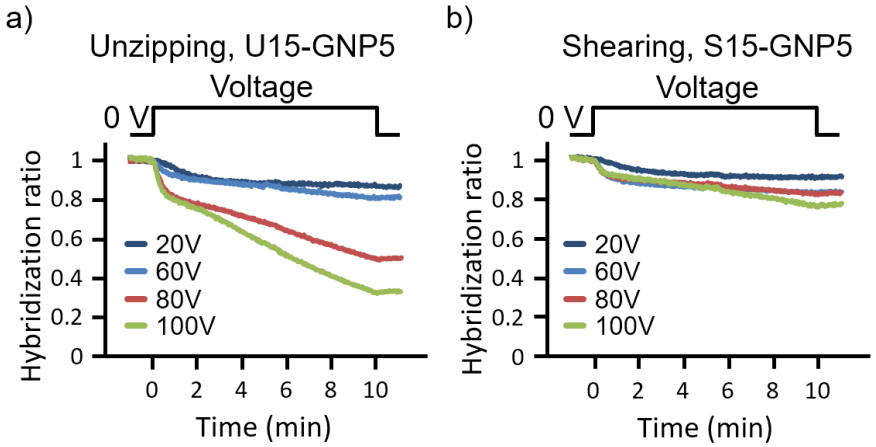

Figure 5.11: Unzipping and shearing of 15nt over time for different voltages. a) Unzipping and b) shearing.

Under 100 V, Un-GNP5 and Sn-GNP5 are tested for different DNA

lengths (n = 20, 25, 30, 49 nt). Results are shown in Figure 5.13a. In case of the unzipping and shearing, there is a direct dependency between the HR and the DNA duplex length. For example, in case of U20-GNP5, the maximum dehybridization ratio is about 15%.

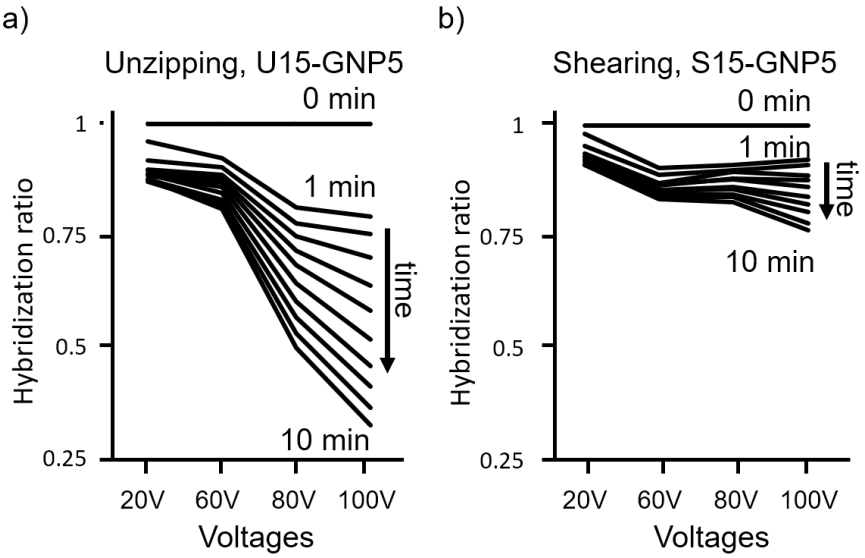

Figure 5.12: Unzipping and shearing of 15nt over different voltages for different times. a) Unzipping and b) shearing.

Un-GNP10 and Sn-GNP10 are tested for n = 15, 20, 25, 30, 49 nt, under 100 V (Figure 5.13b). Dehybridization with GNP10 is different than with GNP 5. In the case of 15 nt, unzipping with GNP10 is achieved within 4 min, which is faster than with GNP5. Shearing of 15 nt with GNP10 shows significant dehybridization compared with shearing with GNP5. Other DNA lengths do not significant dehybridize within the application time of 10 min. These results agrees with the increment of the GNP size, which leads to a surface-charge increment. If the surface-charge increases, the electrophoretic

force increases. In turn, the time-scale for dehybridization or release are sped up as found. These results also demonstrate that the linkage between gold and DNA (which is due to the thiol modification) is stable under 100 V.

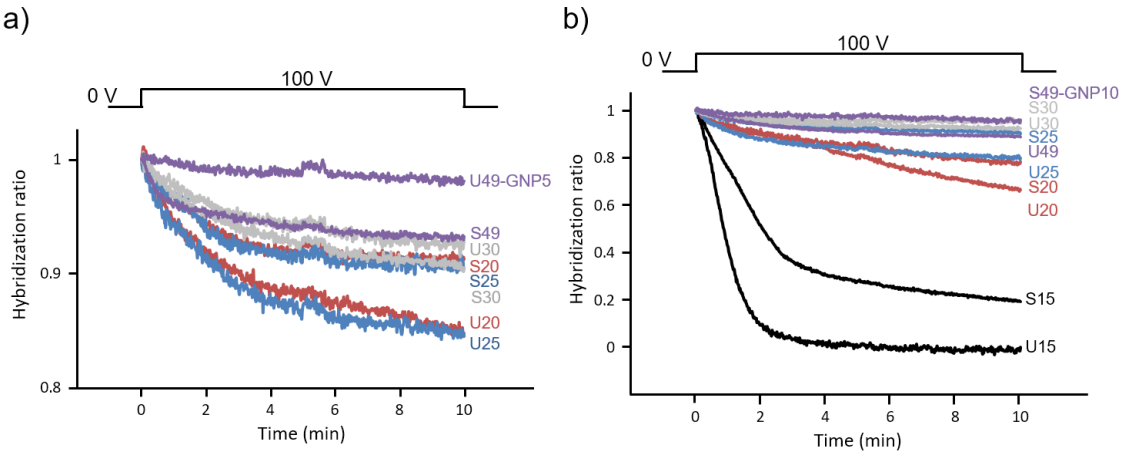

Figure 5.13: Unzipping and shearing for different DNA lengths and GNP under 100 V. a) With 5 nm GNP. b) With 10 nm GNP.

To prove the effect of GNPs under voltage, a control experiment without GNP is realized. In particular, 100 V are applied on 15 nt DNA modified with FAM and observed by fluorescent microscopy (Figure 5.14). The FAM intensity change over time is not significant; it decreases about 10% within 10 min. This result supports the effect of GNP, because the electric field of 25 V cm^{-1} is too weak for dehybridizing the bare DNA duplex (without GNP) as compared with the theoretical required electric field for dehybridization. The required electric field can be calculated considering the free energy of the DNA duplex and the electrical work on the negative charge backbone done by the external electric field. The required field has an

order magnitude of 10^4 V cm^{-1} (this is also in the same order as shown by a statistical mechanics [170]). This order of magnitude is two orders greater than the one in the present experiments. In summary, this results suggests that the DNA duplex alone is stable enough under electric field, and that when using GNP it is possible to drive the dehybridization of the DNA duplex.

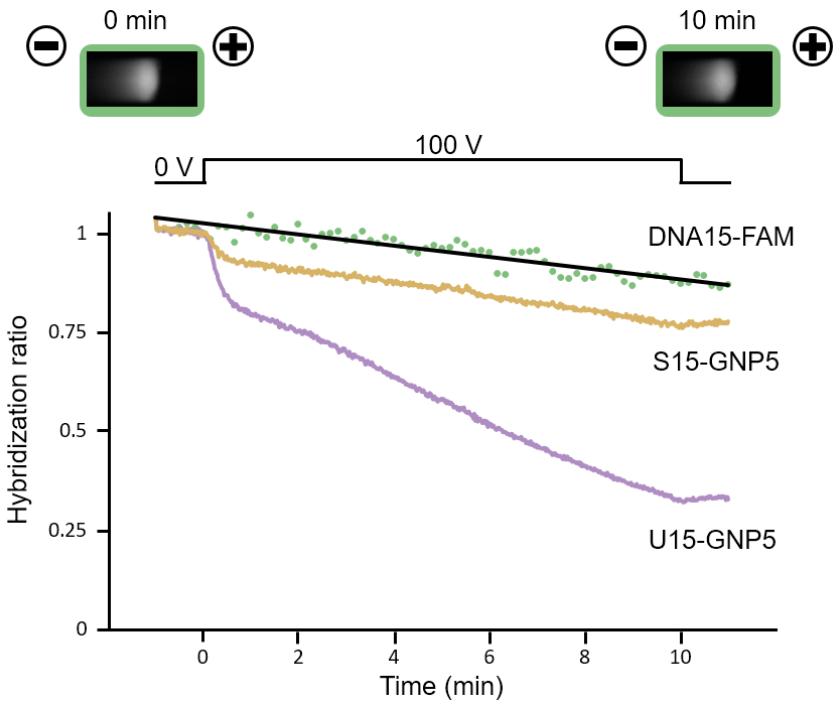

Figure 5.14: Fluorescent microscope of DNA with FAM molecule at its 5' end under 100V.

It is also possible to calculate the electrophoretic force on the GNPs. By assuming a constant surface charge density of the GNP [171,172] and evaluating based on the measured zeta potential (-42 ± 1 mV for GNP5 is obtained in water with 10xBSPP by using Zetasizer Nano (Malvern) under default conditions), the obtained force is approximately 11 fN. This fN force

order of magnitude agrees with the gradual dehybridization or release of DNA-GNPs. Furthemore, this agrees with the claim that any force magnitude can drive DNA dehybridization given sufficient application time [151], which is 10 min in the present experiments.

5.6 Conclusions

DNA dehybridization in hydrogel have been achieved by using electrophoretic force on negatively-charged GNPs (electric field of 25 V cm^{-1}). The gradual release of unzipping molecule was faster than shearing, which indicated that unzipping configuration is weaker than shearing as reported by optical trapping fields [152]. For the first-time, it was demonstrated that the hybridization ratio depends on the voltage application time.

In the future, GNPs will be used as electromechanical actuators. The proposed method will be applied in real-world devices for DNA computing, theragnostics (therapeutics/diagnosis) and mechanobiology. For example, by using metastable DNA molecules such as DNA hairpins [173,174], seesaw gates [175] or DNA origami [176], reusable DNA molecular circuits will be realized. The release of DNA-GNP will be used for simultaneous cell poration and DNA vaccine delivery in cells [177]. The propsed experimental setup is general and can be applied with other types of hydrogels,[156][178] microfluidics [179,180] and nanofabrication [181-183]. This method will contribute to

DNA nanotechnology for manipulating DNA molecules in a sequence-specific manner.

This chapter is summarized with the Table 5.2.

Table 5.2: Summary of the method proposed and demonstrated in this chapter.

METHOD	INTERACTION Applied	STRUCTURE Fabricated	FUNCTION Achieved
4	Electric • Gold nanoparticle electrophoresis • Tensile force on DNA duplex	DNA-integrated hydrogel • Hydrogel with anchored DNA duplexes	Decomposition (Dehybridization and release from hydrogel) • Sequence-specific control (tested with sequences from 15 nt to 49 nt) • Dehybridization modes (unzipping/shearing) • Unzipping is faster than shearing

6

Conclusions of This Thesis

The main question of this thesis, "how to use physico-chemical interactions for novel dynamic structures?", has been answered by designing 4 methods for dynamic DNA structures. These four methods were published in five papers from peer-reviewed journals including the PCCP of the Royal Society of Chemistry, ChemBioChem of John Wiley & Sons, and Nanomaterials of MDPI.

The four methods presented opens new directions for the state of the art. The four methods are summarized in the following Table 6.1, which adds to the methods showed in Introduction chapter.

Table 6.1: Novel methods presented in this thesis. It can be read as "physico-chemical interaction X is applied on structures fabricated with Y to achieve function Z"

METHOD	INTERACTION Applied	STRUCTURE Fabricated	FUNCTION Achieved
1	Mechanical force (molecular)	DNA origami	Self-assembly
2.1	Hydrophobicity	DNA tiles	Separation
2.2	Mechanical force (macro-scale)	DNA origami	Self-assembly
3	UV light	DNA hydrogel	Gel-sol transition
4	Electric	DNA-integrated hydrogel	Decomposition

Specific conclusions are shown in each chapter conclusion section. However, here the main conclusions are briefly described. In chapter 1, a

general background and specialized background are introduced to grasp the context of the thesis. Contents of this chapter belongs to the "Chapter 8 - Engineering DNA Molecules for Morphological Reconfiguration" in the book "Supra-Materials Nanoarchitectonics" [184].

In chapter 2, the self-assembly of rings made of shape-variable monomers has been studied by experiments and a chemical kinetic simulation of flexible monomers, which makes a first-time study of this type at the nanoscale. The diameter of the rings can range from 100 nm to 200 nm, which makes them useful as scaffold for long-term experimental investigations such microtubules running in circles. In the future, the design and construction of reconfigurable rings will be aided by our concept and simulations. Contents of this chapter belongs to the published peer-reviewed paper "Polymorphic Ring-Shaped Molecular Clusters Made of Shape-Variable Building Blocks" [29].

In chapter 3, I have shown, for the first-time, in-situ lipid-modification of DNA nanostructures deposited on surface substrate. DNA nanostructures became hydrophobic with its structural properties preserved. With this insight, it was developed an extraction method of DNA nanostructures from 2D surface to another 2D surface by 3D migration and novel flip-flop mechanism. Substantial extraction was obtained after 10 min. Hydrophobic DNA nanostructures were put at the air–water interface to form Langmuir–Blodgett

films. By applying pressure to the confined are at the air-water interface, hydrophobic nanostructures underwent supramolecular anisotropic self-assembly (1D self-assembly). The 1D self-assembly was controlled up to 2 μm after two compression/expansion cycles. In the future, with the help of the presented lipid-modification methods, researchers will extract sophisticated DNA devices from surfaces, create DNA architectures on complex patterns, and use the LB film to actuate by pressure multi-degrees-of-freedom 2D and 3D structures. Contents of this chapter belongs to two published peer-reviewed paper "In situ 2D-extraction of DNA wheels by 3D through-solution transport" [185] and "Supra molecular 1-D polymerization of DNA origami through a dynamic process at the 2-dimensionally confined air–water interface" [115].

In chapter 4, for the first time, a novel DNA hydrogel with designed gel-sol phase transition properties based on reversible photo reaction when irradiating UV light was implemented. It was found that the minimum concentration for each DNA component should be as low as 40 μM. Gel-sol transitions were observed for at least 5 cycles. In the future, the proposed photo-responsive hydrogel will be useful as medical device in applications including drug delivery and molecular diagnostics by delivering sensing molecules in cells. The reversible gel-sol transition will be utilized as a mechanical actuator in biochemical-mechanical devices, i.e. molecular robots [68]. Contents of this chapter belongs to the published peer-reviewed paper "Reversible Gel–Sol Transition of a Photo-Responsive DNA Gel" [186].

In chapter 5, I have achieved DNA dehybridization in hydrogel by using electrophoretic force on negatively-charged GNPs (electric field of 25 V cm $^{-1}$). The gradual release of unzipping molecule was faster than shearing. For the first-time, it was shown that the hybridization ratio depends on the voltage application time. In the future, GNPs will be used as electromechanical actuators, and our proposed method will be applied in real-world devices for DNA computing including resetting the logic-circuitry of slime-type molecular robots [68], theragnostics (therapeutics/diagnosis) and mechanobiology using hydrogels. Contents of this chapter belongs to the published peer-reviewed paper "Unzipping and Shearing DNA with Electrophoresed Nanoparticle in Hydrogel" [187].

References

[1] Buriak, J. M., 2016, "2016 Chemistry Nobel Prize - Molecular Machines Are Real," Chem. Mater., 28(20), pp. 7179–7180.

[2] 2016, "Foresight Institute Feynman Prize in Nanotechnology," Wikipedia.

[3] Watson, J. D., and Crick, F. H. C., 1953, "Molecular Structure of Nucleic Acids: A Structure for Deoxyribose Nucleic Acid," Nature, 171(4356), pp. 737–738.

[4] Sander, J. D., and Joung, J. K., 2014, "CRISPR-Cas Systems for Editing, Regulating and Targeting Genomes," Nat. Biotechnol., 32(4), pp. 347–355.

[5] Bloomfield, V. A., Crothers, D. M., and Tinoco, I., 2000, Nucleic Acids: Structures, Properties, and Functions, University Science Books.

[6] Mergny, J.-L., and Lacroix, L., 2003, "Analysis of Thermal Melting Curves," Oligonucleotides, 13(6), pp. 515–537.

[7] Smith, S. B., Cui, Y., and Bustamante, C., 1996, "Overstretching B-DNA: The Elastic Response of Individual Double-Stranded and Single-Stranded DNA Molecules," Science, 271(5250), pp. 795–799.

[8] Egli, M., and Saenger, W., 1988, Principles of Nucleic Acid Structure, Springer, New York.

[9] Genereux, J. C., and Barton, J. K., 2010, "Mechanisms for DNA Charge Transport," Chem. Rev., 110(3), pp. 1642–1662.

[10] O'Brien, E., Holt, M. E., Thompson, M. K., Salay, L. E., Ehlinger, A. C., Chazin, W. J., and Barton, J. K., 2017, "The [4Fe4S] Cluster of Human DNA Primase Functions as a Redox Switch Using DNA Charge Transport," Science, 355(6327), p. eaag1789.

[11] Xiang, L., Palma, J. L., Li, Y., Mujica, V., Ratner, M. A., and Tao, N., 2017, "Gate-Controlled Conductance Switching in DNA," Nat. Commun., 8, p. 14471.

[12] Seeman, N. C., 2003, "DNA in a Material World," Nature, 421(6921), pp. 427–431.

[13] Winfree, E., Liu, F., Wenzler, L. A., and Seeman, N. C., 1998, "Design and Self-Assembly of Two-Dimensional DNA Crystals," Nature, 394(6693), pp. 539–544.

[14] Evans, C. G., Hariadi, R. F., and Winfree, E., 2012, "Direct Atomic Force Microscopy Observation of DNA Tile Crystal Growth at the Single-Molecule Level," J. Am. Chem. Soc., 134(25), pp. 10485–10492.

[15] Rothemund, P. W. K., 2006, "Folding DNA to Create Nanoscale Shapes and Patterns," Nature, 440(7082), pp. 297–302.

[16] Castro, C. E., Kilchherr, F., Kim, D.-N., Shiao, E. L., Wauer, T., Wortmann, P., Bathe, M., and Dietz, H., 2011, "A Primer to Scaffolded DNA Origami," Nat. Methods, 8(3), pp. 221–229.

[17] Woo, S., and Rothemund, P. W. K., 2011, "Programmable Molecular Recognition Based on the Geometry of DNA Nanostructures," Nat. Chem., 3(8), pp. 620–627.

[18] Marchi, A. N., Saaem, I., Vogen, B. N., Brown, S., and LaBean, T. H., 2014, "Toward Larger DNA Origami," Nano Lett., 14(10), pp. 5740–5747.

[19] Dietz, H., Douglas, S. M., and Shih, W. M., 2009, "Folding DNA into Twisted and Curved Nanoscale Shapes," Science, 325(5941), pp. 725–730.

[20] Han, D., Pal, S., Nangreave, J., Deng, Z., Liu, Y., and Yan, H., 2011, "DNA Origami with Complex Curvatures in Three-Dimensional Space," Science, 332(6027), pp. 342–346.

[21] Ke, Y., Douglas, S. M., Liu, M., Sharma, J., Cheng, A., Leung, A., Liu, Y., Shih, W. M., and Yan, H., 2009, "Multilayer DNA Origami Packed on a Square Lattice," J. Am. Chem. Soc., 131(43), pp. 15903–15908.

[22] Ke, Y., Voigt, N. V., Gothelf, K. V., and Shih, W. M., 2012, "Multilayer DNA Origami Packed on Hexagonal and Hybrid Lattices," J. Am. Chem. Soc., 134(3), pp. 1770–1774.

[23] Zhang, F., Jiang, S., Wu, S., Li, Y., Mao, C., Liu, Y., and Yan, H., 2015, "Complex Wireframe DNA Origami Nanostructures with Multi-Arm Junction Vertices," Nat. Nanotechnol., 10(9), pp. 779–784.

[24] Benson, E., Mohammed, A., Gardell, J., Masich, S., Czeizler, E., Orponen, P., and Högberg, B., 2015, "DNA Rendering of Polyhedral Meshes at the Nanoscale," Nature, 523(7561), pp. 441–444.

[25] Douglas, S. M., Dietz, H., Liedl, T., Högberg, B., Graf, F., and Shih, W. M., 2009, "Self-Assembly of DNA into Nanoscale Three-Dimensional Shapes," Nature, 459(7245), pp. 414–418.

[26] Padirac, A., Fujii, T., and Rondelez, Y., 2013, "Nucleic Acids for the Rational Design of Reaction Circuits," Curr. Opin. Biotechnol., 24(4), pp. 575–580.

[27] Li, J., Wijeratne, S. S., Qiu, X., and Kiang, C.-H., 2015, "DNA under Force: Mechanics, Electrostatics, and Hydration," Nanomaterials, 5(1), pp. 246–267.

[28] Zhou, L., Marras, A. E., Su, H.-J., and Castro, C. E., 2015, "Direct Design of an Energy Landscape with Bistable DNA Origami Mechanisms," Nano Lett.

[29] Cervantes-Salguero, K., Hamada, S., Nomura, S. M., and Murata, S., 2015, "Polymorphic Ring-Shaped Molecular Clusters Made of Shape-Variable Building Blocks," Nanomaterials, 5(1), pp. 208–217.

[30] Zhou, L., Marras, A. E., Su, H.-J., and Castro, C. E., 2013, "DNA Origami Compliant Nanostructures with Tunable Mechanical Properties," ACS Nano, 8(1), pp. 27–34.

[31] Liedl, T., Högberg, B., Tytell, J., Ingber, D. E., and Shih, W. M., 2010, "Self-Assembly of Three-Dimensional Prestressed Tensegrity Structures from DNA," Nat. Nanotechnol., 5(7), pp. 520–524.

[32] Yurke, B., Turberfield, A. J., Mills, A. P., Simmel, F. C., and Neumann, J. L., 2000, "A DNA-Fuelled Molecular Machine Made of DNA," Nature, 406(6796), pp. 605–608.

[33] Zhang, D. Y., and Winfree, E., 2009, "Control of DNA Strand Displacement Kinetics Using Toehold Exchange," J. Am. Chem. Soc., 131(47), pp. 17303–17314.

[34] Zhang, D. Y., and Seelig, G., 2011, "Dynamic DNA Nanotechnology Using Strand-Displacement Reactions," Nat. Chem., 3(2), pp. 103–113.

[35] Kuzuya, A., Sakai, Y., Yamazaki, T., Xu, Y., and Komiyama, M., 2011, "Nanomechanical DNA Origami 'Single-Molecule Beacons' Directly Imaged by Atomic Force Microscopy," Nat. Commun., 2, p. 449.

[36] Marras, A. E., Zhou, L., Su, H.-J., and Castro, C. E., 2015, "Programmable Motion of DNA Origami Mechanisms," Proc. Natl. Acad. Sci., p. 201408869.

[37] List, J., Weber, M., and Simmel, F. C., 2014, "Hydrophobic Actuation of a DNA Origami Bilayer Structure," Angew. Chem. Int. Ed., p. n/a-n/a.

[38] Rajendran, A., Endo, M., Hidaka, K., and Sugiyama, H., 2013, "Direct and Real-Time Observation of Rotary Movement of a DNA Nanomechanical Device," J. Am. Chem. Soc., 135(3), pp. 1117–1123.

[39] Tanaka, F., Mochizuki, T., Liang, X., Asanuma, H., Tanaka, S., Suzuki, K., Kitamura, S., Nishikawa, A., Ui-Tei, K., and Hagiya, M., 2010, "Robust and Photocontrollable DNA Capsules Using Azobenzenes," Nano Lett, 10(9), pp. 3560–3565.

[40] Sato, Y., Hiratsuka, Y., Kawamata, I., Murata, S., and Nomura, S. M., 2017, "Micrometer-Sized Molecular Robot Changes Its Shape in Response to Signal Molecules," Sci. Robot., 2(4), p. eaal3735.

[41] Murakami, Y., and Maeda, M., 2005, "DNA-Responsive Hydrogels That Can Shrink or Swell," Biomacromolecules, 6(6), pp. 2927–2929.

[42] Baccouche, A., Montagne, K., Padirac, A., Fujii, T., and Rondelez, Y., 2014, "Dynamic DNA-Toolbox Reaction Circuits: A Walkthrough," Methods, 67(2), pp. 234–249.

[43] Braich, R. S., Chelyapov, N., Johnson, C., Rothemund, P. W. K., and Adleman, L., 2002, "Solution of a 20-Variable 3-SAT Problem on a DNA Computer," Science, 296(5567), pp. 499–502.

[44] Klapper, Y., Sinha, N., Ng, T. W. S., and Lubrich, D., 2010, "A Rotational DNA Nanomotor Driven by an Externally Controlled Electric Field," Small, 6(1), pp. 44–47.

[45] Hamad-Schifferli, K., Schwartz, J. J., Santos, A. T., Zhang, S., and Jacobson, J. M., 2002, "Remote Electronic Control of DNA Hybridization through Inductive Coupling to an Attached Metal Nanocrystal Antenna," Nature, 415(6868), pp. 152–155.

[46] Wang, T., Sha, R., Dreyfus, R., Leunissen, M. E., Maass, C., Pine, D. J., Chaikin, P. M., and Seeman, N. C., 2011, "Self-Replication of Information-Bearing Nanoscale Patterns," Nature, 478(7368), pp. 225–228.

[47] Liang, X., Zhou, M., Kato, K., and Asanuma, H., 2013, "Photoswitch Nucleic Acid Catalytic Activity by Regulating Topological Structure with a Universal Supraphotoswitch," ACS Synth. Biol., 2(4), pp. 194–202.

[48] Kamiya, Y., and Asanuma, H., 2014, "Light-Driven DNA Nanomachine with a Photoresponsive Molecular Engine," Acc. Chem. Res.

[49] Ogura, Y., Nishimura, T., and Tanida, J., 2009, "Self-Contained Photonically-Controlled DNA Tweezers," Appl. Phys. Express, 2(2), p. 025004.

[50] Cademartiri, L., Bishop, K. J. M., Snyder, P. W., and Ozin, G. A., 2012, "Using Shape for Self-Assembly," Philos. T rans. R. Soc. Lond. Math. Phys. Eng. Sci., 370(1969), pp. 2824–2847.

[51] Sacanna, S., Pine, D. J., and Yi, G.-R., 2013, "Engineering Shape: The Novel Geometries of Colloidal Self-Assembly," Soft Matter.

[52] Glotzer, S. C., and Solomon, M. J., 2007, "Anisotropy of Building Blocks and Their Assembly into Complex Structures," Nat. Mater., 6(8), pp. 557–562.

[53] Kim, J.-W., Kim, J.-H., and Deaton, R., 2011, "FIJA-DNA-Linked Nanoparticle Building Blocks for Programmable Matter," Angew. Chem. Int. Ed., 50(39), pp. 9185–9190.

[54] Wang, Y., Wang, Y., Breed, D. R., Manoharan, V. N., Feng, L., Hollingsworth, A. D., Weck, M., and Pine, D. J., 2012, "Colloids with Valence and Specific Directional Bonding," Nature, 491(7422), pp. 51–55.

[55] Zhang, C., Macfarlane, R. J., Young, K. L., Choi, C. H. J., Hao, L., Auyeung, E., Liu, G., Zhou, X., and Mirkin, C. A., 2013, "A General Approach to DNA-Programmable Atom Equivalents," Nat. Mater., advance online publication.

[56] Walker, D. A., Leitsch, E. K., Nap, R. J., Szleifer, I., and Grzybowski, B. A., 2013, "Geometric Curvature Controls the Chemical Patchiness and Self-Assembly of Nanoparticles," Nat. Nanotechnol., 8(9), pp. 676–681.

[57] Mao, C., Thalladi, V. R., Wolfe, D. B., Whitesides, S., and Whitesides, G. M., 2002, "Dissections: Self-Assembled Aggregates That Spontaneously Reconfigure Their Structures When Their Environment Changes," J. Am. Chem. Soc., 124(49), pp. 14508-14509.

[58] He, Y., Ye, T., Su, M., Zhang, C., Ribbe, A. E., Jiang, W., and Mao, C., 2008, "Hierarchical Self-Assembly of DNA into Symmetric Supramolecular Polyhedra," Nature, 452(7184), pp. 198–201.

[59] Sacanna, S., Irvine, W. T. M., Chaikin, P. M., and Pine, D. J., 2010, "Lock and Key Colloids," Nature, 464(7288), pp. 575–578.

[60] Yoo, J.-W., and Mitragotri, S., 2010, "Polymer Particles That Switch Shape in Response to a Stimulus," Proc. Natl. Acad. Sci., 107(25), pp. 11205–11210.

[61] Lee, K. J., Yoon, J., Rahmani, S., Hwang, S., Bhaskar, S., Mitragotri, S., and Lahann, J., 2012, "Spontaneous Shape Reconfigurations in Multicompartmental Microcylinders," Proc. Natl. Acad. Sci., 109(40), pp. 16057–16062.

[62] Murata, S., and Kurokawa, H., 2007, "Self-Reconfigurable Robots," IEEE Robot. Autom. Mag., 14(1), pp. 71–78.

[63] Nguyen, T. D., and Glotzer, S. C., 2010, "Reconfigurable Assemblies of Shape-Changing Nanorods," ACS Nano, 4(5), pp. 2585–2594.

[64] Nguyen, T. D., Jankowski, E., and Glotzer, S. C., 2011, "Self-Assembly and Reconfigurability of Shape-Shifting Particles," ACS Nano, 5(11), pp. 8892–8903.

[65] Gang, O., and Zhang, Y., 2011, "Shaping Phases by Phasing Shapes," ACS Nano, 5(11), pp. 8459–8465.

[66] Guo, R., Liu, Z., Xie, X.-M., and Yan, L.-T., 2013, "Harnessing Dynamic Covalent Bonds in Patchy Nanoparticles: Creating Shape-Shifting Building Blocks for Rational and Responsive Self-Assembly," J. Phys. Chem. Lett., 4(8), pp. 1221–1226.

[67] Kohlstedt, K. L., and Glotzer, S. C., 2013, "Self-Assembly and Tunable Mechanics of Reconfigurable Colloidal Crystals," Phys. Rev. E, 87(3), p. 032305.

[68] Hagiya, M., Konagaya, A., Kobayashi, S., Saito, H., and Murata, S., 2014, "Molecular Robots with Sensors and Intelligence," Acc. Chem. Res., 47(6), pp. 1681–1690.

[69] Bombelli, F. B., Gambinossi, F., Lagi, M., Berti, D., Caminati, G., Brown, T., Sciortino, F., Nordén, B., and Baglioni, P., 2008, "DNA Closed Nanostructures: A Structural and Monte Carlo Simulation Study," J. Phys. Chem. B, 112(48), pp. 15283–15294.

[70] Yin, P., Hariadi, R. F., Sahu, S., Choi, H. M. T., Park, S. H., LaBean, T. H., and Reif, J. H., 2008, "Programming DNA Tube Circumferences," Science, 321(5890), pp. 824–826.

[71] Hamada, S., and Murata, S., 2009, "Substrate-Assisted Assembly of Interconnected Single-Duplex DNA Nanostructures," Angew. Chem., 121(37), pp. 6952–6955.

[72] Hosokawa, K., "Dynamics of Self-Assembling Systems - Analogy with Chemical Kinetics."

[73] Hariadi, R. F., Appukutty, A. J., and Sivaramakrishnan, S., 2016, "Engineering Circular Gliding of Actin Filaments Along Myosin-Patterned DNA Nanotube Rings To Study Long-Term Actin–Myosin Behaviors," ACS Nano, 10(9), pp. 8281–8288.

[74] Pinheiro, A. V., Han, D., Shih, W. M., and Yan, H., 2011, "Challenges and Opportunities for Structural DNA Nanotechnology," Nat. Nanotechnol., 6(12), pp. 763–772.

[75] Zhang, F., Nangreave, J., Liu, Y., and Yan, H., 2014, "Structural DNA Nanotechnology: State of the Art and Future Perspective," J. Am. Chem. Soc., 136(32), pp. 11198–11211.

[76] Ma, Y., Zheng, H., Wang, C., Yan, Q., Chao, J., Fan, C., and Xiao, S.-J., 2013, "RCA Strands as Scaffolds To Create Nanoscale Shapes by a Few Staple Strands," J. Am. Chem. Soc., 135(8), pp. 2959–2962.

[77] Gates, E. P., Jensen, J. K., Harb, J. N., and Woolley, A. T., 2015, "Optimizing Gold Nanoparticle Seeding Density on DNA Origami," RSC Adv., 5(11), pp. 8134–8141.

[78] Koirala, D., Shrestha, P., Emura, T., Hidaka, K., Mandal, S., Endo, M., Sugiyama, H., and Mao, H., 2014, "Single-Molecule Mechanochemical Sensing Using DNA Origami Nanostructures," Angew. Chem., 126(31), pp. 8275–8279.

[79] Deng, Z., Samanta, A., Nangreave, J., Yan, H., and Liu, Y., 2012, "Robust DNA-Functionalized Core/Shell Quantum Dots with Fluorescent Emission Spanning from UV–vis to Near-IR and Compatible with DNA-Directed Self-Assembly," J. Am. Chem. Soc., 134(42), pp. 17424–17427.

[80] Vesenka, J., Guthold, M., Tang, C. L., Keller, D., Delaine, E., and Bustamante, C., 1992, "Substrate Preparation for Reliable Imaging of DNA Molecules with the Scanning Force Microscope," Ultramicroscopy, 42, pp. 1243–1249.

[81] Börjesson, K., Lundberg, E. P., Woller, J. G., Nordén, B., and Albinsson, B., 2011, "Soft-Surface DNA Nanotechnology: DNA Constructs Anchored and Aligned to Lipid Membrane," Angew. Chem. Int. Ed., 50(36), pp. 8312–8315.

[82] Langecker, M., Arnaut, V., Martin, T. G., List, J., Renner, S., Mayer, M., Dietz, H., and Simmel, F. C., 2012, "Synthetic Lipid Membrane Channels Formed by Designed DNA Nanostructures," Science, 338(6109), pp. 932–936.

[83] Burns, J. R., Stulz, E., and Howorka, S., 2013, "Self-Assembled DNA Nanopores That Span Lipid Bilayers," Nano Lett., 13(6), pp. 2351–2356.

[84] Suzuki, Y., Endo, M., Katsuda, Y., Ou, K., Hidaka, K., and Sugiyama, H., 2014, "DNA Origami Based Visualization System for Studying Site-Specific Recombination Events," J. Am. Chem. Soc., 136(1), pp. 211–218.

[85] Czogalla, A., Kauert, D. J., Seidel, R., Schwille, P., and Petrov, E. P., 2015, "DNA Origami Nanoneedles on Freestanding Lipid Membranes as a Tool To Observe Isotropic–Nematic Transition in Two Dimensions," Nano Lett., 15(1), pp. 649–655.

[86] Langecker, M., Arnaut, V., List, J., and Simmel, F. C., 2014, "DNA Nanostructures Interacting with Lipid Bilayer Membranes," Acc. Chem. Res., 47(6), pp. 1807–1815.

[87] Tanaka, K., and Okahata, Y., 1996, "A DNA-Lipid Complex in Organic Media and Formation of an Aligned Cast Film1," J. Am. Chem. Soc., 118(44), pp. 10679–10683.

[88] Yonamine, Y., Kawasaki, T., and Okahata, Y., 2009, "Covalent Modification of DNA with Azetidinium Lipids," Chem. Lett., 39(2), pp. 84–85.

[89] Kershner, R. J., Bozano, L. D., Micheel, C. M., Hung, A. M., Fornof, A. R., Cha, J. N., Rettner, C. T., Bersani, M., Frommer, J., Rothemund, P. W. K., and Wallraff, G. M., 2009, "Placement and Orientation of Individual DNA Shapes on Lithographically Patterned Surfaces," Nat. Nanotechnol., 4(9), pp. 557–561.

[90] Hung, A. M., Micheel, C. M., Bozano, L. D., Osterbur, L. W., Wallraff, G. M., and Cha, J. N., 2010, "Large-Area Spatially Ordered Arrays of Gold Nanoparticles Directed by Lithographically Confined DNA Origami," Nat. Nanotechnol., 5(2), pp. 121–126.

[91] Endo, M., Sugita, T., Katsuda, Y., Hidaka, K., and Sugiyama, H., 2010, "Programmed-Assembly System Using DNA Jigsaw Pieces," Chem. – Eur. J., 16(18), pp. 5362–5368.

[92] Rajendran, A., Endo, M., Katsuda, Y., Hidaka, K., and Sugiyama, H., 2011, "Programmed Two-Dimensional Self-Assembly of Multiple DNA Origami Jigsaw Pieces," ACS Nano, 5(1), pp. 665–671.

[93] Endo, M., Sugita, T., Rajendran, A., Katsuda, Y., Emura, T., Hidaka, K., and Sugiyama, H., 2011, "Two-Dimensional DNA Origami Assemblies Using a Four-Way Connector," Chem. Commun., 47(11), pp. 3213–3215.

[94] Liu, W., Zhong, H., Wang, R., and Seeman, N. C., 2011, "Crystalline Two-Dimensional DNA-Origami Arrays," Angew. Chem. Int. Ed., 50(1), pp. 264–267.

[95] Li, Z., Liu, M., Wang, L., Nangreave, J., Yan, H., and Liu, Y., 2010, "Molecular Behavior of DNA Origami in Higher-Order Self-Assembly," J. Am. Chem. Soc., 132(38), pp. 13545–13552.

[96] Deng, Z., and Mao, C., 2004, "Molecular Lithography with DNA Nanostructures," Angew. Chem. Int. Ed., 43(31), pp. 4068–4070.

[97] Hamada, S., and Murata, S., 2012, "Theoretical Model of Substrate-Assisted Self-Assembly of DNA Nanostructures," RSC Adv., 2(19), pp. 7406–7412.

[98] Aghebat Rafat, A., Pirzer, T., Scheible, M. B., Kostina, A., and Simmel, F. C., 2014, "Surface-Assisted Large-Scale Ordering of DNA Origami Tiles," Angew. Chem. Int. Ed., 53(29), pp. 7665–7668.

[99] Woo, S., and Rothemund, P. W. K., 2014, "Self-Assembly of Two-Dimensional DNA Origami Lattices Using Cation-Controlled Surface Diffusion," Nat. Commun., 5.

[100] Kocabey, S., Kempter, S., List, J., Xing, Y., Bae, W., Schiffels, D., Shih, W. M., Simmel, F. C., and Liedl, T., 2015, "Membrane-Assisted Growth of DNA Origami Nanostructure Arrays," ACS Nano, 9(4), pp. 3530–3539.

[101] Suzuki, Y., Endo, M., and Sugiyama, H., 2015, "Lipid-Bilayer-Assisted Two-Dimensional Self-Assembly of DNA Origami Nanostructures," Nat. Commun., 6, p. 8052.

[102] Lee, J., Kim, S., Kim, J., Lee, C.-W., Roh, Y., and Park, S. H., 2011, "Coverage Control of DNA Crystals Grown by Silica Assistance," Angew. Chem. Int. Ed., 50(39), pp. 9145–9149.

[103] Sun, X., Hyeon Ko, S., Zhang, C., Ribbe, A. E., and Mao, C., 2009, "Surface-Mediated DNA Self-Assembly," J. Am. Chem. Soc., 131(37), pp. 13248–13249.

[104] Ariga, K., Yamauchi, Y., Mori, T., and Hill, J. P., 2013, "25th Anniversary Article: What Can Be Done with the Langmuir-Blodgett Method? Recent Developments and Its Critical Role in Materials Science," Adv. Mater., 25(45), pp. 6477–6512.

[105] Mori, T., Okamoto, K., Endo, H., Hill, J. P., Shinoda, S., Matsukura, M., Tsukube, H., Suzuki, Y., Kanekiyo, Y., and Ariga, K., 2010, "Mechanical Tuning of Molecular Recognition To Discriminate the Single-Methyl-Group Difference between Thymine and Uracil," J. Am. Chem. Soc., 132(37), pp. 12868–12870.

[106] Sakakibara, K., Joyce, L. A., Mori, T., Fujisawa, T., Shabbir, S. H., Hill, J. P., Anslyn, E. V., and Ariga, K., 2012, "A Mechanically Controlled Indicator Displacement Assay," Angew. Chem. Int. Ed., 51(38), pp. 9643–9646.

[107] Ishikawa, D., Mori, T., Yonamine, Y., Nakanishi, W., Cheung, D. L., Hill, J. P., and Ariga, K., 2015, "Mechanochemical Tuning of the Binaphthyl Conformation at the Air–Water Interface," Angew. Chem. Int. Ed., 54(31), pp. 8988–8991.

[108] Finch, A. S., Anton, C. M., Jacob, C. M., Proctor, T. J., and Stratis-Cullum, D. N., 2012, "Assembly of DNA Architectures in a Non-Aqueous Solution," Nanomaterials, 2(3), pp. 275–285.

[109] Okuyama, K., Soboi, Y., Hirabayashi, K., Harada, A., Kumano, A., Kaziyama, T., Takayanagi, M., and Kunitake, T., 1984, "Single Crystals of Totally Synthetic Amphiphiles, Dialkyldimethylammonium Bromides," Chem. Lett., 13(12), pp. 2117–2120.

[110] Rozenfeld, J. H. K., Duarte, E. L., Oliveira, T. R., Lonez, C., Ruysschaert, J.-M., and Lamy, M. T., 2013, "Oligonucleotide Adsorption Affects Phase Transition but Not Interdigitation of diC14-Amidine Bilayers," Langmuir, 29(35), pp. 11102–11108.

[111] Kim, H., Surwade, S. P., Powell, A., O'Donnell, C., and Liu, H., 2014, "Stability of DNA Origami Nanostructure under Diverse Chemical Environments," Chem. Mater.

[112] Herzer, N., Hoeppener, S., and Schubert, U. S., 2010, "Fabrication of Patterned Silane Based Self-Assembled Monolayers by Photolithography and Surface Reactions on Silicon-Oxide Substrates," Chem. Commun., 46(31), pp. 5634–5652.

[113] Malik, R., Burch, D., Bazant, M., and Ceder, G., 2010, "Particle Size Dependence of the Ionic Diffusivity," Nano Lett., 10(10), pp. 4123–4127.

[114] Dhôtel, A., Li, H., Fernandez-Ballester, L., Delbreilh, L., Youssef, B., Zeng, X. C., and Tan, L., 2011, "Supramolecular Nanolayer Reconfiguration after Molecular Intercalation," J. Phys. Chem. C, 115(21), pp. 10351–10356.

[115] Yonamine, Y., Cervantes-Salguero, K., Minami, K., Kawamata, I., Nakanishi, W., P. Hill, J., Murata, S., and Ariga, K., 2016, "Supramolecular 1-D Polymerization of DNA Origami through a Dynamic Process at the 2-Dimensionally Confined Air–water Interface," Phys. Chem. Chem. Phys., 18(18), pp. 12576–12581.

[116] Sukhorukov, G. B., Montrel, M. M., Petrov, A. I., Shabarchina, L. I., and Sukhorukov, B. I., 1996, "Multilayer Films Containing Immobilized Nucleic

Acids. Their Structure and Possibilities in Biosensor Applications," Biosens. Bioelectron., 11(9), pp. 913–922.

[117] Kajiyama, T., Oishi, Y., Uchida, M., Tanimoto, Y., and Kozuru, H., 1992, "Morphological and Structural Studies of Crystalline and Amorphous Monolayers on the Water Surface," Langmuir, 8(6), pp. 1563–1569.

[118] Onda, M., Yoshihara, K., Koyano, H., Ariga, K., and Kunitake, T., 1996, "Molecular Recognition of Nucleotides by the Guanidinium Unit at the Surface of Aqueous Micelles and Bilayers. A Comparison of Microscopic and Macroscopic Interfaces," J. Am. Chem. Soc., 118(36), pp. 8524–8530.

[119] Sakurai, M., Tamagawa, H., Inoue, Y., Ariga, K., and Kunitake, T., 1997, "Theoretical Study of Intermolecular Interaction at the Lipid-Water Interface. 1. Quantum Chemical Analysis Using a Reaction Field Theory," J. Phys. Chem. B, 101(24), pp. 4810–4816.

[120] Howorka, S., 2013, "DNA Nanoarchitectonics: Assembled DNA at Interfaces," Langmuir.

[121] Grzybowski, B. A., Stone, H. A., and Whitesides, G. M., 2000, "Dynamic Self-Assembly of Magnetized, Millimetre-Sized Objects Rotating at a Liquid–air Interface," Nature, 405(6790), pp. 1033–1036.

[122] Whitesides, G. M., and Grzybowski, B., 2002, "Self-Assembly at All Scales," Science, 295(5564), pp. 2418–2421.

[123] Yang, D., Hartman, M. R., Derrien, T. L., Hamada, S., An, D., Yancey, K. G., Cheng, R., Ma, M., and Luo, D., 2014, "DNA Materials: Bridging Nanotechnology and Biotechnology," Acc. Chem. Res., 47(6), pp. 1902–1911.

[124] Jiang, F. X., Yurke, B., Verma, D., Previtera, M., Schloss, R., and Langrana, N. A., 2011, "Development of DNA Based Active Macro–Materials for Biology and Medicine: A Review."

[125] Um, S. H., Lee, J. B., Park, N., Kwon, S. Y., Umbach, C. C., and Luo, D., 2006, "Enzyme-Catalysed Assembly of DNA Hydrogel," Nat. Mater., 5(10), pp. 797–801.

[126] Xing, Y., Cheng, E., Yang, Y., Chen, P., Zhang, T., Sun, Y., Yang, Z., and Liu, D., 2011, "Self-Assembled DNA Hydrogels with Designable Thermal and Enzymatic Responsiveness," Adv. Mater., 23(9), pp. 1117–1121.

[127] Lee, J. B., Peng, S., Yang, D., Roh, Y. H., Funabashi, H., Park, N., Rice, E. J., Chen, L., Long, R., Wu, M., and Luo, D., 2012, "A Mechanical Metamaterial Made from a DNA Hydrogel," Nat. Nanotechnol., 7(12), pp. 816–820.

[128] Rovigatti, L., Smallenburg, F., Romano, F., and Sciortino, F., 2014, "Gels of DNA Nanostars Never Crystallize," ACS Nano, 8(4), pp. 3567–3574.

[129] Liu, J., 2011, "Oligonucleotide-Functionalized Hydrogels as Stimuli Responsive Materials and Biosensors," Soft Matter, 7(15), pp. 6757–6767.

[130] Lin, D. C., Yurke, B., and Langrana, N. A., 2004, "Mechanical Properties of a Reversible, DNA-Crosslinked Polyacrylamide Hydrogel," J. Biomech. Eng., 126(1), pp. 104–110.

[131] Jiang, F. X., Yurke, B., Firestein, B. L., and Langrana, N. A., 2008, "Neurite Outgrowth on a DNA Crosslinked Hydrogel with Tunable Stiffnesses," Ann. Biomed. Eng., 36(9), p. 1565.

[132] Gao, M., Gawel, K., and Stokke, B. T., 2011, "Toehold of dsDNA Exchange Affects the Hydrogel Swelling Kinetics of a polymer–dsDNA Hybrid Hydrogel," Soft Matter, 7(5), pp. 1741–1746.

[133] Cheng, E., Xing, Y., Chen, P., Yang, Y., Sun, Y., Zhou, D., Xu, L., Fan, Q., and Liu, D., 2009, "A pH-Triggered, Fast-Responding DNA Hydrogel," Angew. Chem. Int. Ed., 48(41), pp. 7660–7663.

[134] Guo, W., Orbach, R., Mironi-Harpaz, I., Seliktar, D., and Willner, I., 2013, "Fluorescent DNA Hydrogels Composed of Nucleic Acid-Stabilized Silver Nanoclusters," Small, 9(22), pp. 3748–3752.

[135] Zhang, L., Lei, J., Liu, L., Li, C., and Ju, H., 2013, "Self-Assembled DNA Hydrogel as Switchable Material for Aptamer-Based Fluorescent Detection of Protein," Anal. Chem., 85(22), pp. 11077–11082.

[136] Kang, H., Liu, H., Zhang, X., Yan, J., Zhu, Z., Peng, L., Yang, H., Kim, Y., and Tan, W., 2011, "Photoresponsive DNA-Cross-Linked Hydrogels for Controllable Release and Cancer Therapy," Langmuir, 27(1), pp. 399–408.

[137] Yoshimura, Y., Ito, Y., and Fujimoto, K., 2005, "Interstrand Photocrosslinking of DNA via P-Carbamoylvinyl Phenol Nucleoside," Bioorg. Med. Chem. Lett., 15(5), pp. 1299–1301.

[138] Fujimoto, K., Yamada, A., Yoshimura, Y., Tsukaguchi, T., and Sakamoto, T., 2013, "Details of the Ultrafast DNA Photo-Cross-Linking Reaction of 3-Cyanovinylcarbazole Nucleoside: Cis–Trans Isomeric Effect and the Application for SNP-Based Genotyping," J. Am. Chem. Soc., 135(43), pp. 16161–16167.

[139] Yoshimura, Y., and Fujimoto, K., 2008, "Ultrafast Reversible Photo-Cross-Linking Reaction: Toward in Situ DNA Manipulation," Org. Lett., 10(15), pp. 3227–3230.

[140] Luo, D., and Roh, Y. H., 2012, "Photo-Crosslinked Nucleic Acid Hydrogels."

[141] Tagawa, M., Shohda, K., Fujimoto, K., and Suyama, A., 2011, "Stabilization of DNA Nanostructures by Photo-Cross-Linking," Soft Matter, 7(22), pp. 10931–10934.

[142] Kuijpers, A. J., Engbers, G. H. M., Meyvis, T. K. L., de Smedt, S. S. C., Demeester, J., Krijgsveld, J., Zaat, S. A. J., Dankert, J., and Feijen, J., 2000, "Combined Gelatin-Chondroitin Sulfate Hydrogels for Controlled Release of Cationic Antibacterial Proteins," Macromolecules, 33(10), pp. 3705–3713.

[143] Islam, M. A., 2004, "Einstein–Smoluchowski Diffusion Equation: A Discussion," Phys. Scr., 70(2–3), p. 120.

[144] Chirieleison, S. M., Allen, P. B., Simpson, Z. B., Ellington, A. D., and Chen, X., 2013, "Pattern Transformation with DNA Circuits," Nat. Chem., 5(12), pp. 1000–1005.

[145] Scalise, D., and Schulman, R., 2014, "Emulating Cellular Automata in Chemical Reaction-Diffusion Networks," DNA Computing and Molecular Programming, Springer, Cham, pp. 67–83.

[146] Zenk, J., Scalise, D., Wang, K., Dorsey, P., Fern, J., Cruz, A., and Schulman, R., 2017, "Stable DNA-Based Reaction–diffusion Patterns," RSC Adv., 7(29), pp. 18032–18040.

[147] Baltierra-Jasso, L. E., Morten, M. J., Laflör, L., Quinn, S. D., and Magennis, S. W., 2015, "Crowding-Induced Hybridization of Single DNA Hairpins," J. Am. Chem. Soc., 137(51), pp. 16020–16023.

[148] Bae, W., Kim, K., Min, D., Ryu, J.-K., Hyeon, C., and Yoon, T.-Y., 2014, "Programmed Folding of DNA Origami Structures through Single-Molecule Force Control," Nat. Commun., 5.

[149] Bleichert, F., Botchan, M. R., and Berger, J. M., 2017, "Mechanisms for Initiating Cellular DNA Replication," Science, 355(6327), p. eaah6317.

[150] Wang, X., and Ha, T., 2013, "Defining Single Molecular Forces Required to Activate Integrin and Notch Signaling," Science, 340(6135), pp. 991–994.

[151] Mosayebi, M., Louis, A. A., Doye, J. P. K., and Ouldridge, T. E., 2015, "Force-Induced Rupture of a DNA Duplex: From Fundamentals to Force Sensors," ACS Nano, 9(12), pp. 11993–12003.

[152] Lang, M. J., Fordyce, P. M., Engh, A. M., Neuman, K. C., and Block, S. M., 2004, "Simultaneous, Coincident Optical Trapping and Single-Molecule Fluorescence," Nat. Methods, 1(2), pp. 133–139.

[153] Hatch, K., Danilowicz, C., Coljee, V., and Prentiss, M., 2008, "Demonstration That the Shear Force Required to Separate Short Double-Stranded DNA Does Not Increase Significantly with Sequence Length for Sequences Longer than 25 Base Pairs," Phys. Rev. E, 78(1), p. 011920.

[154] Bustamante, C., Macosko, J. C., and Wuite, G. J. L., 2000, "Grabbing the Cat by the Tail: Manipulating Molecules One by One," Nat. Rev. Mol. Cell Biol., 1(2), pp. 130–136.

[155] Yang, D., Ward, A., Halvorsen, K., and Wong, W. P., 2016, "Multiplexed Single-Molecule Force Spectroscopy Using a Centrifuge," Nat. Commun., 7, p. 11026.

[156] Sosnowski, R. G., Tu, E., Butler, W. F., O'Connell, J. P., and Heller, M. J., 1997, "Rapid Determination of Single Base Mismatch Mutations in DNA Hybrids by Direct Electric Field Control," Proc. Natl. Acad. Sci., 94(4), pp. 1119–1123.

[157] Baeissa, A., Moghimi, N., and Liu, J., 2012, "Hydrogel Porosity Controlling DNA-Directed Immobilization of Gold Nanoparticles Revealed by DNA Melting and Scanning Helium Ion Microscopy," RSC Adv., 2(7), pp. 2981–2987.

[158] Sun, J.-Y., Zhao, X., Illeperuma, W. R. K., Chaudhuri, O., Oh, K. H., Mooney, D. J., Vlassak, J. J., and Suo, Z., 2012, "Highly Stretchable and Tough Hydrogels," Nature, 489(7414), pp. 133–136.

[159] Rehman, F. N., Audeh, M., Abrams, E. S., Hammond, P. W., Kenney, M., and Boles, T. C., 1999, "Immobilization of Acrylamide-Modified Oligonucleotides by Co-Polymerization," Nucleic Acids Res., 27(2), pp. 649–655.

[160] Brudno, Y., and Mooney, D. J., 2015, "On-Demand Drug Delivery from Local Depots," J. Controlled Release, 219, pp. 8–17.

[161] Kearney, C. J., and Mooney, D. J., 2013, "Macroscale Delivery Systems for Molecular and Cellular Payloads," Nat. Mater., 12(11), pp. 1004–1017.

[162] Roche, E. T., Horvath, M. A., Wamala, I., Alazmani, A., Song, S.-E., Whyte, W., Machaidze, Z., Payne, C. J., Weaver, J. C., Fishbein, G., Kuebler, J., Vasilyev, N. V., Mooney, D. J., Pigula, F. A., and Walsh, C. J., 2017, "Soft Robotic Sleeve Supports Heart Function," Sci. Transl. Med., 9(373), p. eaaf3925.

[163] Wang, D., Hu, Y., Liu, P., and Luo, D., 2017, "Bioresponsive DNA Hydrogels: Beyond the Conventional Stimuli Responsiveness," Acc. Chem. Res.

[164] Mahajan, S., Richardson, J., Brown, T., and Bartlett, P. N., 2008, "SERS-Melting: A New Method for Discriminating Mutations in DNA Sequences," J. Am. Chem. Soc., 130(46), pp. 15589–15601.

[165] Johnson, R. P., Gale, N., Richardson, J. A., Brown, T., and Bartlett, P. N., 2013, "Denaturation of dsDNA Immobilised at a Negatively Charged Gold Electrode Is Not Caused by Electrostatic Repulsion," Chem. Sci., 4(4), pp. 1625–1632.

[166] Trau, M., Saville, D. A., and Aksay, I. A., 1996, "Field-Induced Layering of Colloidal Crystals," Science, 272(5262), pp. 706–709.

[167] Barsotti, R. J., Vahey, M. D., Wartena, R., Chiang, Y.-M., Voldman, J., and Stellacci, F., 2007, "Assembly of Metal Nanoparticles into Nanogaps," Small, 3(3), pp. 488–499.

[168] Toma, H. E., Zamarion, V. M., Toma, S. H., and Araki, K., 2010, "The Coordination Chemistry at Gold Nanoparticles," J. Braz. Chem. Soc., 21(7), pp. 1158–1176.

[169] Ross, D., Gaitan, M., and Locascio, L. E., 2001, "Temperature Measurement in Microfluidic Systems Using a Temperature-Dependent Fluorescent Dye," Anal. Chem., 73(17), pp. 4117–4123.

[170] Hill, T. L., 1958, "Some Possible Biological Effects of an Electric Field Acting on Nucleic Acids or Proteins1," J. Am. Chem. Soc., 80(9), pp. 2142–2147.

[171] J. Hill, R., 2016, "Electrokinetics of Nanoparticle Gel-Electrophoresis," Soft Matter, 12(38), pp. 8030–8048.

[172] Agnihotri, S. M., Ohshima, H., Terada, H., Tomoda, K., and Makino, K., 2009, "Electrophoretic Mobility of Colloidal Gold Particles in Electrolyte Solutions," Langmuir, 25(8), pp. 4804–4807.

[173] Yin, P., Choi, H. M. T., Calvert, C. R., and Pierce, N. A., 2008, "Programming Biomolecular Self-Assembly Pathways," Nature, 451(7176), pp. 318–322.

[174] Zhang, Y., Ge, C., Zhu, C., and Salaita, K., 2014, "DNA-Based Digital Tension Probes Reveal Integrin Forces during Early Cell Adhesion," Nat. Commun., 5.

[175] Qian, L., and Winfree, E., 2011, "A Simple DNA Gate Motif for Synthesizing Large-Scale Circuits," J. R. Soc. Interface, p. rsif20100729.

[176] Gan, L., Camacho-Alanis, F., and Ros, A., 2015, "Polarizability of Six-Helix Bundle and Triangle DNA Origami and Their Escape Characteristics from a Dielectrophoretic Trap," Anal. Chem., 87(24), pp. 12059–12064.

[177] Draz, M. S., Wang, Y.-J., Chen, F. F., Xu, Y., and Shafiee, H., 2016, "Electrically Oscillating Plasmonic Nanoparticles for Enhanced DNA Vaccination against Hepatitis C Virus," Adv. Funct. Mater., p. 1604139.

[178] Kearney, C. J., Skaat, H., Kennedy, S. M., Hu, J., Darnell, M., Raimondo, T. M., and Mooney, D. J., 2015, "Switchable Release of Entrapped Nanoparticles from Alginate Hydrogels," Adv. Healthc. Mater., 4(11), pp. 1634–1639.

[179] Erickson, D., Liu, X., Krull, U., and Li, D., 2004, "Electrokinetically Controlled DNA Hybridization Microfluidic Chip Enabling Rapid Target Analysis," Anal. Chem., 76(24), pp. 7269–7277.

[180] Zangmeister, R. A., and Tarlov, M. J., 2004, "DNA Displacement Assay Integrated into Microfluidic Channels," Anal. Chem., 76(13), pp. 3655–3659.

[181] Santini, J. T., Cima, M. J., and Langer, R., 1999, "A Controlled-Release Microchip," Nature, 397(6717), pp. 335–338.

[182] Yoshida, R., Omata, K., Yamaura, K., Ebata, M., Tanaka, M., and Takai, M., 2006, "Maskless Microfabrication of Thermosensitive Gels Using a Microscope and Application to a Controlled Release Microchip," Lab. Chip, 6(10), pp. 1384–1386.

[183] Liu, J., Gao, D., Li, H.-F., and Lin, J.-M., 2009, "Controlled Photopolymerization of Hydrogel Microstructures inside Microchannels for Bioassays," Lab. Chip, 9(9), pp. 1301–1305.

[184] Cervantes-Salguero, K., and Murata, S., 2017, "Chapter 8 - Engineering DNA Molecules for Morphological Reconfiguration," Supra-Materials Nanoarchitectonics, William Andrew Publishing, pp. 195–206.

[185] Yonamine, Y., Cervantes-Salguero, K., Nakanishi, W., Kawamata, I., Minami, K., Komatsu, H., Murata, S., Hill, J. P., and Ariga, K., 2015, "In Situ 2D-Extraction of DNA Wheels by 3D through-Solution Transport," Phys. Chem. Chem. Phys.

[186] Kandatsu, D., Cervantes-Salguero, K., Kawamata, I., Hamada, S., Nomura, S. M., Fujimoto, K., and Murata, S., 2016, "Reversible Gel–Sol

Transition of a Photo-Responsive DNA Gel," ChemBioChem, 17(12), pp. 1118–1121.

[187] Cervantes-Salguero, K. A., Kawamata, I., Nomura, S. M., and Murata, S., 2017, "Unzipping and Shearing DNA with Electrophoresed Nanoparticle in Hydrogel," Phys. Chem. Chem. Phys.

List of Figures

List of Tables

A

Appendix

A Simulation of Abstract Flexible Monomers

A.1 Hosokawa Model

In 1995, Kazuo Hosokowa *et al.* did a pioneer work in the field of artificial self-assembling systems by utilizing chemical kinetics as a mathematical model for the formation of clusters of homogeneous triangles [49]. They created macroscopic rigid triangles that moved in a 2D shaking box. Two sides of the triangles incorporated magnets of complementary polarity (north and south in such a way that six triangles can self-assemble into hexamers. However, after the experiment some intermediate products were present indicating kinetic barriers in the formation of the final hexamers. The intermediate products (hereinafter referred to as clusters) are characteristic of any self-assembly system and belong to what is known as the yield problem. The insight of this model is to use an analogy with chemical kinetics for modeling the dynamic formation of the clusters.

The self-assembly process of any cluster was modeled as the reaction of monomers and intermediate clusters as in the bimolecular reactions in Equation A.1 (simultaneous reactions of more than three clusters are neglected). X_i $(1 \leq i \leq 6)$ indicates the type of cluster in the simulation. Monomers (1-mer) are indicated as X (Figure A.1a). The intermediate clusters are described as X_2 (2-mer), X_3 (3-mer), X_4 (4-mer) and X_5 (5-mer), and the target cluster is

indicated as X_6 (6-mer) (Figure A.1c). The symbol x_i is the state variable that represents the number of clusters for an specific type X_i at a certain time. All monomers are disassembled as initial condition and move in a plane with the same side facing up (Figure A.1b).

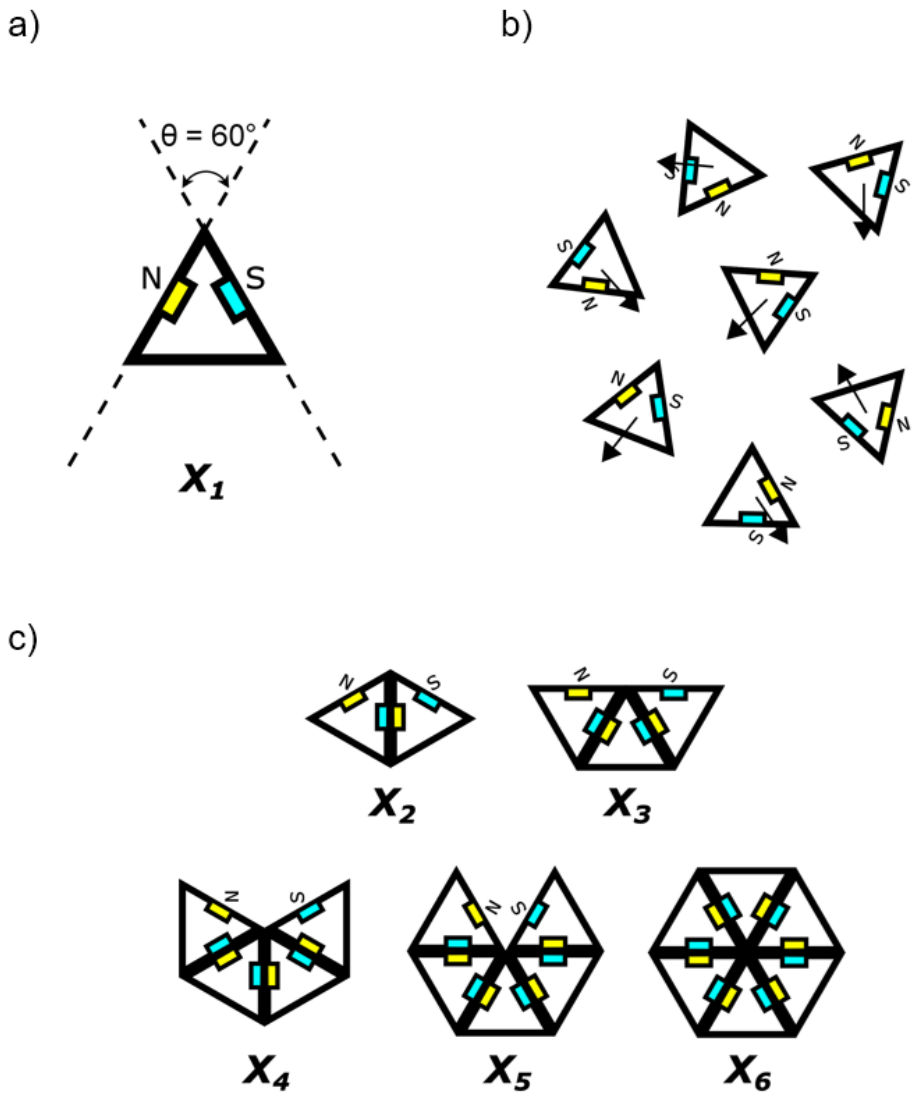

Figure A.1: Concept of rigid monomers. (a) Rigid monomer in its fixed configuration. (b) Rigid monomers interacting with other rigid monomers. (c)

$$2X \rightarrow X_2 \tag{A.1a}$$

$$X + X_2 \rightarrow X_3 \tag{A.1b}$$

$$X + X_3 \rightarrow X_4 \tag{A.1c}$$

$$X + X_4 \rightarrow X_5 \tag{A.1d}$$

$$X + X_5 \rightarrow X_6 \tag{A.1e}$$

$$2X_2 \rightarrow X_4 \tag{A.1f}$$

$$X_2 + X_3 \rightarrow X_5 \tag{A.1g}$$

$$X_2 + X_4 \rightarrow X_6 \tag{A.1h}$$

$$2X_3 \rightarrow X_6 \tag{A.1i}$$

For a large enough x_i, the state vector $\mathbf{x} = (x_1, ..., x_6)$ obeys the a differential equation (Equation A.2). t in the differential equation is the number of steps in the simulation (collisions between clusters or time evolution of the self-assembly system).

$$\mathbf{x}(t+1) = \mathbf{x}(t) + \mathbf{F}(t) \tag{A.2}$$

Where each $F_i = F_i(x_1, ..., x_6) = \sum_j v_{ij} P_j$ $(1 \leq i \leq 6)$ in $\mathbf{F} = (F_1, ..., F_6)$ is the expected value of increment of x_i for one step (from t

to $t+1$). The term v_{ij} corresponds to the stoichiometric number (coefficient of X_i in the j-th reaction in Equation A.1). v_{ij} is positive if X_i is a product (right side of the reaction, meaning generation of clusters), and negative if X_i is a reactant (left side of the reaction, meaning consumption of clusters for generating new clusters). The term is shown in Equation A.4 and is the probability of the j-th reaction.

$$P_j = P_{lm}^b P_{lm}^c \tag{A.3}$$

P_j depends on the two factors: the collision probability P_{lm}^c and the bonding probability P_{lm}^b (if they collide) for clusters X_l and X_m reacting. P_{lm}^c is assumed to be equal to the probability of picking up clusters whose type is X_l and X_m from $S = x_1 + x_2 + x_3 + x_4 + x_5 + x_6$ clusters. Equation AA.2 is constructed based on the assumption that x_i is large enough ($x_i \gg 1$), then Equation AA.4 shows the probability of collision P_{lm}^c.

$$P_{lm}^c = \begin{cases} 2x_l x_m / S^2, \ l \neq m \\ x_l / S^2, \ l = m \end{cases} \tag{A.4}$$

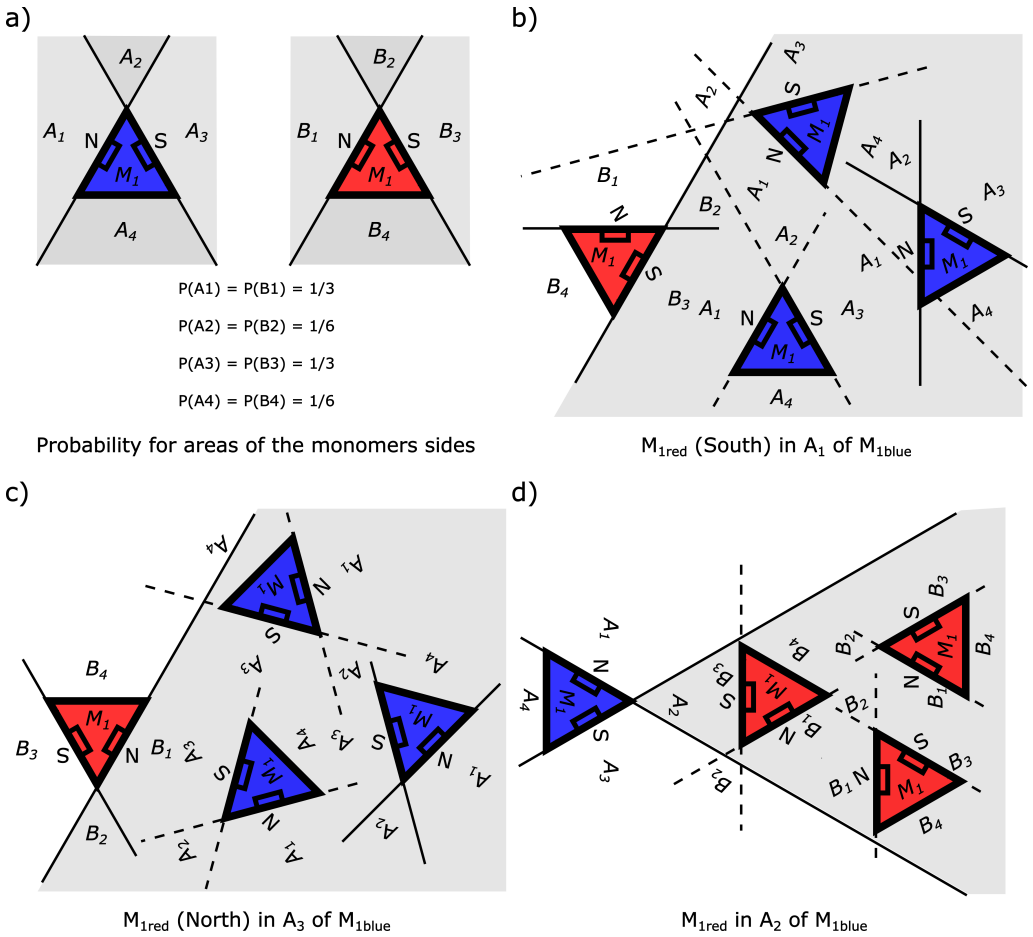

Figure A.2: Schemes for calculating the bonding probabilities of two rigid monomers. (a) Scheme of rigid monomer. (b) Rigid monomers interacting with other rigid monomers for one configuration. (c) Rigid monomers interacting with other rigid monomers for other configuration. (d) Rigid monomers interacting with other rigid monomers for another configuration.

The bonding probability P^b_{lm} depends on the geometry and orientation of the clusters when facing each other. Two clusters face each other on a 2D plane. Depending on which side of a cluster is facing the side of another cluster it is possible to calculate a probability of bonding. For example, consider the two monomers as in Figure A.2. The sides of the monomers M_{1red} and M_{1blue} can be divided into four areas: A_1, A_2, A_3, A_4 and B_1, B_2, B_3, B_4, respectively

(Figure A.2a). The probabilities of the divisions can be calculated according to the geometry of the monomer. Its shape is an equilateral triangle. Then the probability of the North side is $P(A_1) = P(B_1) = 1/3$, the South side is $P(A_3) = P(B_3) = 1/3$, the overlapping region between North and South side is $P(A_2) = P(B_2) = 1/6$. The region in where there is no magnet has a probability $P(A_4) = P(B_4) = 1/6$.

The bonding probabilities can be calculated from how the sides of the monomers face each other. There are four probabilistic independent cases:

- The probability for facing each other the South side of M_{1red} and North side of M_{1blue} (Figure A.2b). The conditional probability is $P(M_{1red} \text{ in } A_1)P(M_{1blue} \text{ in } B_2 \cup B_3) = 1/3 \times 1/2 = 1/6$.

- The probability for facing each other the North side of M_{1red} and South side of M_{1blue} (Figure A.2c). The conditional probability is $P(M_{1red} \text{ in } A_3)P(M_{1blue} \text{ in } B_1 \cup B_2) = 1/3 \times 1/2 = 1/6$.

- The probability for facing each other the side A_2 of M_{1red}, and North and South sides of M_{1blue} (Figure A.2d). The conditional probability is $P(M_{1red} \text{ in } A_2)P(M_{1blue} \text{ in } B_1 \cup B_2 \cup B_3) = 1/6 \times 5/6 = 5/36$.

- M_{1red} in A_4. The probability of bonding is zero since there is no magnet in A_4.

Then the bonding probability of two monomers is the summation of all the four cases: $1/6+1/6+5/36 = 17/36 \approx 0.472$. Other bonding probabilities are calculated in similar way. All bonding probabilities for the reaction of clusters X_l and X_m are summarized in Table A.1.

Table A.1: Bonding probabilities for clusters X_l and X_m

m\l	1	2	3	4	5	6
1	0.472	0.444	0.417	0.278	0.139	-
2		0.389	0.333	0.222	-	-
3			0.250	-	-	-
4				-	-	-
5					-	-
6						-

The vector $F_i = F_i(x_1, ..., x_6)$ can be expressed explicitly as the Equation A.5.

$$
\begin{aligned}
F_1(\mathbf{x}) &= (-2P^b_{11}x_1^2 - 2P^b_{12}x_1x_2 - 2P^b_{13}x_1x_3 - 2P^b_{14}x_1x_4 - 2P^b_{14}x_1x_5)/S^2) \\
F_2(\mathbf{x}) &= (P^b_{11}x_1^2 - 2P^b_{12}x_1x_2 - 2P^b_{22}x_2^2 - 2P^b_{23}x_2x_3 - 2P^b_{24}x_2x_4)/S^2) \\
F_3(\mathbf{x}) &= (2P^b_{12}x_1x_2 - 2P^b_{13}x_1x_3 - 2P^b_{23}x_2x_3 - 2P^b_{33}x_2^2)/S^2) \\
F_4(\mathbf{x}) &= (2P^b_{13}x_1x_3 + P^b_{22}x_2^2 - 2P^b_{14}x_1x_4 - 2P^b_{24}x_2x_4)/S^2) \\
F_5(\mathbf{x}) &= (2P^b_{14}x_1x_4 + P^b_{23}x_2x_3 - 2P^b_{15}x_1x_5)/S^2) \\
F_6(\mathbf{x}) &= (2P^b_{15}x_1x_5 + P^b_{24}x_2x_4 + 2P^b_{33}x_3^2)/S^2)
\end{aligned}
\tag{A.5}
$$

Finally, the vector $\mathbf{x} = (x_1, ..., x_6)$ is solved by introducing the Equation A.5 into Equation A.2. The result is plotted in Figure A.3.

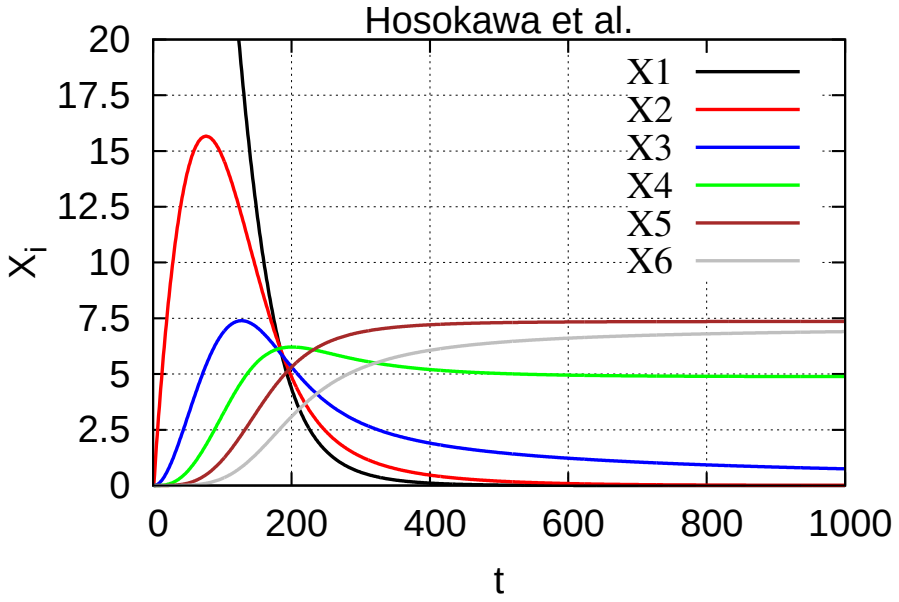

Figure A.3: Simulation for the monomers described in the original paper of Hosokowa *et al*

.

A.2 Flexible Monomers Model

The method of Hosokowa *et al* is extended to the case in which the monomers are not rigid and have some degree of flexibility. These monomers are called flexible monomers. In general, the flexible monomer is an abstraction for simulating the behavior of the shape-variable monomers and the fixed monomers. In our model, the behavior of the flexible monomer is abstracted as an isosceles triangle of variable angle Figure A.4). The angle oscillate between θ_{min} (θ_{X_1min}) and θ_{max} (θ_{X_1max}).

Flexible monomers move randomly on a surface colliding each other. Sides A and B of different monomers can stack, thus forming a flexible dimer. Over time (after many collisions) the monomers self-assemble into multiple clusters whose size depends on the angle range of θ_{X_1}.

$$\begin{aligned} P(A_1) &= \tfrac{1}{2} - \tfrac{\theta_{X_1}}{2\pi} \\ P(A_2) &= \tfrac{\theta_{X_1}}{2\pi} \\ P(A_3) &= \tfrac{1}{2} - \tfrac{\theta_{X_1}}{2\pi} \\ P(A_4) &= \tfrac{\theta_{X_1}}{2\pi} \end{aligned} \tag{A.6}$$

Where $\theta_{X_1min} \leq \theta_{X_1} \leq \theta_{X_1max}$

The sides of a flexible monomer are divided into four areas: A_1, A_2,

A_3 and A_4. For a monomer of angle θ the probability of the sides can be described as in Equation (A.6).

In general, the probability of the sides of any cluster X_i can be described as Equation (A.7).

$$\begin{aligned} P(A_1 \text{ of } X_i) &= \tfrac{1}{2} - \tfrac{\theta_{X_i}}{2\pi} \\ P(A_2 \text{ of } X_i) &= \tfrac{\theta_{X_i}}{2\pi} \\ P(A_3 \text{ of } X_i) &= \tfrac{1}{2} - \tfrac{\theta_{X_i}}{2\pi} \\ P(A_4 \text{ of } X_i) &= \tfrac{\theta_{X_i}}{2\pi} \end{aligned} \tag{A.7}$$

Where $\theta_{X_i min} \leq \theta_{X_i} \leq \theta_{X_i max}$

The bonding probability can be obtained from the relative position of the colliding clusters X_l and X_m (with angles θ_{X_l} and θ_{X_m}, respectively). Fig. S11.4b shows the orientation of the North and South sides of the clusters for bonding each other. Assume that the angles of the clusters just before colliding are fixed. Then, the expression for the bonding probability g_{X_l,X_m} is developed in similar way as in SI S11.1 (Equation (A.8)).

$$g_{X_l,X_m} = P(A_1 \text{ of } X_l)(P(B_2 \text{ of } X_m) + P(B_3 \text{ of } X_m)) +$$
$$P(A_3 \text{ of } X_l)(P(B_1 \text{ of } X_m) + P(B_3 \text{ of } X_m)) +$$
$$P(A_2 \text{ of } X_l)(P(B_1 \text{ of } X_m) + P(B_2 \text{ of } X_m) + P(B_3 \text{ of } X_m))$$

$$g_{X_l,X_m} = 2P(A_1 \text{ of } X_l)(P(B_2 \text{ of } X_m) + P(B_3 \text{ of } X_m)) +$$
$$P(A_2 \text{ of } X_l)(P(B_1 \text{ of } X_m) + P(B_2 \text{ of } X_m) + P(B_3 \text{ of } X_m))$$

$$g_{X_l,X_m} = g(\theta_{X_l}, \theta_{X_m}) = \frac{1}{2} - \frac{\theta_{X_l}\theta_{X_m}}{4\pi^2} \mid \theta_{X_l} \wedge \theta_{X_m} \in R^*$$

Where $R^* = [\theta_{X_l}, \theta_{X_m}]$

$$= \{\theta_{X_l min} \leq \theta_{X_l} \leq \theta_{X_l max} \cup \theta_{X_m min} \leq \theta_{X_m} \leq \theta_{X_m max} \cup \theta_{X_l} + \theta_{X_m} \leq 2\pi\}$$

(A.8)

R^* defines all possible values of θ_{X_l} and θ_{X_m} for assembling the new cluster X_{l+m}; in this case, there should be enough space for one cluster to insert itself into the other cluster. Note here that it is assummed $\theta_{X_l} + \theta_{X_m} \leq 2\pi$, meaning that assembled clusters keep their shape on the plane.

The function $g_{X_l,X_m} = g(\theta_{X_l}, \theta_{X_m})$ is the bonding probability function of the clusters X_l and X_m. Clusters are also flexible and can change their angle. The probability density function of θ_{X_l} and θ_{X_m} are $f_{X_l} = f_{X_l}(\theta_{X_l})$ and

$f_{X_m} = f_{X_m}(\theta_{X_m})$, respectively. Then, the differential of bonding probability $p^b_{X_l,X_m} = p^b_{X_l,X_m}(\theta_{X_l}, \theta_{X_m})$ for fixed angles can be described in terms of f_{X_l}, f_{X_m} and g_{X_l,X_m} (Equation (A.9)).

$$p^b_{X_l,X_m} = (\text{Probability of } \theta_{X_l} \wedge \theta_{X_m} \in R^* \mid \theta_{X_l} \wedge \theta_{X_m} \in R)$$

$$(\text{Bonding probability} \mid \theta_{X_l} \wedge \theta_{X_m} \in R^*)$$

$$p^b_{X_l,X_m} = \left(\frac{\iint\limits_{R^*} f_{X_l}\, f_{X_m}\, d\theta_{X_l}\, d\theta_{X_m}}{\iint\limits_{R} f_{X_l}\, f_{X_m}\, d\theta_{X_l}\, d\theta_{X_m}}\right)\ \left(f_{X_l}\, f_{X_m}\, g_{X_l,X_m}\, d\theta_{X_l}\, d\theta_{X_m}\right) \mid \theta_{X_l} \wedge \theta_{X_m} \in R^*$$

$$p^b_{X_l,X_m} = \left(\frac{\iint\limits_{R^*} f_{X_l}(\theta_{X_l})\, f_{X_m}(\theta_{X_m})\, d\theta_{X_l}\, d\theta_{X_m}}{\iint\limits_{R} f_{X_l}(\theta_{X_l})\, f_{X_m}(\theta_{X_m})\, d\theta_{X_l}\, d\theta_{X_m}}\right)\ \left(f_{X_l}(\theta_{X_l})\, f_{X_m}(\theta_{X_m})\right.$$

$$\left.\left(\tfrac{1}{2} - \tfrac{\theta_{X_l}\theta_{X_m}}{4\pi^2}\right) d\theta_{X_l}\, d\theta_{X_m}\right) \mid \theta_{X_l} \wedge \theta_{X_m} \in R^*$$

Where $R = [\theta_{X_l}, \theta_{X_m}] = \{\theta_{X_l min} \leq \theta_{X_l} \leq \theta_{X_l max} \cup \theta_{X_m min} \leq \theta_{X_m} \leq \theta_{X_m max}\}$

$R^* = [\theta_{X_l}, \theta_{X_m}] = \{\forall [\theta_{X_l}, \theta_{X_m}] \in R \mid \theta_{X_l} + \theta_{X_m} \leq 2\pi\}$

(A.9)

R defines all possible values of θ_{X_l} and θ_{X_m} independently if they interact or not.

The differential of bonding probability depends on θ_{X_l} and θ_{X_m} just before colliding (Equation (A.9)). Then, this differential should be integrated

over R and R^* resulting in an integral form (Equation (A.10)).

$$P^b_{X_l,X_m} = \iint_{R^*} p^b_{X_l,X_m}$$

$$P^b_{X_l,X_m} = \frac{\iint_{R^*} f_{X_l}(\theta_{X_l})\, f_{X_m}(\theta_{X_m})\, d\theta_{X_l}\, d\theta_{X_m}}{\iint_{R} f_{X_l}(\theta_{X_l})\, f_{X_m}(\theta_{X_m})\, d\theta_{X_l}\, d\theta_{X_m}} \iint_{R^*} f_{X_l}(\theta_{X_l})\, f_{X_m}(\theta_{X_m}) \left(\frac{1}{2} - \frac{\theta_{X_l}\theta_{X_m}}{4\pi^2}\right) d\theta_{X_l}\, d\theta_{X_m} \tag{A.10}$$

Expression (Equation (A.10)) depends on the probability density function of the angles. Throughout all the simulations, a continuous uniform distribution is used by basing on the minimum and maximum angles of the particular cluster.

In these calculations there is no distinction between an open and closed cluster: clusters open and close at all times.

A.2.1 Simulation for Shape-Variable Monomers

In order to simulate the behaviour of the shape-variable monomers on a surface it is required to set the angle of the flexible monomer between 60° and 120°. The angle is approximated by an uniform function. Flexible monomers move randomly on a surface colliding each other. Sides A and B

a)

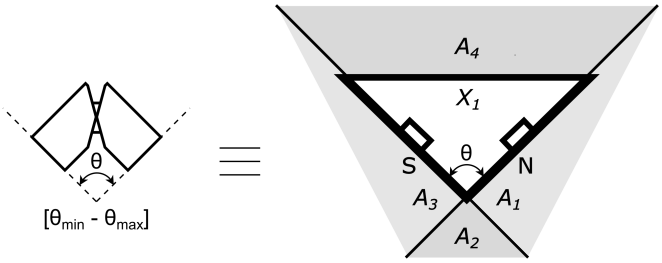

Flexible monomer as equivalent of shape-variable monomer

b)

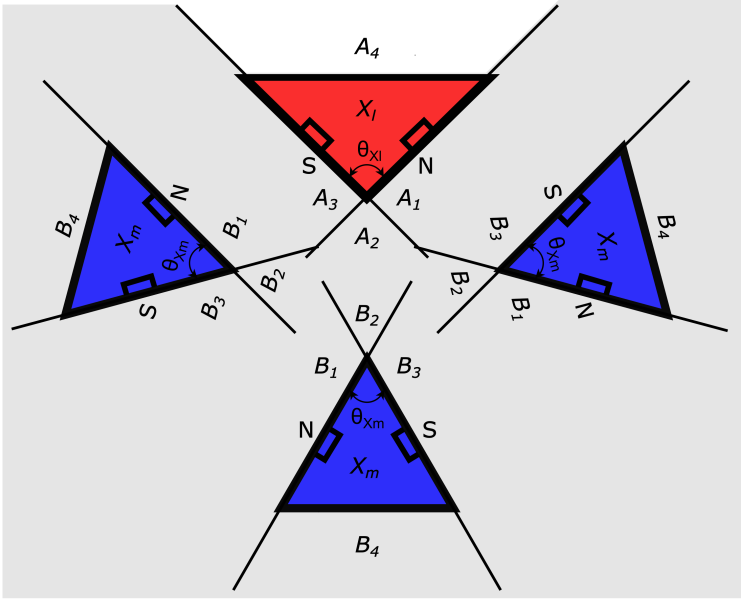

Scheme of the possible positions for clusters X_I and Xz to bond

Figure A.4: Flexible monomers and scheme for possible bonding.

of different monomers can stack, thus forming a flexible dimer. Over time (after many collisions) the monomers self-assemble into clusters from dimers up to hexamers. Table A.2 shows the bonding probability values used in the simulation.

Table A.2: Bonding probabilities for clusters X_l and X_m made of flexible monomers (60°-120°)

m\l	1	2	3	4	5	6
1	0.438	0.375	0.087	0.021	0	-
2		0.076	0.002	0	-	-
3			0	-	-	-
4				-	-	-
5					-	-
6						-

Figure A.5 shows the cluster formation for 50000 Number of collisions (time steps for the simulation). The simulation shows that the amount of trimers overcomes the tetramers. However, dimers and pentamers have similar yield. In addition, hexamers are highly improbable due to flexibility range of the flexible monomer; the probability of the angle to be 120° is neglectable.

Of course other geometries are possible by this model, as for example linear self-assembly with rotational connections. The proposed simulation

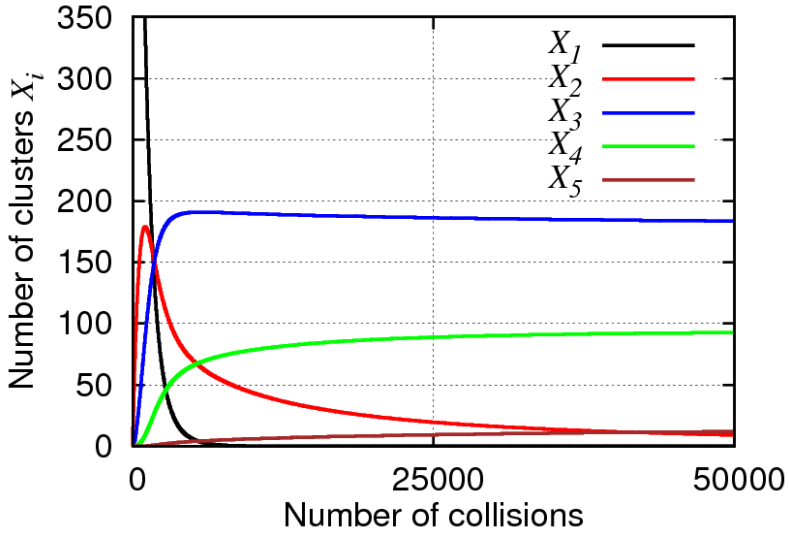

Figure A.5: Simulation of the formation dynamics of self-assemble clusters made of flexible monomers with an internal angle between 60° and 120°.

for flexible monomers will be used elsewhere, as for example in the study of reconfigurable structures.

Acknowledgements

I would like to acknowledge and recognize all the people and circumstances that accompanied me during my life as student in Japan, towards my doctoral degree.

I would like to start by showing gratitude towards my advisor, Prof. Satoshi Murata, whom I appreciate from the bottom of my heart. His trust and opportune advice, alongside his everlasting patience and kind compliments, have made me not only good at what I pursue but also a better human being. I truly thank him for taking care of me as in good, bad and uncertain times throughout my studies here at Tohoku University. Most importantly, he taught me the exclusive pleasure of building things in the real world and to recognize the nuance in writing.

I would like to acknowledge laboratory staff. I truly acknowledge Prof. Nomura for his continuous encouragement, his readily disposition for challenges, his friendly caring attitude and his ever sense of humor. Perhaps, my life at the laboratory would have been very different without his persona. Mr Kawamata for his sharp remarks, evidence-based speaking and unconditional

criticism. I am grateful for his continue encouragement at all moment. I truly appreciate and acknowledge our laboratory secretary Mrs Abe for helping me in many ways. Her assistance in non-academic issues have helped me to work at the laboratory with little worries. Ms Kawagishi, Mrs Tanabe and Ms Minegishi are acknowledged for their help and cheering up the laboratory environment.

The laboratory for being an interesting place for experiencing creation, sharing knowledge at international conferences and competitions, and for providing me with the tools and companionship necessary for studying. My gratitude is directed to each and every colleague for his/her support, valuable discussions and unconditional disposition in supporting me during laboratory routines. Indeed, sharing equipment with them has been a real pleasure that I will never forget. It is impossible to forget those colleagues who are not with us now but have been important figures in setting up the laboratory and my life here; especially to former lab members Daisuke Kandatsu, Shogo Hamada, Kei Fujiwara, Fumi Takabatake and former secretary Shizuka Mitoma.

I would like to acknowledge the doctoral committee Prof. Nishizawa and Prof. Tanaka for useful comments. I also acknowledge Yonamine-san, Prof. Ariga (NIMS), and Prof. Fujimoto (JAIST) for fruitful collaboration.

Previous to starting studying in Japan, I was selected by the Japanese Embassy in Peru to receive the prestigious MEXT scholarship. I am very

grateful to the support given by Ms Moreno, Ms Umeoka and the former ambassador, Mr Megata. I am truly grateful to the Japanese government for kindly supporting my studies and research in Japan.

Additionally, I would like to acknowledge both my international and local friends for making, in particular ways, my life in Japan more interesting and pleasant. I would like to recognize their kindness, friendship and love not only in such moments; I cannot express in words how much I learned from them. Special thank go to my host family Mrs Kokubun for taking care of me and my wife. Special thanks go to Lazaro, Vinicius and Carlos for friendly moments. I acknowledge the Peruvian crew consisting of Jorge, Luis, Bruno, Daniel and Erick. I also thank the other Latino crew including Irina, Seth, Evelyn and Marco. Matias and the other members. My friends abroad: Karim, Alfie, Wudmir, Paul, Enver and Grace, Samantha, Oscar, Jimy, Christian Cuba S., Christian Cuba T., Sadao, Luis Jauregui and family. I appreciate all of these people for carefree conversations. I really acknowledge them from the bottom of my heart.

I would like to recognize with all my heart the love of my family in Peru, relatives in the United States and my wife. Their unconditional trust in me, comprehension and strength have been fundamental support on my life. The colorful cheerfulness, strong character and lively passion of my mother have been the push and fuel that accompanied me during my studies. Lastly

and most importantly, I would like to recognize that my investigations should not end here. They will definitely continue with new endeavors as I take a leap of intuition.

Contributions

A Peer-reviewed Articles

- K. Cervantes-Salguero, I. Kawamata, S.-i. M. Nomura, S. Murata. "Unzipping and Shearing DNA with Electrophoresed Nanoparticle in Hydrogel", Physical Chemistry Chemical Physics, 2017. DOI: 10.1039/c7cp02214j.

- D. Kandatsu, K. Cervantes-Salguero, I. Kawamata, S. Hamada, S.-i. M. Nomura, K. Fujimoto, S. Murata. "Reversible Gel-Sol Transition of a Photo-Responsive DNA Gel", ChemBioChem, 2016.

- Y. Yonamine, K. Cervantes-Salguero, K. Minami, I. Kawamata, W. Nakanishi,a J. P. Hill, S. Murata, K. Ariga. "Supramolecular 1-D polymerization of DNA origami through a dynamic process at the 2-dimensionally confined air-water interface", Physical Chemistry Chemical Physics, 2016.

- Y. Yonamine, K. Cervantes-Salguero, W. Nakanishi, I. Kawamata, K. Minami, H. Komatsu, S. Murata, J. P. Hill, K. Ariga. "In situ 2D-extraction of DNA wheels by 3D through-solution transport", Physical Chemistry Chemical Physics, 2015.

- K. Cervantes-Salguero, S. Hamada, S.M. Nomura, S. Murata. "Polymorphic ring-shaped molecular clusters made of shape-variable building blocks", Nanomaterials, 2015.

B Book Chapter

- K. Cervantes-Salguero, S. Murata., "Chapter 8: Engineering DNA Molecules for Morphological Reconfiguration", Katsuhiko Ariga, Masakazu Aono Eds. "Supra-Materials Nanoarchitectonics" p.195-206 Elsevier, (2016).

C International Conferences

- 5th International Conference On The Theory And Practice Of Natural Computing (Sendai, Japan, Dec 2016). K. Cervantes-Salguero, I. Kawamata, S.-i. M. Nomura, S. Murata. Poster and talk presentation: "Design and Construction of Reusable DNA Logic Gates Based on Electric Field Actuation".

- DNA21: 21th International Conference on DNA Computing and Molecular Programming (Harvard, Boston, US, Aug 2015). K. Cervantes-Salguero, Y. Yonamine, W. Nakanishi, I. Kawamata, K. Minami, H. Komatsu, S. Murata, J. P. Hill, K. Ariga. Poster presentation: "Lipid-Modified DNA Rings on Hydrophobic Surfaces".

- DNA20: 20th International Conference on DNA Computing and Molecular Programming (Kyoto, Japan, Sept 2014). K. Cervantes-Salguero, Y. Yonamine, W. Nakanishi, I. Kawamata, K. Minami, H. Komatsu, S. Murata, J, P. Hill, K. Ariga. Poster presentation: "Hydrophobic Control of DNA Nanostructures".

- FNANO: Foundations of Nanoscience 2014 (Snowbird, USA. Apr 2014). S. Murata, K. Cervantes-Salguero, S. Hamada, S.M. Nomura, S. Murata. Poster and invited talk: "Shape-Variable Building Blocks for Reconfiguring Closed Molecular Clusters".

- FNANO: Foundations of Nanoscience 2013 (Snowbird, USA. Apr 2013). K. Cervantes-Salguero, S. Hamada, S.M. Nomura, S. Murata. Poster presentation: "Reconfigurable Ring-Shaped Clusters".

- DNA18: 18th International Conference on DNA Computing and Molecular Programming (Aarhus, Denmark, Aug 2012). K. Cervantes-Salguero, S. Hamada, S.M. Nomura, S. Murata. Poster presentation: "Controlling the Size of Molecular-Clusters".